Universidad Autónoma de Madrid

Facultad de Ciencias

Departamento de Biología Molecular

Regulating NOTCH ligands

The role of Mind bomb1 during cardiac development and disease

Doctoral thesis

Guillermo de Luxán García

October 2013

Director: José Luis de la Pompa Mínguez

Tutor: Antonio Rodríguez Márquez

To C, C, F, N and M

“The saddest aspect of life right now is that science gathers knowledge faster than society gathers wisdom.”

Isaac Asimov

This work was performed in Dr José Luis de la Pompa´s laboratory in the Cardiovascular Developmental Biology and Repair Department at the Centro Nacional de Investigaciones Cardiovasculares (CNIC) in Madrid.

This study was funded by grants SAF2007-62445, SAF2010-17555, RD06/0014/0038 (RECAVA) and RD06/0010/1013 (TERCEL) from the Spanish Ministry of Economy and Competition (MINECO) to José Luis de la Pompa.

Guillermo de Luxán has a PhD fellowship from the MINECO (FPI Program, BES-2008-002904).

Index of contents

Index of figures, tables and videos

Figures

Tables

Videos

1. 6-month-old wild-type (WT) echocardiography analysis. ep, epicardium; en, endocardium.
2. 6-month-old Mib1flox;cTnT-Cre echocardiography analysis. ep, epicardium. Asterisks mark where prominent trabeculae can be observed.
3. 6-month-old WT CMRI. 4 chambers view.
4. 6-month-old WT CMRI. Short axis view.
5. 6-month-old Mib1flox;cTnT-Cre CMRI 4 chambers view.
6. 6-month-old Mib1flox;cTnT-Cre CMRI short axis view.
7. Healthy control CMRI 4 chamber view
8. Patient 1.II.3 CMRI 4 chamber view.
9. Patient 2.I.2 CMRI 4 chamber view.

10. Healthy control CMRI 2 chamber view.
11. Patient 1.II.3 CMRI 2 chamber view.
12. Patient 2.I.2 CMRI 2 chamber view.
13. Healthy control CMRI short axis view.
14. Patient 1.II.3 CMRI short axis view.
15. Patient 2.I.2 CMRI short axis view.

Abbreviations

ACTC: Actin

ADAMTS1: A disintegrin and metalloproteinase with thrombospondin motifs 1

Anf: Atrial natriuretic factor

AoV: Aortic valve

AP: Aortic-pulmonary

AV: Atrio-ventricular

AVC: Atrioventricular canal

BAV: Bicuspid aortic valve

BMP: Bone morphogenetic proteins

CBF1: See RBPJK

CHD: Congenital heart disease

CMRI: Cardiac magnetic resonance imaging

coIP: Coimmunoprecipitation

Cx40: Connexin 40

Dll: Delta like

DSL: Delta, Serrate, Lin12 domain

DTX1: Human deltex-1 protein

Egf: Epidermal growth factor

EMT: Epithelial-to-mesenchyme transition

FHF: Fist heart field

FRET: Fluorescence resonance energy tranfer

G4.5: Tafazzin

GATA3: Trans-acting T-cell-specific transcription factor GATA-3

HEK: Human Embryonic Kidney

Hes: Hairy and enhancer of split

Hey/HRT/Hesr: Hairy and enhancer of split repressor

Irx4/ 5: Iroquois-class homeodomain protein 4/ 5

Jag: Jagged

La: Left atrium

LDB3: LIM domain binding 3

LMNA: Lamin A/C

Lv: Left ventricle

LVNC: Left ventricular non-compaction

MIB: MIND BOMB

MYBPC3: Cardiac Myosin binding protein-C

MyH7: myosin heavy chain beta (MHC-β) isoform

MYL2/ 3: Myosin regulatory light chain 2/3

NECD: Notch extracellular domain

Neurl: Neuralized

NICD: Notch intracellular domain

NMD: Nonsense-mediated decay

NRARP: Notch regulated ankyrin repeat protein

Nrg1: Neuregulin 1

OFT: Out flow tract

Ra: Right atrium

RBPJK: Recombination Signal-binding protein 1 for J-kappa sequences, equivalent to Drosophila's Suppressor of Hairless (Su(H)) and CSL, for CBF1 (in mammals) Supressor of Hairless (in Drosophila) and Lag-1 (in C. elegans).

Rv: Right ventricle

Sema3C: Semaphorin-3C

SHF: Second heart field

Tbx20: T-box transcription factor 20

TCF7: Transcription factor 7

TNNI3: Troponin I

TNNT2: Troponin T type 2

TPM1: Tropomyosin alpha-1

WT: Wild-type

SUMMARY

Heart development is the result of the tightly regulated spatio-temporally embryonic processes of lineage specification, tissue patterning, cellular proliferation, differentiation and morphogenesis that ultimately lead to the adult, fully functional heart. Congenital heart disease (CHD) occurs when normal cardiac development is impaired and the structure of the heart and great vessels is abnormal. It is very frequent and approximately nine people in 1000 are born with a congenital heart defect. A great research effort is under way to understand the molecular and genetic bases of CHD, as they can be manifested in the neonate but also in the adult individual. In this work, we have used a conditional loss-of-function model of the Notch regulator Mib1, to show that Notch acting from the endocardium not only regulates early heart development, as it has been described previously, but also plays a crucial later role in the maturation of the cardiac valves and chambers. In the OFT valves, Notch regulates in a non-cell autonomous manner BMP signalling, repressing *Bmp6* and cellular proliferation in the valvular mesenchyme, allowing the valves to undergo the morphogenetic processes required for their maturation. In the ventricles, Notch activity in the endocardium activated from the myocardium sends maturation signals to the myocardium, so that compact and trabecular myocardium are established by the expression of trabecular markers (*Anf*, *Bmp10* or *Cx40*) and compact zone markers (*Hey2*, *N-myc* or *Tbx20*), allowing ventricular compaction, and thus the formation of the adult contractile wall of the heart. Absence of these Notch-dependent signals produces LVNC in humans, the third most important cardiomyopathy, with a very poorly understood etiology, characterized by prominent and excessive trabeculations, with deep recesses in the ventricular wall. LVNC manifests as depressed systolic function. Classical complications include systemic embolism, malignant arrhythmias, heart failure and sudden death. The importance of NOTCH in heart development and its impact in cardiomyopathies such as LVNC, opens a new research avenue into the identification of novel diagnostic and eventually, therapeutic targets.

INTRODUCTION

In this PhD thesis we have studied the role of the Notch signalling pathway in heart development, paying particular attention to two structures that are important substrates of CHD, the valves of the outflow tract (OFT) and the ventricles, that are essential components of the pumping machinery of the adult heart: the valves allow the flow of the blood from one cardiac chamber to another and prevent retrograde flow, the ventricles are the muscular wall that in the case of the left ventricle has to send the oxygenated blood to the rest of the body through the aortic valve. Failure to properly develop valves or ventricles causes CHD that severely compromises the life of the neonate and may cause its death if not treated on due time.

Heart development

Development of the heart starts at embryonic day 7 in the mouse (E7) when pre-cardiac precursor cells move forward bilaterally into the lateral plate mesoderm to form the cardiac crescent (Fig. 1 A) (Harvey, 2002). By E8, folding of the mesodermal layers from both sides of the embryo results in the formation of the linear heart tube that is not yet compartmentalised. The two mains tissues of the heart are present, the endocardium in the inside and the myocardium in the outside. The cells forming the original heart tube come from the first heart field (FHF), that will give rise later to part of the atria, left ventricle and atrio-ventricular canal (AVC) (Buckingham et al., 2005) (Fig. 1 A, B).

At E9.0, the heart starts to bend rightwards to relocate the tube in a manner that the future atria of the heart are located posterior to the common ventricle, this process is called cardiac looping. At the same time, it expands by the addition of cells from the second heart field (SHF) (Kelly and Buckingham, 2002). In the arterial pole of the heart, the SHF will contribute to the OFT, the right ventricle and the ventricular septum (Zaffran et al., 2004), whereas in the venous pole of the heart, the SHF contributes to atria and atrial septum (Snarr et al., 2008) (Fig. 1 A, B).

The heart divides afterwards into developmental domains that would allow the formation of two regions, the valvular and the chamber regions (Moorman and Christoffels, 2003, Moorman et al., 2007, Aanhaanen et al., 2011) (Fig.1 B). Cardiac valve formation is restricted to AVC and OFT. It is in these two regions where the endocardial cushions, the primitive valves, are formed. Endocardial cells undergo an epithelial-to-mesenchyme transition (EMT) and populate the cardiac jelly that separates endocardium and myocardium. In the endocardium Notch is essential for the activation of EMT (Timmerman et al., 2004, Luna-Zurita et al., 2010). The transcription factors *Snail1* (Timmerman et al., 2004, Luna-Zurita et al., 2010) and *Snail2* (Niessen et al., 2008) are required for this process downstream of Notch, as they repress *vascular endothelial cadherin* (*VE-C* or *Cdh5*) so that the endocardial cells are capable of undergo EMT and invade the cardiac jelly (Timmerman et al., 2004). A complex signalling network that integrates different pathways such as Bmp, Tgf-β and Notch regulates the EMT process (Luna-Zurita et al., 2010, de la Pompa and Epstein, 2012). There are four cushions formed in the AVC and four in the OFT (Fig. 1B). By E10.5 the endocardial cushions are formed and the morphogenesis and maturation of the valves begins.

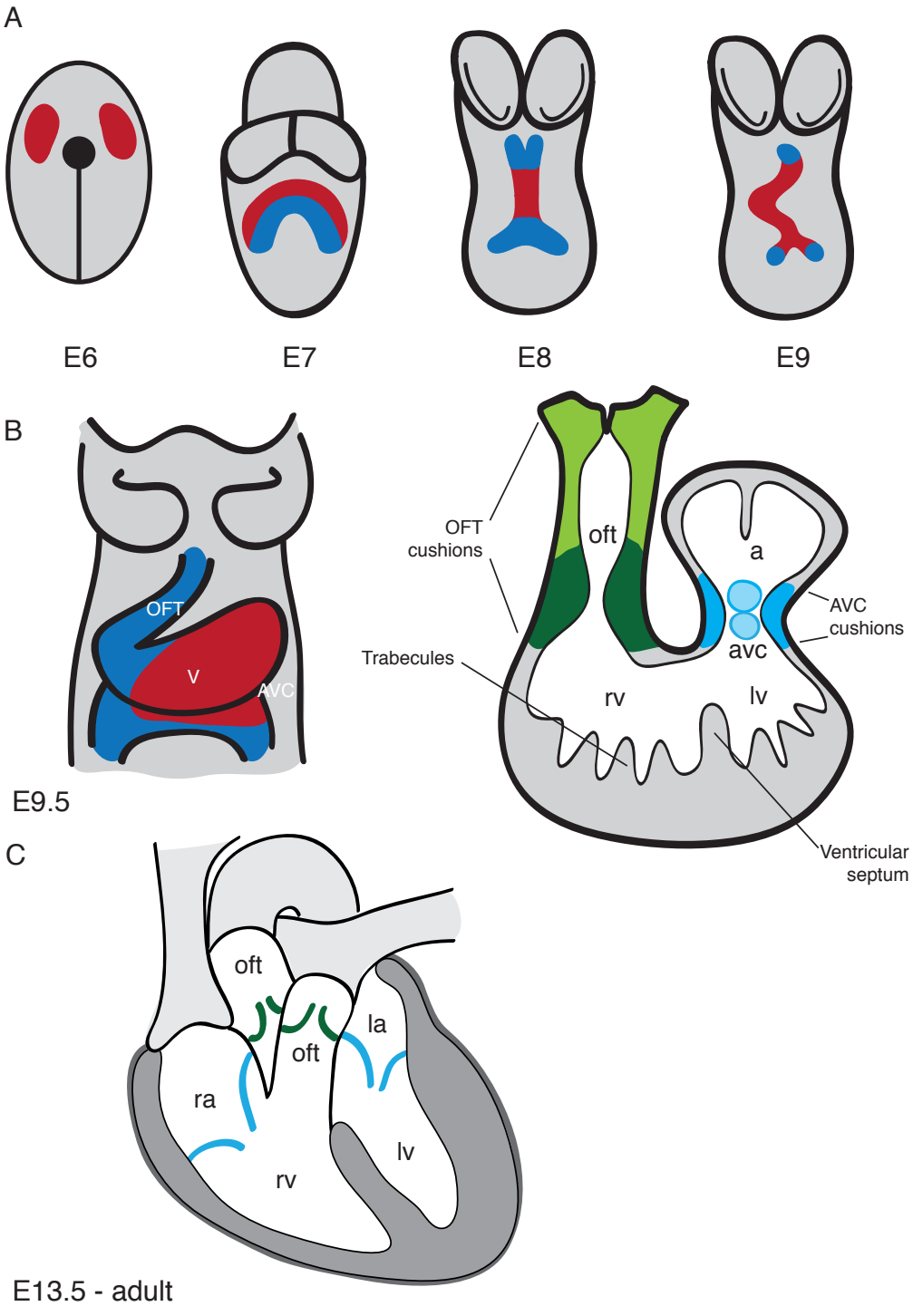

At around the same time (E9.5), the process of trabeculation begins in the primitive ventricles. Trabeculae are highly organized sheets of cardiomyocytes that protrude towards the light of the ventricles (Ben-Shachar et al., 1985). Trabeculae are the first structure that differentiates the ventricles in the developing heart (Sedmera et al., 1997). They increase the ventricular surface and allow the myocardium to grow in the absence of coronary vessels that will be formed later. They are important for contractibility, formation of the conduction system and blood flow direction in the ventricle. Although trabeculae start to form first in the left ventricle and then later in the right ventricle, there are

Figure 1. Overview of early heart development.

(A) Ventral views of the developing mouse embryo. At E7.0, cardiac progenitors (red) migrate to the center of the embryo to form the cardiac tube and at E7.5, two cardiac fields can be distinguished: the first heart field (FHF; red) and the second heart field (SHF; blue). By E8.0, the cardiac tube is formed where endocardium and myocardium are already present. At E9.0, the tube loops and the different cardiac regions become apparent. (B) Ventral view of the E9.5 heart, which consists of four anatomically distinct regions: atrium, atrioventricular canal (AVC), ventricle (V) and outflow tract (OFT). Endocardial cushions are formed in valvulogenic regions of the heart (green, OFT and blue, AVC) and trabeculae appear in the ventricles. (C) Longitudinal section depicting the heart. Once valve primordia (OFT, green and AVC, blue) and trabeculae are formed, the heart needs to mature and these structure undergo morphogenesis.

no differences between these structures in the two ventricles. Formed trabeculae have no free ends and they make the ventricle look like a sponge (Sedmera et al., 2000) (Fig.1 B). The Notch signalling pathway is essential for early trabeculation (Grego-Bessa et al., 2007).

From E10.5 onwards, the ventricular myocardium has two well-defined regions, morphologically and molecularly, the outer compact myocardium and the inner trabecular layer. The compact myocardium is less differentiated and shows a higher proliferation rate, than the trabecular myocardium more differentiated (Sedmera et al., 2000). Differentiated cardiomyocytes will give rise to the working myocardium and the conduction system (Sedmera et al., 2000). After ventricular septation is complete, around E13.5-E14.5, trabeculae are mature and they have to be remodel to continue ventricular development (Fig. 1 C).

When endocardial cushions and trabeculae are formed, a second phase in heart development begins. The structures that have risen during this first part of development have to mature in order to form a fully functional heart. AVC and OFT are septated, endocardial cushions are fused and finally they will be sculpted to form the mature leaflets of the heart. Simultaneously, the ventricular walls are compacted when the trabeculae become part of the ventricular wall. Little is known about the molecular networks that guide cardiac maturation, one aim of this PhD thesis has been to gain some knowledge about these later stages of heart development (Fig. 1 C).

Cardiac valve morphogenesis and maturation

The morphogenetic events that transform the endocardial cushions into mature valves are related to the septation of the heart and the separation of pulmonary and systemic blood circuitries. The correct maturation of the endocardial cushions is crucial for later function of the heart, and the consequences of defective morphogenesis of the leaflets at this stages will be observed later in the form of congenital heart disease (CHD), such as bicuspid aortic valve (BAV) (Srivastava, 2006).

After EMT has taken place, four endocardial cushions are formed in the AVC and in the OFT. Two mayor leaflets and two smaller lateral ones (Fig.1 B) (Wessels and Sedmera, 2003). The mayor leaflets of the AVC form a fused bulk of mesenchyme that occupies

the lumen of the AVC and it is required for the ventricular septation that will divide the systemic and pulmonary flows. The lateral leaflets do not fuse and will not be part of the atrio-ventricular (AV) complex, instead they will give rise to the mural leaflets of the mitral valve (Snarr et al., 2008). Something similar happens in the OFT, the major cushions fuse to form the aortic-pulmonary (AP) septum, while the intercalating cushions do not fuse and contribute only to the definitive leaflets.

The endocardial cushions are not only formed by EMT-derived mesenchymal cells, there are other lineages that contribute to the cushions and drive its maturation. Thus, by E11.5 the OFT mesenchyme derived from the endocardium by EMT is invaded by mesenchyme cells that migrate rostro-caudally from the neural crest. They form two prongs of mesenchyme in both sides of the future AP septum (de Lange et al., 2004). Although neural crest cells make little contribution to the mature valves, they can still be observed in the adult valves (Jiang et al., 2000). There is an important cross-talk between the two populations of mesenchymal cells, endocardial- and neural crest- derived in the cushions, crucial for the maturation of the leaflets. Neural crest-derived, mesenchymal cells induce cell death in the mesenchyme, which is crucial for the delamination and sculpting of the leaflets (Jain et al., 2011, de la Pompa and Epstein, 2012). The neural crest does not contribute to the formation of the AV valves (Wessels et al., 2012). At E12.0, epicardial derived cells migrate through the AV junction into the endocardial cushions of the AVC. The contribution of these cells to the mature AV valves is mainly to the lateral cushions and only a few cells can be observed in the major AV cushions, but during development they will populate most of the leaflet (Wessels et al., 2012). After the invasion of the other lineages, the expansion of the cushions via cellular proliferation is driven by different signals such as Bmp (Eisenberg and Markwald, 1995), Wnt (Alfieri et al., 2010) or Egf (Iwamoto et al., 2003). Two Bmp molecules, Bmp6 and Bmp7, are expressed in the OFT and required for cushion formation in the OFT. The double mutant *Bmp6*;*Bmp7* shows a marked delay and hypoplasia of the OFT cushions (Kim et al., 2001).

The last phases of valve development are characterized by the differentiation of the mesenchyme that has grown from EMT and invasion of the other lineages (Fig. 2). This forms a highly organized and stratified structure guided by the extracellular matrix. The exact mechanism that underlies these structural changes is unclear (de Vlaming et al., 2012). The elongation of the leaflets occurs between E15.5 and E18.5 and is due to an increase of cellular density and a reorganization of the extracellular matrix (Kruithof et al., 2007). Periostin that binds to collagen fibers modulates the diameter and the assembly of the fibers promoting fibrillogenesis by cross-linking (Norris et al., 2009). The reorganization of the matrix is regulated by Periostin and the coordinated actions of zinc metallopreoteases, ie: ADAMTS1 that cleaves versican and facilitates the dense packing of the mesenchyme, the sculpting of valves (Kern et al., 2006), and the differentiation of endocardial-, epicardial- and neural crest-derived mesenchyme will give rise to mature valves.

The leaflets of the AV valves will be attached

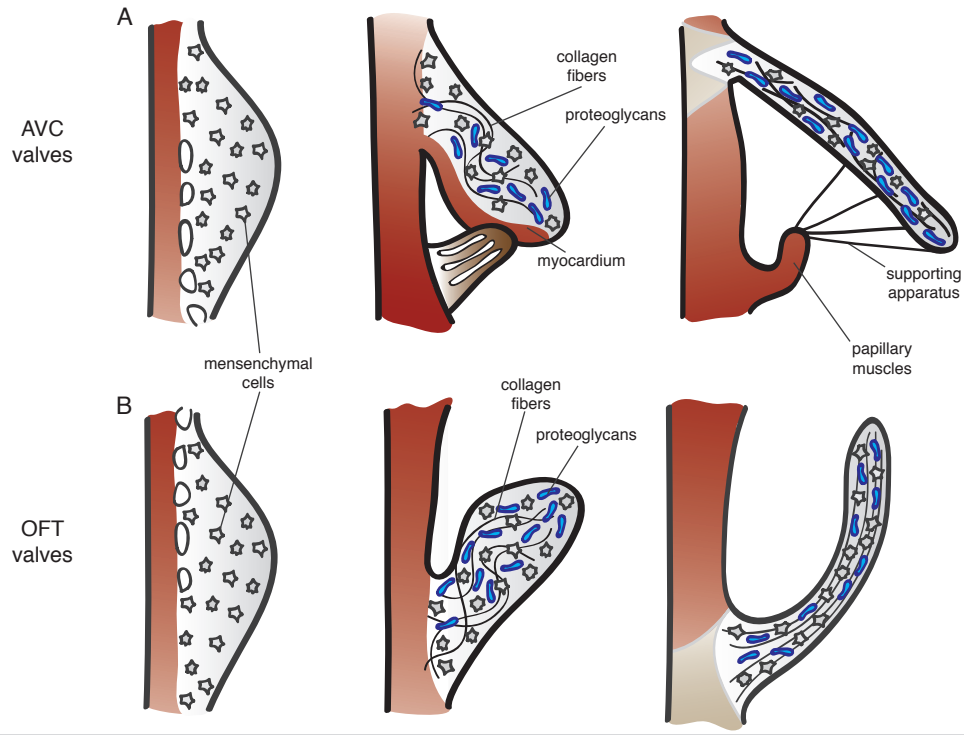

Figure 2. Valve maturation.

(A) Morphogenesis of the AVC valves. From E13.5 onwards the leaflets and tensile apparatus (dark red) of the AVC valves form predominantly by delamination of the inner layers of the inlet zone from the ventricular septal wall. The chordae tendinae that will form the supporting apparatus develop at this time. These structures and the leaflet itself are derived from the endocardium. (B) Morphogenesis of the OFT valves. The excavation of the cusps takes place by an initial solid ingrowth of the endothelium at the arterial face of the cusp, and subsequent lumenation. Elongation and remodeling of the primordia into mature valve structures is associated with regionalized cell proliferation and matrix alignment guided by hemodynamic forces. Myocardium is depicted in dark red, proteoglycans in blue and mesenchyme in gray.

to the base of the ventricular walls by tendon-like cords tendinae, the supporting apparatus of the valves, via the papillary muscles (Guy and Hill, 2012) that are formed by coalescence of trabeculae in the ventricles (Sedmera et al., 2000) (Fig. 2 A) while the OFT are self-supporting and attach to the arterial wall (Fig. 2 B).

Finally, in mature valves the remodelled extracellular matrix is aligned to the blood flow. This suggests that there is a role for hemodynamic forces in the maturation of the valves that should be taken into account (Combs and Yutzey, 2009). Interestingly, endocardial expression of the active Notch1 receptor is restricted to the flow side of the valves (Del Monte et al., 2007), suggesting that there is an endothelial response to shear stress produced by the hemodynamic forces (Combs and Yutzey, 2009) (Fig. 2).

Failure of cardiac cushion remodelling giving rise to dysmorphic valves is a characteristic of some CHD such as tetralogy of Fallot in which, a dysmorphic pulmonary

valve is accompanied by an overriding aorta (Greenway et al., 2009, Jain et al., 2011).

Ventricular maturation and trabecular compaction

After completion of ventricular septation around E14.5, further growth and maturation of the ventricular chambers requires a complete trabecular remodelling and reorganization into an apico-basal orientation that determines the shape of the ventricles. Trabeculae become compacted and as a result, there is a significant change in the ratio of compact vs. trabecular myocardium in the ventricle. Some of the trabeculae coalesce to produce part of the papillary muscles of the AV valves (Sedmera et al., 2000).

Trabeculae compaction is accompanied by the hypoxia-dependent invasion of the coronary vasculature from the epicardium into the compact layer of the myocardium (Tao et al., 2013). As they compact, the intertrabecular recesses are transformed into capillaries of the rising coronary plexus. This is followed by a reorganization of the muscle fibres of the heart that organize in a three-layered spiral around the heart reflecting the twisting pattern of heart contraction (Sedmera et al., 2000).

Trabeculae stop proliferating while the proliferation of the compact zone sustains the growth of the chamber and the contribution of the compact layer to the heart becomes more significant than the one of the luminal trabeculations that will eventually disappear. How exactly this happens and what molecular mechanisms drive this process is unknown.

Left ventricular non-compaction (LVNC)

LVNC is a cardiomyopathy of poorly understood etiology that is characterized by prominent and excessive trabeculations with deep recesses in the ventricular wall (Jenni et al., 2007) (Fig.3). It is caused by the intrauterine arrest of myocardial morphogenesis that leads to the presence of persistent trabeculae (Ritter et al., 1997).

LVNC was first diagnosed in 1984, in a 33-year old woman assessed by echocardiography (Engberding and Bender, 1984). Since then, the heterogeneity of its symptoms might have left many LVNC cases undiagnosed (Jenni et al., 2007), giving a lower estimation of its real impact as a cardiomyopathy. The improvement in imaging technologies and the advent of CMRI, allows now a better diagnose of this disease and ten years after the first description, LVNC was included in the World Health Organization (WHO) catalogue of cardiomyopathies (Richardson et al., 1996). In 2006, the American Heart Association included LVNC to its list of genetic cardiomyopathies (Maron et al., 2006).

Although LVNC can manifest as depressed systolic function (Captur and Nihoyannopoulos, 2010), its clinical manifestation and the age of the affected individual at symptom onset are highly variable. Classical complications include systemic embolism, malignant arrhythmias, heart failure and sudden death (Oechslin et al., 2000). LVNC is the third most common cardiomyopathy after dilated and hypertrophic cardiomyopathy, and its prevalence ranges from 0.05% to 0.3% of the general population (Ritter et al., 1997, Oechslin et al., 2000,

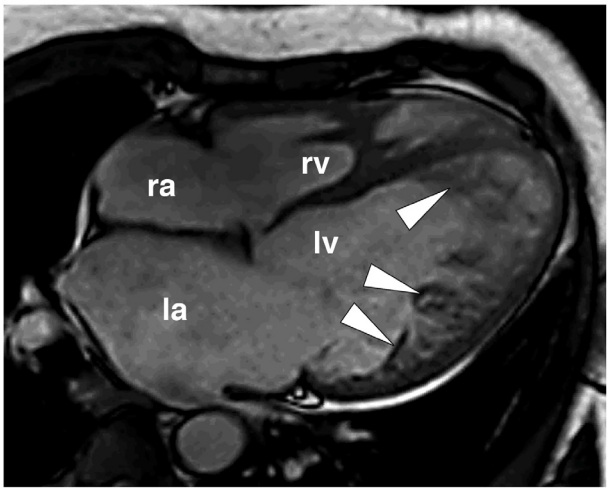

Figure 3. Example of LVNC heart CMRI.

Presence of persistent trabeculae in an adult LVNC heart (arrowheads) characteristic of the diseased hearts. rv, right ventricle; lv, left ventricle; ra, right atria; la, left atria. Image courtesy of Dr L. J. Jimenez-Borreguero.

Stollberger and Finsterer, 2004).

Previously, it has been described that LVNC is caused by mutations in genes encoding mainly structural proteins of the muscle fibres (Klaassen et al., 2008), cytoskeletal (Ichida et al., 2001), nuclear-membrane (Hermida-Prieto et al., 2004) and chaperone proteins (Shou et al., 1998). With the exception of infantile cases in which the disease is ligated to chromosome X (Bione et al., 1996), familial forms of LVNC are transmitted as an autosomal-dominant trait (Captur and Nihoyannopoulos, 2010). The underlying molecular mechanisms producing the structural abnormalities leading to LVNC are still unknown (Towbin, 2010, Finsterer, 2009).

The NOTCH signalling pathway

Notch is an evolutionary conserved signalling pathway that during embryonic development regulates cell-fate specification, differentiation and tissue patterning (Artavanis-Tsakonas et al., 1999). In the adult organism, Notch maintains tissue homeostasis via the regulation of a variety of cellular processes (Billiard et al., 2011, Kim and Shivdasani, 2011). In general, the cells in which the pathway is active maintain an undifferentiated state (Kimble and Crittenden, 2007). Notch functions between adjacent cells, it is a local signalling pathway whereby one cell expressing higher levels of ligand becomes the signalling cell and the neighbouring one becomes the receiving cell, although this is a generalization that cannot be made extensive to all Notch settings.

Notch takes its name from the *Drosophila* mutants that show notches in their wing edge (Mohr, 1919) and the gene was initially cloned in *Drosophila* in 1985 (Wharton et al., 1985). In mammals there are four Notch genes, *Notch1-Notch4*, which are expressed in different tissues and at different times during embryonic development and in the adult (Del Amo et al., 1992, Weinmaster et al., 1992, Lardelli et al., 1994, Uyttendaele et al., 1996) (Fig. 5). The

Notch genes encode a long transmembrane receptor that has two distinct domains, an extracellular domain (NECD) responsible for the interaction with the ligands and an intracellular domain (NICD) responsible for signal transduction.

The NECD contains tandem arrays of Epidermal Growth Factor (EGF)-like repeats (Artavanis-Tsakonas and Muskavitch, 2010). The number of EGF-like repeats varies by species and receptor subtype, ranging from 36 in *Drosophila* to as few as 11 in *C. elegans* (Artavanis-Tsakonas and Muskavitch, 2010). The EGF repeats are implicated in the interaction with the ligand (Fehon et al., 1990, Rebay et al., 1991), three Lin/Notch repeats and the heterodimerization domain, which is in contact with the NICD. The NICD is composed of the RAM23 domain and 6 ankyrin repetitions responsible for the interaction with RBPJK, the transcriptional effector of the pathway; two nuclear localization signals (NLS), a transcriptional activation domain only present in Notch1 and Notch2, and a terminal PEST domain, that negatively regulates the stability of the receptor (Rechsteiner, 1988, Kopan, 2002). The NECD and NICD are synthetized as a single polypeptide, which is directly cleaved after translation by a Furin-convertase in the Golgi. This first (S1) cleavage (Blaumueller et al., 1997, Logeat et al., 1998) is necessary to form the functional heterodimeric receptor that will be translocated to the membrane where the two domains are still associated by Ca^{2+}-dependent non-covalent bonds (Rand et al., 2000).

There are two families of ligands that are expressed in the signalling cell, Delta-like (Dll) and Jagged (Jag). In mammals there are three Delta-like genes, *Delta-like 1* (Bettenhausen et al., 1995), *Delta-like 3* (Dunwoodie et al., 1997) and *Delta-like 4* (Shutter et al., 2000), and two Jagged, *Jagged1* (Lindsell et al., 1995) and *Jagged2* (Shawber et al., 1996) (Fig. 5). The mammalian Notch ligands are homologues to *Delta* and *Serrate* from *Drosophila*. The ligands are type I transmembrane proteins and their extracellular domains are composed by a variable number of EGF-like domains responsible for the interaction with the receptor and the DSL (Delta, Serrate, Lin12) domain (Fig. 4, yellow) (Kopan, 2002). The EGF-like repetitions are continuous in the case of Delta while in Jagged they are interspersed by a short linker sequence. The Jagged ligands also have a cysteine-enriched domain (Kopan, 2002).

The glycosil transferase Fringe can modify the EGF-like domain in the NECD of the receptor by adding O-fucose glycans (Blair, 2000) (Fig. 5). This modification determines which ligand preferentially binds to the receptor. Delta ligands bind to the Fringe-modified receptors and, on the contrary, Jagged ligands bind to the not modified Notch receptors (Panin et al., 1997). Fringe introduces an additional level of regulation in the Notch pathway by selecting which ligand is able to activate Notch. There is evidence that the presence of Fringe shifts the activation balance towards Delta-like ligands at the expense of Jagged ligands when both molecules are expressed at the same time in the same tissue (Benedito et al., 2009, Golson et al., 2009).

Mind bomb

There are two families of E3 ubiquitin ligases that regulate the endocytosis of the Notch

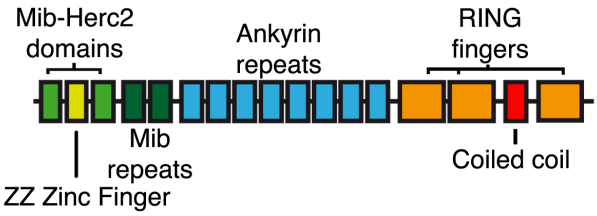

Figure 4. Structure of Mib1 protein.

Schematic representation of Mib1 domains. Two Mib-Herc2 domains (green) separated by one ZZ Zinc finger (olive green) followed by two Mib domains (dark green) responsible for the interaction with the ligand. Eight ankyrin repeats (blue) that fold the protein together and towards the C-terminus three RING fingers (orange) with a Coiled coil domain (red) in between them responsible for the enzymatic activity of the pathway. Modified from (Barsi et al., 2005)

ligands when bound to NECD, a prerequisite for Notch activation. These E3 ubiquitin ligases are Neuralized (Neurl) (Deblandre et al., 2001) and Mind bomb (Mib) (Itoh et al., 2003). Although there are two members of the Neurl family in mammals they are dispensable during embryonic development and mice with targeted mutations in either *Neurl* genes do not show any phenotypic alteration and are viable (Vollrath et al., 2001, Ruan et al., 2001, Koo et al., 2007). In the case of the Mib family, there are two members Mib1 (Itoh et al., 2003) and Mib2 (Koo et al., 2005b). Only *Mib1* is required for development (Koo et al., 2007) although *Mib2* is highly expressed in adult tissue (Koo et al., 2005b). Mib1 binds specifically to the two families of Notch ligands, Delta-like (Chen and Casey Corliss, 2004, Itoh et al., 2003) and Jagged (Hansson et al., 2010, Koo et al., 2007), and it is a point of regulation of the pathway in the signalling cell. The 110kDa protein encoded by the *Mib1* gene contains five domains, two Mib-Herc2 domains separated by one ZZ Zinc finger domain, followed by two Mib domains responsible for the interaction with the ligand, eight ankyrin repeats that fold the protein together, and towards the C-terminus and spaced by a coiled-coil domain, three RING fingers responsible for the enzymatic activity of the pathway (Barsi et al., 2005) (Fig. 4).

Mib1 is expressed ubiquitously throughout the developing embryo (Barsi et al., 2005). Various studies have shown the importance of Mib1 during development and that targeted inactivation of *Mib1* in mice produces Notch loss of function-like phenotypes (Koo et al., 2007). Thus, *MIb1* is required for vascular development and its inactivation leads to a Dll4-like phenotype, skin epithelial cells differentiation and cerebellum development, its inactivation producing a Jag1-like phenotype or in the ectordermal ridge where the deletion of *Mib1* produces a Jag2-like phenotype (Koo et al., 2007). *Mib1* is also required for development of the collecting tubes of the kidney (Jeong et al., 2009), pancreatic β-cell formation (Horn et al., 2012), T-cell development (Shah et al., 2012, Jeong et al., 2012), gastrointestinal secretory cell maturation (Capoccia et al., 2013) and in the control of neurogenesis and gliogenesis in the spinal cord (Kang et al., 2013).

The importance of Mib1 during development and the fact that the two families

of Notch ligands are its substrates, make this E3 ubiquitin ligase a powerful tool to study the role of Notch in development. Mib1 is ubiquitously expressed and thus is essential for Notch signalling activation as it regulates all the input from the Notch ligands so that *Mib1* deletion would allow us to explore the total loss of function of the Notch pathway. Thus, tissue-specific inactivation of *Mib1* will give us insights in the importance of the origin of Notch signalling and the particular role of the different ligands in the heart.

NOTCH activation

Upon interaction of ligand and receptor, Mib1 targets by ubiquitylation the ligand to endocytosis (Itoh et al., 2003). The ligands are endocytosed, mechanically pulling NECD producing a conformational change that liberates the S2 cleavage site (Parks et al., 2000) (Fig. 5). The liberation of the S2 site allows a metalloprotease of the ADAM family to cleave the NECD (Hartmann et al., 2002) that is finally endocytosed into the signalling cell together with the ligand. Immediately after, γ-secretase/Presenilin cleaves the receptor in the S3 site, liberating the NICD in the cytoplasm of the receiving cell (Okochi et al., 2002) (Fig. 5). Due the NLS, the NICD translocates to the nucleus where it binds to the transcription factor CSL or RBPJK via by the RAM23 domain (Tamura et al., 1995).

In the absence of Notch signalling activation, RBPJK is bound to transcriptional repressors as Mint (Tanigaki and Honjo, 2007) or SMRT (Silencing mediator of retinoic and thyroid hormone receptors) (Mumm and Kopan, 2000) that inhibit gene expression. Upon the interaction of NICD with RBPJK the transcriptional repressors are released and transcriptional activators such as Master mind (Maml) (Wu et al., 2000) are recruited, forming a protein complex that activates the expression of the target genes of the pathway (Fig. 5).

The most studied target genes of the pathway in cardiac development are the basic-helix-loop-helix (bHLH) repressor transcription factors of the Hes (Hairy and enhancer of split) and Hey (HESR) (Hairy and enhancer of split repressor) (Kokubo et al., 1999, Iso et al., 2001, Iso et al., 2003) (Fig. 5). The spectrum of immediate targets is large and include those encoding the oncogene c-myc, another bHLH protein that enhances cellular growth in leukaemia (Palomero et al., 2006, Weng et al., 2006), the cell cycle regulator p21 (Devgan et al., 2005, Rangarajan et al., 2001) or the repressor transcription factor Snail1 (Timmerman et al., 2004, Sahlgren et al., 2008) required for EMT and valvular development (Fig. 5). The Notch negative regulator NRARP (Notch regulated ankyrin repeat protein) (Krebs et al., 2001, Lamar et al., 2001) is also a direct target gene of the pathway (Fig. 5).

NOTCH and cardiac development

Notch is implicated in several processes during the development of the heart (Rones et al., 2000, Nemir et al., 2006, High and Epstein, 2008, de la Pompa and Epstein, 2012).

In the mid-gestation mouse embryo, Notch1 is active (implying that N1ICD can be detected) throughout the endocardium of the AVC and OFT, where the valves will form (Del Monte et al., 2007). During valve primordium formation,

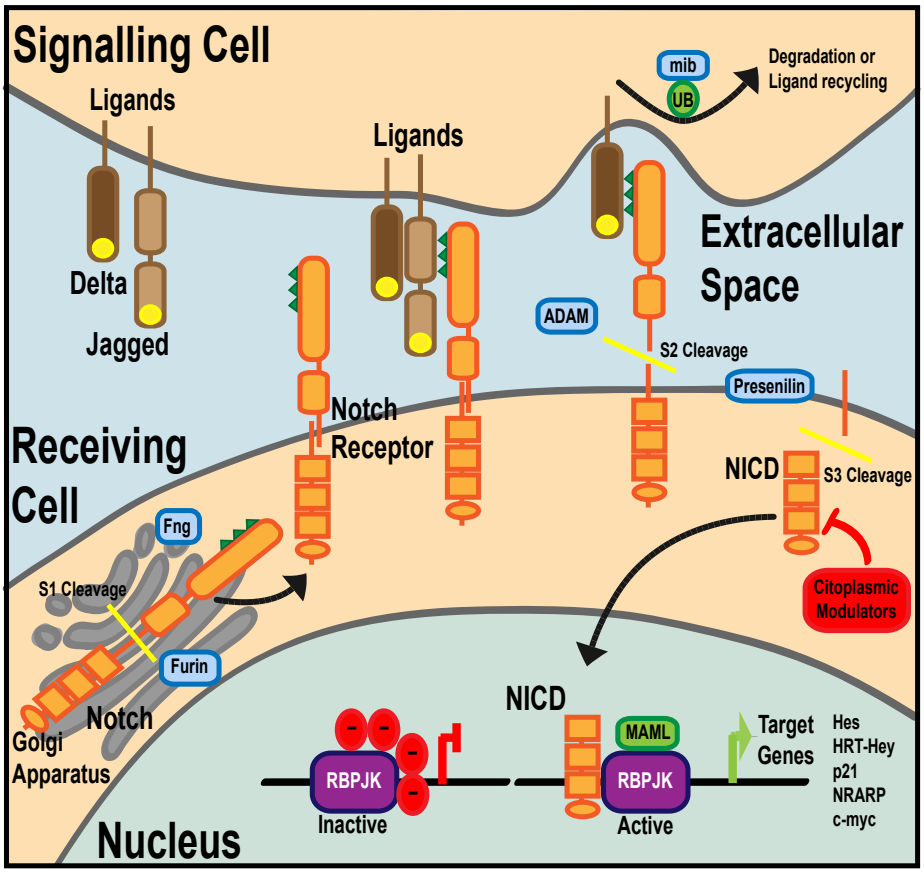

Figure 5. Notch signalling pathway.

The Notch ligands Delta and Jagged are expressed in the membrane of the signalling cell and are characterized by the DSL motif (yellow) located in the extracellular domain. Notch receptors are processed in the Golgi apparatus, S1-cleavaged by Furin, and sugar-modified by Fringe to form the functional heterodimer that is located in the membrane of the receiving cell. Upon ligand-receptor interaction two cleavage events, S2 by an ADAM protease and S3 by γ-secretase/Presenilin, liberate N1ICD in the cytoplasm of the receiving cell. NICD translocates to the nucleus and together with MAML, forms an transcriptional activation complex with RBPJK that activates the transcription of the target genes of the pathway including Hes, Hey, p21 etc.

Notch activates the expression of *Snail1* that represses Vascular Endothelial Cadherin (*VE-C* or *Cdh5*), allowing endocardial cells in the AVC and OFT to undergo EMT and invade the cardiac jelly in between endocardium and myocardium to form the endocardial cushions, the valve primordia (Timmerman et al., 2004). Hey1 and Hey2 restrict *Bmp2* expression to the AVC and OFT restricting valve formation to non-chamber territorires (Rutenberg et al., 2006, Kokubo et al., 2004). Although Notch is not responsible for the expression of *Hey* genes in the myocardium (Timmerman et al., 2004) the overexpression of the N1ICD in the myocardium is accompanied by ectopic expression of *Hey1*, disrupting AVC development (Watanabe et al., 2006, Luna-Zurita et al., 2010). The double mutant *Hey1;Hey2* is not able to produce endocardial cushions and EMT is totally blocked (Kokubo et al., 2005).

At E9.5, Notch1 is expressed throughout

the endocardium of the developing ventricles, but it is only active at the base of the trabeculae (Del Monte et al., 2007), where it signals to the myocardium to induce its proliferation and differentiation and form the trabeculae (Grego-Bessa et al., 2007). Analysis of standard and endothelial-specific *Notch1* and *RBPJk* mutants shows that trabeculation is severely impaired and only primitive, poorly organized trabeculae can be observed in these mutants (Grego-Bessa et al., 2007). Molecular analysis indicates that during trabeculation Notch modulates three different signals: EphrinB2 (Adams et al., 1999), expressed in the endocardium is a direct Notch target (Grego-Bessa et al., 2007). Nrg1 (Hertig et al., 1999) also expressed in the endocardium, is an indirect Notch target and its expression depends both of Notch and EphrinB2 (Grego-Bessa et al., 2007). Nrg1 induces the formation of the ventricular conduction system, a feature of ventricular maturation (Rentschler et al., 2002). A third signalling pathway is Bmp10 (Chen et al., 2004), expressed in trabecular myocardium and whose expression is severely down-regulated in Notch pathway mutants, suggesting that Notch is required to produce a signal that activates Bmp10 in the myocardium (Grego-Bessa et al., 2007).

Notch is also active in the proepicardium and later in the epicardium during the formation of epicardial derivatives. Epicardial Notch modulates cell differentiation in the proepicardium organ and later it is required for the arterial commitment and coronary vessel formation that will sustain myocardial growth during ventricular maturation (del Monte et al., 2011, Grieskamp et al., 2011).

INTRODUCCIÓN

En este trabajo hemos estudiado el papel de la vía de señalización Notch en el desarrollo del corazón, prestando especial atención a dos estructuras por su relación con CHD, las válvulas del tracto de salida (OFT) y los ventrículos, que son esenciales para función cardíaca. Las válvulas permiten que el flujo sanguíneo avance de manera unidireccional por el corazón y evitan el reflujo. Los ventrículos son la pared muscular, que en caso del ventrículo izquierdo se encarga de bombear sangre oxigenada por el resto del cuerpo a través de la válvula aortica. Errores durante los procesos de desarrollo de las válvulas o los ventrículos causan CHD, que compromete la vida de los recién nacidos y pueden causar su muerte si no son tratadas a tiempo.

Desarrollo del corazón

El desarrollo cardíaco comienza en el día de desarrollo embrionario 7.0 en ratón (E7), cuando los precursores cardiacos migran bilateralmente hacia delante al interior del mesodermo lateral, donde forman la media luna cardiaca (Harvey, 2002). A E8.0, la fusión de las capas mesodérmicas de ambos lados, produce un tubo linear que todavía no está compartimentalizado. Los dos tejidos principales del corazón, el endocardio en el interior y el miocardio en el exterior, ya están presentes en el tubo cardiaco. Las células que forman el tubo cardiaco original provienen del campo cardiaco primario (FHF), el cuál dará lugar a parte de las aurículas, el ventrículo izquierdo y el canal atrio ventricular (AVC) (Buckingham et al., 2005) (Fig. 1 A, B).

A día E9.0, comienza el proceso de torsión cardíaca durante el cual el tubo cardíaco gira hacia la derecha, de manera que las futuras aurículas se sitúan en una posición posterior al ventrículo común. Simultáneamente, el tubo se expande por la adición del células del campo cardiaco secundario (SHF) (Kelly and Buckingham, 2002). En el polo arterial del corazón, el SHF contribuye al OFT, al ventrículo derecho y a parte del septo interventricular (Zaffran et al., 2004); por otro lado, en el polo venoso del corazón el SHF contribuye a parte de las aurículas y al septo arterial (Snarr et al., 2008) (Fig.1 A, B).

Inmediatamente después pueden distinguirse dos territorios en los que se desarrollarán las válvulas cardíacas y los ventrículos (Moorman and Christoffels, 2003, Moorman et al., 2007, Aanhaanen et al., 2011) (Fig. 1 B). Los territorios donde se formarán las válvulas del corazón son el AVC y el OFT. Inicialmente, a E9.5 en el AVC y E10.5 en el OFT, las células del endocardio sufren un proceso de transición epitelio-mesénquima (EMT) e invaden la gelatina cardiaca que separa el endocardio y el miocardio. En el endocardio, Notch juega un papel crucial en la activación de la EMT mediante la activación directa de los factores de transcripción *Snail1* (Timmerman et al., 2004, Luna-Zurita et al., 2010) y *Snail2* (Niessen et al., 2008) que reprimen la cadherina del endotelio vascular (*VE-C* o *Cdh5*), permitiendo que las células del endocardio se despeguen unas de otras, adquieran un fenotipo mesenquimal e invadan la gelatina cardiaca. Una compleja red de señalización que integra diferentes vías de señalización como Bmp, Tgf-β y Notch regula la EMT (Luna-Zurita et al., 2010, de la Pompa and Epstein, 2012). En el AVC se forman cuatro colchones endocárdicos, al igual que en el OFT. Posteriormente, tienen lugar los

procesos de morfogénesis y maduración valvular.

Igualmente a E9.5, comienza la trabeculación ventricular. Las trabéculas son crestas de cardiomiocitos que crecen hacía la luz del ventrículo (Ben-Shachar et al., 1985). Las trabéculas son las primeras estructuras que se diferencian en los ventrículos (Sedmera et al., 1997). Incrementan la superficie ventricular y permiten que el miocardio se desarrolle en ausencia de los vasos coronarios que se formarán más adelante. A pesar de que las trabéculas comienzan a desarrollarse primero en el ventrículo izquierdo y después en el derecho, no hay diferencias estructurales entre ambos. Una vez que se forman las trabéculas, no tienen el limite superior libre sino que se unen, de manera que el interior del ventrículo parece una esponja (Sedmera et al., 2000) (Fig. 1 B). La vía de señalización Notch es crucial para la formación de las trabéculas y las maduración de los ventrículos (Grego-Bessa et al., 2007).

A E10.5, en los ventriculos puede distinguirse la zona compacta, situada hacia la parte exterior y que contiene cardiomiocitos inmaduros con una elevada proliferación, e internamente, la zona trabecular ocupada por las trabéculas que contiene cardiomiocitos en diferenciación con una baja proliferación (Sedmera et al., 2000). Estos cardiomiocitos se diferenciarán tanto en cardiomiocitos contráctiles como en células del sistema de conducción (Sedmera et al., 2000).

A E13.5-E14.5, se completa la septación interventricular y la pared del ventrículo se compacta y las trabéculas pasan a formar parte de la pared ventricular (Fig. 1 B). Igualmente, después de la septación del AVC y OFT (Fig. 1 B), los colchones del endocardio se fusionan primero y se transforman después en las valvas maduras de las válvulas. Los mecanismos moleculares que regulan estos procesos no se conocen bien. Uno de los objetivos de esta tesis doctoral ha sido el de contribuir a entender estos procesos del desarrollo cardíaco (Fig. 1 C).

Morfogénesis y maduración valvular

Los eventos morfogenéticos que transforman los colchones del endocardio en válvulas cardiacas maduras están relacionados con la septación del corazón y con la separación de los circuitos pulmonar y sistémico. La correcta maduración de los colchones es crucial para la función cardíaca y las consecuencias de los defectos en estos procesos puede manifestarse más tarde en forma de enfermedades congénitas del corazón (CHD) (Srivastava, 2006).

La EMT resulta en la formación de cuatro colchones del endocardio en el AVC y cuatro en el OFT, en ambos casos dos principales y dos laterales (Wessels and Sedmera, 2003) (Fig. 1 B). Los colchones principales del AVC se fusionan y forman una masa de mesénquima que ocupa el lumen del AVC y es necesario para la septación ventricular que va a dividir los flujos pulmonar y sistémico. Los colchones laterales no se fusionan y no forman parte del complejo atrio-ventricular (AV), directamente darán lugar a las valva mural de la válvula mitral. (Snarr et al., 2008). Algo similar ocurre en el OFT, donde los colchones principales se fusionan para formar el septo aórtico-pulmonar (AP) y los colchones laterales no se fusionan y sólo forman parte de las valvas

definitivas.

Los colchones del endocardio no sólo están formados por células que derivan de la EMT, otros linajes celulares invaden los colchones y contribuyen a la maduración de las válvulas. A E11.5, el mesénquima del OFT ha sido invadido por células mesenquimáticas que migran rostro-caudalmente desde la cresta neural formando dos olas a ambos lados del futuro septo AP (de Lange et al., 2004). Aunque la participación de las células de la cresta neural en el desarrollo de las válvulas es pequeña, estas células están presentes en las valvas maduras (Jiang et al., 2000). Sin embargo, la interacción entre ambas poblaciones de células en los colchones endocárdicos es esencial para la maduración de las válvulas. Las células derivadas de la cresta neural inducen muerte celular en el mesénquima del colchón, necesaria para la remodelación de las valvas (Jain et al., 2011, de la Pompa and Epstein, 2012). Estas células no participan en el desarrollo de las válvulas (Wessels et al., 2012). A E12.0, células derivadas del epicardio migran a través de la unión AV en los colchones endocárdicos del AVC. Estas células participarán sobre todo en los colchones laterales, donde durante el desarrollo terminarán poblando finalmente la mayoría de la valva, mientras que sólo algunas células formarán parte de las valvas de la válvula madura (Wessels et al., 2012). Después de la invasión de las células derivadas de la cresta neural y del epicardio la expansión de los colchones por medio de proliferación celular está regulada por diferentes señales como Bmp (Eisenberg and Markwald, 1995), Wnt (Alfieri et al., 2010) o Egf (Iwamoto et al., 2003). Dos moléculas de la vía de Bmp, Bmp6 y Bmp7, se expresan en el OFT y son necesarias para la formación de los colchones del endocardio en esta estructura. El doble mutante *Bmp6*;*Bmp7* muestra un marcado retraso en el desarrollo de los colchones endocárdicos en el OFT (Kim et al., 2001).

Las últimas fases del desarrollo de las válvulas está caracterizada por la diferenciación y morfogénesis del mesénquima valvular (Fig. 2). Este proceso aún poco conocido, resulta en una estructura altamente organizada y estratificada guiada por la matriz extracelular (de Vlaming et al., 2012). La elongación de las valvas ocurre entre E15.5 y E18.5 mediante un incremento de la densidad celular y reorganización de la matriz extracelular (Kruithof et al., 2007). Periostina, que se une a las fibras de colágeno modula el diámetro de éstas y su interacción mediante *cross-linking,* lo que promueve la fibrilogénesis (Norris et al., 2009). La reorganización de la matriz está regulada por Periostina y la acción coordinada de metaloproteasas de Zinc como ADAMTS1 que proteolizan Versican, esto facilita un denso empaquetamiento del mesénquima (Kern et al., 2006). Esto promueve la diferenciación de las células que derivan del endocardio, epicardio y cresta neural que darán lugar a las válvulas maduras.

Las valvas del AVC están unidas a la base de la pared ventricular por cuerdas tendinosas parecidas a tendones a través de los músculos papilares (Guy and Hill, 2012), esto constituye el aparato de soporte de las válvulas. El aparato de soporte se forma por la unión de varias trabéculas en el ventrículo (Sedmera et al., 2000). Sin embargo, las válvulas del OFT se mantienen sin soporte externo y se unen a la pared de la arteria (Fig. 2 A).

Finalmente, en las válvulas maduras la matriz extracelular está alineada con el flujo sanguíneo, lo que sugiere un papel de las fuerzas hemodinámicas durante la maduración de las válvulas (Combs and Yutzey, 2009). En este aspecto, es interesante resaltar que la expresión en el endocardio del receptor Notch1 se restringe al lado de las válvulas que se encuentra bajo el flujo sanguíneo (Del Monte et al., 2007), lo que sugiere una reacción al flujo sanguíneo por parte del endotelio valvular que resultaría en la activación mecánica de Notch (Combs and Yutzey, 2009) (Fig. 2).

La falta de remodelación de los colchones endocárdicos que da lugar a válvulas dismórficas es una característica de algunas CHD como la tetralogía de Fallot en la cuál la válvula pulmonar dismórfica está acompañada por el cabalgamiento de la aorta (Greenway et al., 2009, Jain et al., 2011).

Maduración trabecular y compactación ventricular

Después de completarse la septación ventricular a E14.5, la continuación del crecimiento y maduración de los ventrículos requiere una completa remodelación y reorganización de las trabéculas que se orientan de manera apico-basal, lo que determinará la forma de los ventrículos. Las trabéculas se compactan, lo que cambia la relación entre miocardio compacto y miocardio trabecular en el ventrículo. Algunas de estas trabéculas se unirán para formar los músculos papilares de las válvulas AV (Sedmera et al., 2000).

La compactación de las trabéculas está acompañada por la invasión dependiente de hipoxia del miocardio compacto por parte de la vasculatura coronaria que provienen del epicardio (Tao et al., 2013). Simultáneamente a la compactación trabecular, los recesos intertrabeculares pasan a formar parte del emergente plexo coronario. Esto es seguido por una reorganización de las fibras musculares que se organizan en una espiral de tres capas alrededor del corazón. Esta espiral refleja el patrón de contracción del corazón (Sedmera et al., 2000).

Las cardiomiocitos de las trabéculas no proliferan y el crecimiento del órgano lo mantiene la proliferación de los cardiomiocitos de la zona compacta del miocardio compacto. De esta manera cambia la relación del grosor entre el miocardio trabecular y el compacto, y este último se transforma en el más prominente en el corazón, mientras que las trabéculas en el lumen del ventrículo terminarán por desaparecer. Este proceso y los mecanismos moleculares subyacentes, son muy poco conocidos.

Miocardiomiopatía no compactada del ventrículo izquierdo (LVNC)

LVNC es una miocardiopatía de cuya etiología se sabe muy poco y que está caracterizada por unas trabéculas prominentes y excesivamente grandes en la pared del ventrículo izquierdo (Jenni et al., 2007) (Fig. 3). Se ha sugerido que al menos en algunos casos, esta enfermedad se produce por un bloqueo intrauterino de la morfogénesis del miocardio que lleva a la presencia de trabéculas (Ritter et al., 1997).

La primera vez que se diagnosticó la LVNC fue en 1984 en una mujer de 33 años de

edad mediante ecocardiografía (Engberding and Bender, 1984). Desde este primer caso, la heterogeneidad de los síntomas de la enfermedad puede haber hecho que muchos casos de LVNC no hayan sido diagnosticados (Jenni et al., 2007) y como consecuencia atribuirse a esta miocardiopatía una menor prevalencia de la que realmente tiene. El desarrollo de las herramientas diagnósticas (la incorporación de la RMN), han permitido un mejor y más preciso diagnostico, de manera que 10 años después del primer diagnóstico, la LVNC se incluyó en la clasificación de miocardiopatía de la Organización Mundial de la Salud (WHO) como miocardiopatía "sin clasificar" (Richardson et al., 1996). En 2006 la Asociación Americana del Corazón incluyó la LVNC en la lista de miocardiopatías de origen genético (Maron et al., 2006).

La LVNC se puede manifestar como una reducción de la función sistólica (Captur and Nihoyannopoulos, 2010), sin embargo su manifestación clínica y la edad con la que debutan los pacientes afectados es altamente variable. Las complicaciones clásicas que se observan en los pacientes de LVNC pueden ser embolias, arritmias, fallo cardiaco e incluso muerte súbita (Oechslin et al., 2000). La LVNC es la tercera miocardiopatía más común detrás de la miocardiopatía dilatada e hipertrófica y su prevalencia va desde 0.05% a 0.3% de la población general (Ritter et al., 1997, Oechslin et al., 2000, Finsterer, 2009).

Las mutaciones que se han asociado a la LVNC se han relacionado con genes que codifican proteínas estructurales de las fibras musculares; proteínas del sarcómero (Klaassen et al., 2008), citoesqueléticas (Ichida et al., 2001), de membrana nuclear (Hermida-Prieto et al., 2004) y chaperonas (Shou et al., 1998). Con la excepción de los casos pediátricos, en cuyo caso la enfermedad está ligada al cromosoma X (Bione et al., 1996), los casos familiares de LVNC son heredados de manera autosómica dominante. A pesar de la utilidad diagnóstica de estos estudios genéticos, los mecanismos moleculares cuya alteración da lugar a la LVNC son aún desconocidos.

La vía de señalización Notch

Notch es una vía de señalización conservada evolutivamente que está implicada en múltiples procesos durante el desarrollo, ya que regula la especificación de los destinos celulares, la diferenciación celular y la formación de patrón tisular (Artavanis-Tsakonas et al., 1999). En el organismo adulto Notch mantiene la homeostasis tisular (Billiard et al., 2011, Kim and Shivdasani, 2011). Las células en las cuales la vía está activa tienden a mantener un estado más indiferenciado (Kimble and Crittenden, 2007). Notch es una vía de señalización local, ya que implica a células que están en contacto. Aunque el patrón de expresión de los ligandos es muy complejo, podemos decir que la activación de la vía ocurre cuando una célula que expresa altos niveles de ligando (célula señalizadora) interactúa con una célula vecina que expresa el receptor Notch (célula receptora).

Notch recibe su nombre de los mutantes de *Drosophila* que presentan unas muescas (Notch en inglés) en el borde del ala (Mohr, 1919). El gen *Notch* fue inicialmente clonado en *Drosophila* en 1985 (Wharton et al., 1985). En mamíferos hay cuatro receptores Notch, *Notch1-Notch4*, que se expresan

en diferentes tejidos en diferentes estadios durante el desarrollo y más tarde en la vida adulta (Del Amo et al., 1992, Weinmaster et al., 1992, Lardelli et al., 1994, Uyttendaele et al., 1996) (Fig. 5). Los genes *Notch* codifican un gran receptor transmembrana que tiene dos dominios diferenciados, uno extracelular (NECD), responsable de la interacción con los ligandos y otro intracelular (NICD), responsable de la transducción de la señal.

El NECD contiene varias repeticiones del dominio Epidermal Growth Factor (EGF) (Artavanis-Tsakonas and Muskavitch, 2010) implicados en la interacción con los ligandos (Fehon et al., 1990) (Rebay et al., 1991). El número de repeticiones del dominio EGF-likevaría entre especies y receptor, va desde 36 en *Drosophila* hasta sólo 11 en *C. elegans* (Artavanis-Tsakonas and Muskavitch, 2010). Tres repeticiones del dominio Lin/ Notch y un dominio de heterodimerización con el que se mantiene unido con el NICD. El NICD se compone del dominio RAM23 y seis repeticiones de Ankyrina responsables de la interacción con RBPJK, el efector transcripcional de la vía; dos señales de localización nuclear (NLS), un dominio de activación transcripcional que sólo está presente en Notch1 y Notch2, y un dominio terminal PEST que regula negativamente la estabilidad del receptor (Rechsteiner, 1988, Kopan, 2002). El NECD y el NICD son sintetizados como un único polipéptido que después de la traducción, se procesa proteolíticamente en el Golgi por una Furin-convertasa. Este corte S1 (Blaumueller et al., 1997, Logeat et al., 1998) es necesario para formar el receptor heterodimérico que se transloca a la membrana donde los dos dominios NICD y NECD están asociados mediante enlaces no covalentes de Ca^{2+} (Rand et al., 2000).

Hay dos familias de ligandos que se expresan en la célula señalizadora, Delta-like (Dll) y Jagged (Jag). En mamíferos hay tres genes Delta, *Delta-like 1* (Bettenhausen et al., 1995), *Delta-like 3* (Dunwoodie et al., 1997) y *Delta-like 4* (Shutter et al., 2000), y dos Jagged, *Jagged1* (Lindsell et al., 1995) y *Jagged2* (Shawber et al., 1996) (Fig. 5). Estos ligandos de mamíferos son homólogos de *Delta* y *Serrate* de *Drosophila*. Los ligandos son proteínas transmembrana de tipo I cuyo dominio extracelular se compone de una repetición de dominios EGF responsables de la interacción con el receptor y el dominio DSL (Delta, Serrate, Lin12) (Fig. 5 amarillo). Los dominios EGF son continuos en el caso de Delta, mientras que en los ligandos de la familia Jagged, están separados por una pequeña secuencia espaciadora. Los ligandos Jagged además tienen un dominio rico en cisteínas (Kopan, 2002).

La glicosil-transferasa Fringe puede modificar los dominios repetidos de EGF en los receptores Notch añadiendo O-fucosa glicanos (Blair, 2000) (Fig. 5). Esta modificación de los azúcares en los dominios EGF de Notch determina con que ligando interactúa de manera preferente. Por ejemplo, los ligandos Delta se unen preferencialmente con receptores modificados por Fringe en detrimento de Jagged. En caso de que el receptor no esté modificado no hay diferencia entre la unión de uno u otro ligando (Panin et al., 1997). De esta manera, Fringe añade un nuevo nivel de regulación a la activación de Notch, regulando que ligando es capaz de activar la señalización por Notch. Esta función

es muy importante, ya que existen evidencias de que la presencia de Fringe cambia el equilibrio entre Jagged y Delta cuando se expresan en el mismo tejido (Benedito et al., 2009, Golson et al., 2009).

Mind bomb

Existen dos familias de E3 ubiquitina ligasas que regulan la endocitosis de los ligandos una vez que se ha unido al NECD, un requisito esencial para la activación de Notch. Estas ubiquitina ligasas son Neuralized (Neurl) (Deblandre et al., 2001) y Mind bomb (Mib) (Itoh et al., 2003). Aunque existen dos miembros de la familia *Neurl* en mamíferos (*Neurl1* y *Neurl2*), ambos genes son dispensables para el desarrollo embrionario, ya que ratones doble mutantes para estos genes no muestran alteraciones del desarrollo y son viables (Vollrath et al., 2001, Ruan et al., 2001, Koo et al., 2007). En el caso de los dos miembros de la familia *Mib*, *Mib1* (Itoh et al., 2003) y *Mib2* (Koo et al., 2005b), sólo *Mib1* es necesario para el desarrollo, aunque es importante resaltar que *Mib2* se expresa fuertemente en tejido adulto (Koo et al., 2005b). Mib1 interactúa de manera específica con los ligandos de ambas familias de Notch, Delta-like (Chen and Casey Corliss, 2004, Itoh et al., 2003) y Jagged (Hansson et al., 2010, Koo et al., 2007), lo que es un punto de regulación de la activación de la vía en la célula señalizadora. La proteína de 110KDa codificada por *Mib1* contienen cinco dominios, dos dominios Mib-Herc2 separados por un ZZ *Zinc finger*, seguidos por dos dominios Mib que son responsables de la interacción con los ligandos, ocho repeticiones de ankirina que doblan la proteína sobre si misma y en el extremo C-terminal, tres RING *fingers* separados por un dominio en espiral, responsables de la actividad enzimática de la proteína (Barsi et al., 2005) (Fig. 4).

Mib1 se expresa de manera ubicua durante el desarrollo embrionario murino (Barsi et al., 2005). Diferentes estudios que muestran su importancia durante varios procesos del desarrollo y la inactivación de *Mib1* mediante *gene targeting* produce fenotipos similares a la pérdida de función de Notch. Mib1 se requiere para el desarrollo de la vasculatura donde su inactivación produce un fenotipo similar a la perdida de función de Dll4, para el desarrollo de las células epiteliales de la piel y las crestas de ectodermo del cerebelo donde produce un fenotipo similar a la inactivación de *Jag2* (Koo et al., 2007). Mib1 también se requiere para el desarrollo de los tubos colectores renales (Jeong et al., 2009), la formación de células β pancreáticas (Horn et al., 2012), el desarrollo de las células T (Shah et al., 2012, Jeong et al., 2012), la maduración de las células secretoras en el sistema gastrointestinal (Capoccia et al., 2013) y en el control de la neurogénesis y gliogénesis en la médula espinal (Kang et al., 2013).

La importancia de Mib1 durante el desarrollo embrionario y el hecho de que ambas familias de ligandos de Notch son sus substratos, hacen de esta E3 ubiquitina ligasa una poderosa herramienta para estudiar la función de la vía de señalización Notch durante el desarrollo. Mib1 es uno de los primeros miembros de toda la vía de señalización en actuar, se expresa de manera ubicua y regula la señalización proveniente de todos los ligandos, de manera que su inactivación nos permite estudiar la pérdida total de la vía de Notch. La inactivación especifica de tejido de

Mib1 durante el desarrollo permitirá distinguir diferentes efectos en la señalización por Notch dependiendo del origen de la señal y las diferentes funciones de cada ligando.

Activación de la vía de NOTCH

La interacción ligando-receptor permite que Mib ubiquitinice el dominio intracelular del ligando, lo que promueve su internalización y endocitosis (Itoh et al., 2003). La endocitosis del ligando arrastra el NECD de Notch, produciendo un cambio conformacional que libera el sitio de corte S2 (Parks et al., 2000) (Fig. 5). La liberación del sitio S2 permite a una metaloproteasa de la familia ADAM cortar el NECD (Hartmann et al., 2002), el cuál es finalmente endocitado junto al ligando en la célula señalizadora. Inmediatamente después, una actividad γ-secretase corta el receptor por el sitio S3, liberando el NICD en el citoplasma de la célula receptora (Okochi et al., 2002) (Fig. 5). Las NLS de NICD favorecen su translocación al núcleo, donde a través del dominio RAM23 se une a factor de transcripción CSL o RBPJK (Tamura et al., 1995).

En ausencia de activación de la vía de Notch, RBPJK está unido a represores transcripcionales como Mint (Tanigaki and Honjo, 2007) o SMRT (Silencing mediator of retinoic and thyroid hormone receptors) (Mumm and Kopan, 2000) inhibiendo la expresión génica. La interacción de RBPJK con el NICD de Notch hace que estos represores sean liberados y activadores transcripcionales como master mind (Maml) (Wu et al., 2000) son reclutados para formar un complejo activador que inicia la expresión de los genes diana de la vía (Fig. 5).

Los genes diana de la vía más estudiados en el contexto del desarrollo cardiovascular son los factores de transcripción basic-helix-loop-helix (bHLH) de las familias Hes (hairy and enhancer of split) y Hey/Hesr/HRT/HERP/HESR (Hes-related repressor protein) (Kokubo et al., 1999, Iso et al., 2001, Iso et al., 2003) (Fig. 5). El espectro de genes diana directos de la vía es muy amplio y varios genes pueden activarse en paralelo a la vía incluyendo el oncogén c-myc, otra proteína bHLH que promueve el crecimiento celular en leucemia (Palomero et al., 2006, Weng et al., 2006), el regulador del ciclo celular p21 (Devgan et al., 2005, Rangarajan et al., 2001) o el factor de transcripción represor Snail1 que se requiere para la EMT y el desarrollo valvular (Timmerman et al., 2004, Sahlgren et al., 2008) (Fig. 5). El regulador negativo de la vía NRARP (Notch regulated ankyrin repeat protein) (Krebs et al., 2001, Lamar et al., 2001) es también una diana directa de Notch (Fig. 5).

NOTCH y el desarrollo cardiaco

Notch está implicada en diversos procesos durante el desarrollo del corazón (High and Epstein, 2008, Rones et al., 2000, Nemir et al., 2006, de la Pompa and Epstein, 2012).

En el embrión de ratón a mitad de gestación, Notch1 está activo en todo el endocardio del AVC y del OFT donde se formarán las válvulas (Del Monte et al., 2007). Durante la formación de los primordios valvulares, Notch activa la expresión de Snail1 que reprime la cadherina del endotelio vascular (*VE-C* o *Cdh5*) permitiendo que las células del endocardio en el AVC y el OFT realicen EMT e invadan la gelatina cardiaca

entre el endocardio y el miocardio para formar los primordios valvulares (Timmerman et al., 2004). Hey1 y Hey2 restringen la expresión de Bmp2 exclusivamente al miocardio del AVC, de manera que las válvulas sólo se formen en este área (Rutenberg et al., 2006, Kokubo et al., 2004). Aunque Notch no regula la expresión de los genes *Hey* en el miocardio (Timmerman et al., 2004), la sobreexpresión del N1ICD en el miocardio produce la expresión ectópica de los genes *Hey* y bloquea la formación del AVC (Watanabe et al., 2006, Luna-Zurita et al., 2010). El doble mutante *Hey1;Hey2* no produce colchones del endocardio y la EMT está totalmente inhibida (Kokubo et al., 2005).

Aunque esté expresado por todo el endocardio en los ventrículos durante el desarrollo, Notch1 sólo está activo en las base de las trabéculas a E9.5 (Del Monte et al., 2007). Desde la base de las trabéculas Notch señaliza hacia el miocardio para inducir su diferenciación y proliferación que dará lugar a las trabéculas (Grego-Bessa et al., 2007). El análisis de los mutantes estándar y específicos del endocardio de *Notch1* y *RBPJk* revela que en estos ratones la trabeculación está severamente afectada, solamente algunas trabéculas menores y pobremente organizadas pueden observarse (Grego-Bessa et al., 2007). El análisis molecular revela que durante la trabeculación Notch modula tres señales diferentes: EphrinB2 (Adams et al., 1999), que se expresa en el endocardio es una diana directa de Notch (Grego-Bessa et al., 2007), Nrg1 (Hertig et al., 1999) expresado en el endocardio es una diana indirecta de Notch pero su expresión depende tanto de Notch como de EphrinB2 (Grego-Bessa et al., 2007). Nrg1 induce la formación del sistema de conducción cardiaca, necesario para la maduración ventricular (Rentschler et al., 2002). La tercera vía de señalización es Bmp10 (Chen et al., 2004), expresado en el miocardio trabecular y cuya expresión se ve severamente reducida en los mutantes de Notch, sugiriendo que Notch es necesario para producir la señal que active Bmp10 en el miocardio (Grego-Bessa et al., 2007).

Notch está activo en el proepicardio y más tarde en el epicardio durante la formación de las células derivadas del epicardio. Notch modula la diferenciación celular en el proepicardio y posteriormente se requiere para la determinación arterial durante el desarrollo de la vasculatura coronaria que mantendrá el crecimiento del miocardio durante el desarrollo ventricular (del Monte et al., 2011, Grieskamp et al., 2011).

OBJECTIVES

The observations that *Mind bomb 1* is expressed ubiquitously in the developing embryo (Barsi et al., 2005), that it is necessary for the correct development of the mammalian embryo (Koo et al., 2007), that its substrates are all the Notch ligands (Koo et al., 2005a) and that more than one ligand may be expressed in a given cardiac tissue (ie: myocardium, epicardium) makes the mouse with a conditional mutation in this E3 ubiquitin ligase a perfect tool to study the role of the Notch ligands in heart development. Notch has been demonstrated to regulate the development of the valves (Timmerman et al., 2004, Kokubo et al., 2004, Luna-Zurita et al., 2010) and the cardiac chambers (Grego-Bessa et al., 2007). One obvious implication of these developmental studies is that alterations of NOTCH signalling in human cardiac development may lead to CHD.

In this study we have generated cardio-specific mouse loss-of-function models of *Mib1*, in order to evaluate the effect of the abrogation of all the input of the ligands expressed in a given cardiac tissue.

Specific aims:

Study the phenotypic consequences of Notch ligands signalling abrogation in the heart:

Mib1 in the endocardium: *Mib1^{flox};Tie2-Cre*.

Mib1 in the myocardium: *Mib1^{flox};cTnT-Cre*.

Mib1 in endocardium and myocardium: *Mib1^{flox};Nkx2.5-Cre*.

Thus, we will study the consequences of *Mib1* targeted inactivation in the development of the cardiac valves and the chambers, paying special attention to the potential implication in cardiac disease derived from the incorrect development of these structures (Grego-Bessa et al., 2007, Garg et al., 2005).

MATERIAL AND METHODS

Mouse strains and genotyping. The mouse strains used were Tie2-cre (Kisanuki et al., 2001a), *Nkx2.5-cre* (Stanley et al., 2002), *cTnT-cre* (Jiao et al., 2003), *Islet1-Cre* (Cai et al., 2003) and *Mib1^{flox}* (Koo et al., 2007). For simplicity, we use *Mib1^{flox};Tie2-cre* to refer to *Mib1$^{flox/flox}$;Tie2-cre/+* mice, *Mib1^{flox};cTnT-cre* to refer to *Mib1$^{flox/flox}$;cTnT-cre/+* mice, *Mib1^{flox};Nkx2.5-cre* for *Mib1$^{flox/flox}$*; *Nkx2.5-cre/+* mice. All groups of mice were a mix of males and females. Genotyping of the different genes was performed using the following primers: *Tie2-Cre* (forward, 5'-GGGAAGTCGC AAAGTTGTGAGTT-3'; reverse, 5'-CTAGAGCCTGTTTTGCACGTTC-3'), annealing temperature 60ºC, product length 500bp; *Nkx2.5-Cre* (forward, 5'-GCGCACTCACTTTAATGGGAAGAG-3'; reverse, 5'-GCCCTGTCCCTCAGATTTCACACC-3'), annealing temperature 60ºC, product length 583bp; *cTnT-Cre* (forward, 5'-TACTCAAGAACTACGGGCTGC-3'; reverse 5'-GCACTCCAGCTTGGTTCCCGA-3'), annealing temperature 60ºC, product length 350bp; *Islet1-Cre* (forward, 5'-GCTGAAGGATGCCCAGAAGG-3', reverse, 5'-AACTTGCACCATGCCGCCCAC-3'), annealing temperature 60ºC, product length 350bp; *Mib1^{flox}* (forward, 5'-ACACCCAGAGGAAGCCCTAC-3', reverse, 5'-CTCACATCACCAAAGGATTGT-3' and conditional 5'-CCAGTCATAGCCGAATAGCC-3'), forward and reverse primers are used to obtain the WT band, forward and conditional are used to obtain the transgenic band. All three primers can be used in the same time in the PCR mix. Annealing temperature 60ºC, product length 500bp for the transgenic band and 320bp for the WT band. Animal studies were approved by the CNIC Animal Experimentation Ethics Committee. All animal procedures conformed to EU Directive 2010/63EU and Recommendation 2007/526/EC regarding the protection of animals used for experimental and other scientific purposes, enforced in Spanish law under Real Decreto 1201/2005.

Tissue Processing. Mouse embryos were fixed in 4% paraformaldehyde (PFA) at 4ºC overnight. Embedding was performed following dehydratation using graded ethanol series, xylene washes and final paraffin steps.

Histology, and *in situ* hybridization. H&E was performed according to standard protocols. *In situ* hybridization was performed following published protocols (Kanzler et al., 1998).

3D episcopic reconstruction. 3D models were performed in Dr. T. Mohun's laboratory in the MRC National Institute for Medical Research in London following already published protocols (Mohun and Weninger, 2012a, Mohun and Weninger, 2012b, Mohun and Weninger, 2012c).

Scanning Electron Microscopy (SEM). Hearts were analysed in Dr. D. Sedmera's laboratory in the Institute of Anatomy, First Faculty of Medicine, Charles University in Prague.

Immunohistochemistry. Antibodies to Dll4 (1:100, SC28915, Santa Cruz Biotechnology) and Jag1 (1:100, 2620, Cell Signaling Technology) were applied overnight, followed by a 1-h incubation with rabbit horseradish peroxidase (HRP)-coupled

secondary antibody (1:100 in 5% BSA, P0447, Dako Cytomation). The signal was amplified using a tyramide amplification kit (TSA) coupled to Cy3 (1:100, NEL744, Perkin Elmer). Staining with antibodies to N1ICD (1:100, 2421, Cell Signaling Technology) was performed following the protocol described in (Del Monte et al., 2007).

Proliferation analysis and quantification. Cell proliferation was analyzed by detection of BrdU incorporation. Pregnant females were intraperitonally injected with 300ul BrdU at 10mg/ml and two hours later embryos were isolated in sterile PBS. Neonates were intraperitonally inject with 50ul BrdU at 10mg/ml and the hearts were after two hours dissected. Embryos or neonatal hearts were fixed overnight in PFA 4%. BrdU positive cells were detected following the protocol described in (Del Monte et al., 2007). Antibody to BrdU (1:50, B2531, Sigma-Aldritch). Total cells and BrdU-positive cells in the compact myocardium were counted in sections (at least five) in three embryos of each genotype.

Hypertrophy analysis and quantification. Hypertrophy was analyzed by measuring the relative cell area in WT and *Mib1^{flox};cTnT-cre* hearts stained with tetramethylrhodamine-conjugated wheat germ agglutinin (1:100, W849, Molecular Probes). Hearts were fixed overnight in 4% paraformaldehyde and embedded in paraffin. At least 100 cells were measured per section, and at least three sections were measured per embryo. Three embryos were analyzed per genotype.

Microscopy. Stained sections or cells were viewed with an Olympus BX51 microscope fitted with a Nikon DP71 camera and CellA controller software.

Semi- and Quantitative RT-PCR of embryonic mouse heart. E9.5 for semi-quantitative and E15.5 for quantitative WT and mutant mice were dissected in ice-cold PBS and the whole heart was separated from the rest of the body. Total RNA was purified using TRIzol (Invitrogen). cDNA was synthesized with SuperScript III First Strand (Invitrogen), with 1 µg total RNA per reaction.

Semi-quantitative PCR was performed with the following primers: *Hey1* (forward, 5'-AGGGTGGGATCAGTGTGC-3'; reverse 5'-TGCTTCTCAAAGGCACTG-3') annealing temperature 56ºC, product length 355bp (Timmerman et al., 2004); *Hey2* (forward, 5'-GAGGCAGTGATGACATCC-3'; reverse, 5'-CCCTGATGGCATCCGAAGAGC-3'), annealing temperature 58ºC, product length 273bp (Timmerman et al., 2004); *Hey3* (forward, 5'-GGTCCCCACTGCCTTTGAGA-3'; reverse 5'-AGGATGGCGAGCTGACTGTTC-3'), annealing temperature 65ºC, product length 381bp (Wang et al., 2002), *Snail1* (forward, 5'-GGAAGCCCAACTATAGCGAGC-3'; reverse 5'-CAGTTGAAGATCTTCCGCGAC-3'), annealing temperature 57ºC, product length 424bp (Veltmaat et al., 2000), *Nrg1* (forward, 5'-GCACTTGCACAAGTATCTTGAGGG-3'; reverse 5'-CCTCCCAGATTGAAAGAGATGAAA-3') annealing temperature 67ºC, product length 531bp (Miyazaki et al., 2004), *Bmp10* (forward 5'-ACCAAGCTGAGGACACCGGAAGG-3'; reverse 5'-CTTCGTGGGCACACAGCAGGCTTT-3') annealing temperature 59ºC, product length 485bp (Grego-Bessa et al., 2007), *Actin* (forward, 5'-GGACCTGGCTGGCCGGGACC-3', reverse

5'-GCGGTGCACGATGGAGGGGC-3'), annealing temperature 62ºC, product length 583bp (Bi et al., 1999).

Quantitative PCR was performed with Power SYBR Green Master Mix (Applied Biosystems, 4367659) and the following primers: *Tbx20* (forward, 5′-TATTCAGCATACTCCTAC-3′; reverse, 5′-GTTAGTCTTGTCAATACG-3′); *Anf* (forward, 5′-CCTGCCTTCATCTATCAC-3′; reverse, 5′-TGAGGATCTACCTTAATATGC-3′); *Bmp10* (forward, 5′-CCATCTCCATCCTCTATT-3′; reverse, 5′-TCTCCTCTCCTATCTACA-3′); *Cx40* (forward, 5′-AGCAACATACCAGATAGA-3′; reverse, 5′-GCAGATTACTTGATGAATAC-3′); *n-Myc* (forward, 5′-GACGAGGAGGAAGATGAA-3′; reverse, 5′-CTTGTTGTTAGAGGAGGAA-3′); *Hey2* (forward, 5′-GCTCATTGACACCAACTC-3′; reverse, 5′-ATTGCCTGCTTCTTCTCT-3′); β-*actin* (forward, 5′- ATCTTCCGCCTTAATACT-3′; reverse, 5′- GCCTTCATACATCAAGTT-3′).

RNA-seq. RNA was isolated from the ventricles of 16 WT and 16 *Mib1^{flox};cTnT-cre* hearts at E14.5 and then pooled into four replicates. RNA was sequenced with the GAIIx sequencer. The sequencing protocol was single-end 75-bp elongation. The reads were first aligned using Bowtie version 0.12.7 and then mapped to the latest Ensembl transcript set using RSEM v1.16 (Li and Dewey, 2011). Genes showing altered expression with adjusted $P<0.05$ were considered differentially expressed. Gene Ontology analysis was performed using Ingenuity.

Western blots from embryonic samples. Hearts from E13.5 embryos were dissected and lysed in RIPA buffer (50 mM Tris, pH 7.4, 150 mM NaCl, 1% Triton X-100, 0.25% sodium deoxycholate and 1 mM EDTA) containing protease inhibitor cocktail (Roche) and MG-132 (Calbiochem). Total proteins (25 µg) were separated by SDS-PAGE and transferred to a polyvinylidene fluoride (PVDF) membrane. Blots were incubated overnight with primary antibodies. Antibodies to Mib1 (Jin et al., 2002) were used at 1:1,000, and antibodies to N1ICD and Jagged1 (1:1,000) were the same as those used for immunostaining. Other primary antibodies used were antibodies to N2ICD (1:1,000, ab52302, Abcam), Dll4 (1:500, ab7280, Abcam), GFP (1:400, SC9996, Santa Cruz Biotechnology), α-tubulin (Sigma, T8203, 1:4,000) and β-actin (1:6,000, Sigma, A5441). HRP-coupled secondary antibodies (Dako) were used at 1:5,000 dilution. Band intensities were quantified by densitometric analysis using ImageJ software.

Ultrasound. Mice were anesthetized by inhalation of isoflurane and oxygen (1.25% and 98.75%, respectively) and examined with a 30-MHz transthoracic echocardiography probe. Images were obtained with Vevo 770 (VisualSonics, Toronto, Canada) from *Mib1^{flox};cTnT-cre* and WT littermates. Short-axis, long-axis, B-mode and two-dimensional M-mode views were obtained as described previously (Cruz-Adalia et al., 2010). From these images, left ventricle function was estimated by the ejection fraction obtained from the M mode by a blinded echocardiography expert. For the ejection fraction measurements, a long- or short-axis view of the heart was selected to obtain an M mode registration in a line perpendicular to the left ventricular septum and posterior wall at the level of the mitral chordae tendinea. Ultrasound studies were performed in collaboration with Dr. J.

Borreguero (CNIC).

CMRI. Mice were anesthetized by inhalation of isoflurane and oxygen (5% and 95%, respectively) and examined with a Bruker Biospec 70/210 at 7 T and a maximum gradient of 750 mT m^{-1}. Echocardiograph (ECG) synchronization was performed with the Intragate function included in the CMRI software. ECG measures and breathing rhythm were monitored with a system for small animals compatible with MRI (model 1025, S.A. Instruments, Inc.). Data were acquired with the IntraGate_FLASH sequence at TE (echo time) = 2.4 ms and TR (repetition time) = 8 ms. The slice thickness was 1 mm and the field of view was 2.7 cm x 3 cm in a matrix of 256 pixels x 256 pixels.

Studies in human subjects were performed with a 3-T clinical magnet (Ingenuity, Philips Medical Systems, Best, The Netherlands). Patients were scanned using 32-channel phased array surface coils as receivers and retrospective ECG gating. Images were obtained during end-expiratory breath holds. Segmented cine steady-state free precession was performed to acquire 10–15 contiguous short-axis slices covering both ventricles from the base to the apex and also four-chamber and two-chamber views with a slice thickness of 6 mm. The structurally normal hearts analysed by CMRI were from healthy individuals with no mutations in *MIB1*. Left ventricular trabeculation was defined as myocardium protruding from the left ventricular wall into the left ventricular cavity at the end-diastolic phase. To quantify left ventricular volume, left ventricular ejection fraction and compacted left ventricular mass, the endocardial border was traced to include papillary muscle and exclude trabeculation. To quantify global left ventricular mass, the endocardial border was traced to include papillary muscles and trabeculation. The trabeculated left ventricular mass was calculated as (global left ventricular mass – compacted left ventricular mass), and the trabeculated left ventricular mass with respect to the total left ventricular mass was calculated as ((global left ventricular mass – compacted left ventricular mass)/global left ventricular mass) x 100. Left ventricular volume, compacted left ventricular mass and trabeculated left ventricular mass were indexed to the body surface area. The ratio of noncompacted to compacted myocardium was measured in short-axis views at the end-diastolic phase, considering the segment with the most pronounced trabeculations as the noncompacted layer and the compacted myocardium as being perpendicular to this. We used the methods of Jacquier (trabeculated left ventricular mass above 20% of the total left ventricle (Jacquier et al., 2010)) and Petersen (noncompacted to compacted ratio >2.3 in the diastole (Petersen et al., 2005)) for the CMRI analysis, considering a diagnosis of LVNC by CMRI if at least one of those measures were positive. Mouse CMRI was performed in collaboration with Dr. J. Ruiz Cabello (CNIC).

LVNC clinical phenotype evaluation and DNA collection. Clinical evaluations and genetic studies were performed in accordance with human subject guidelines after informed consent according to the protocol approved by the Hospital Universitario Virgen de la Arrixaca, Instituto Cardiovascular Hospital Clínico San Carlos, Hospital General Universitario Gregorio Marañón, Hospital Universitario Puerta de Hierro and Hospital Universitario de La Princesa. We included 100 unrelated index

patients with an echocardiographic diagnosis of LVNC (48 of them familial), defined by the presence of at least three prominent trabeculations in the left ventricle and a ratio of noncompacted to compacted segment >2.0 at the end-diastolic phase (Stollberger and Finsterer, 2004, Stollberger et al., 2002). All subjects underwent a clinical evaluation, including an ECG and two-dimensional and Doppler echocardiography. A pedigree was drawn for each patient and first-degree relatives were screened with the same protocol. Patients were diagnosed by Dr. J. R. Gimeno (Hospital Clínico Universitario Virgen de la Arrixaca, Murcia). Blood samples were taken for genetic analysis and all patients and their relatives gave written informed consent. Genomic DNA for genetic analyses was extracted from peripheral lymphocytes. Patients positive for *MIB1* mutations were then analyzed and found negative for alterations in other genes previously related to LVNC (Captur and Nihoyannopoulos, 2010) (Ichida, 2009). The genes analyzed were *MYH7*, *MYBPC3*, *TNNT2*, *TNNI3*, *TPM1*, *ACTC*, *MYL2*, *MYL3*, *TNNC*, *G4.5*, *LDB3* and *LMNA*. CMRI was performed on all patients with identified *MIB1* mutations, except in patients 2.I.3 and 2.I.4 (Table 3), and in selected healthy individuals.

Identification of human *MIB1* mutations. All human *MIB1* coding exons were sequenced bidirectionally to search for sequence variations in the 100 patients analyzed and the family members of the two probands. Primer pairs for the 20 *MIB1* exons were designed using the PrimerZ algorithm (Tsai et al., 2007). PCR amplification was performed with the Advantage Genomic PCR kit (Clontech). Human *MIB1* mutations were screened with the LIMSTILL platform (http://limstill.niob.knaw.nl/). For controls, echocardiographic studies were carried out on 263 healthy volunteers. Blood from these volunteers was obtained and the two *MIB1* exons that contain the identified mutations in the patients with LVNC were sequenced. All healthy volunteers were negative for these mutations.

URLs. PolyPhen-2 program, http://genetics.bwh.harvard.edu/pph2/index.shtml; GERP, http://genome.ucsc.edu/; 1000 Genomes database, http://browser.1000genomes.org/Homo_sapiens/Transcript/ProtVariations?db=core;g=ENSG00000101752;r=18:19321281-19450918;t=ENST00000261537; National Heart, Lung, and Blood Institute Grand Opportunity Exome Sequencing Project, https://esp.gs.washington.edu/drupal/; Genome-Wide Association Studies, http://www.genome.gov/gwastudies/; Copy Number Variation, http://www.sanger.ac.uk/research/areas/humangenetics/cnv/global_assess.html; Genetic Association Database, http://geneticassociationdb.nih.gov/cgi-bin/index.cgi; International HapMap project, http://hapmap.ncbi.nlm.nih.gov/.

Three-dimensional structure prediction for MIB1 and JAG1. *In silico* models of the MIB1 and JAG1 proteins were calculated using a *de novo* prediction method with a structural homolog comparison approach. The fasta sequence (1006 amino acids (aa)) of MIB1 (UniProtKB: Q86YT6, NCBI: NP_065825.1) and the fasta sequence (1218 aa) of JAG1 (UniProtKB: P78504, NCBI: NP_000205) were submitted to the i-TASSER server (http://zhanglab.ccmb.med.umich.edu/I-TASSER/) (Roy et al., 2010; Roy et al., 2011; Zhang, 2008). The default values (no restriction or model templates) were used for

prediction. The more compact PDB model for MIB1 (C-score = –2.88) was loaded into the PyMOL program (PyMOL Molecular Graphics System, Version 1.4.1, Schrödinger, LLC., http://www.pymol.org/), and a new PDB model with a single mutated position (V943F) was generated. To validate the secondary structure of the transmembrane domain of the best PDB model for JAG1 (C-score = –1.37), the JAG1 fasta sequence was submitted to the Swiss-Model Portal with the MEMSAT option selected (http://swissmodel.expasy.org/) (Arnold et al., 2006, Kiefer et al., 2009, Jones et al., 1994). The helix dihedral angles for the transmembrane domain in the JAG1 PDB model were fixed using Swiss-PdbViewer v 4.04 (http://www.expasy.org/spdbv/). 3D models were performed by Dr. F. Martinez de Benito (CNIC).

Three-dimensional structure prediction for the MIB1 dimer. *In silico* models of the MIB1 WT homodimer (WT-WT) and the heterodimer (WT-V943F) were calculated by submitting PDB models of MIB1 and MIB1-V943F to the Hex server v6.9 (http://hexserver.loria.fr/) (Ritchie, 2005, Ritchie et al., 2008, Ritchie and Venkatraman, 2010, Macindoe et al., 2010, Mustard and Ritchie, 2005, Ritchie, 2003, Ritchie and Kemp, 2000). The docking method in dimer mode with shape plus electrostatic restriction was used for prediction and the minimal energy model for each dimer type was selected. 3D models were performed by Dr. F. Martinez de Benito (CNIC)

Three-dimensional structure prediction for the docking of JAG1 to the MIB1 dimer. *In silico* theoretical models of the docking of JAG1 to MIB1 dimers (WT-WT homodimers and WT-mutant heterodimers) were calculated using a docking prediction method. PDB models for JAG1 as the receptor and the MIB1 dimer as the ligand were submitted to the ClusPro server v2.0 (http://cluspro.bu.edu/) (Kozakov et al., 2010, Kozakov et al., 2006, Comeau et al., 2004). The hydrophobic-favored model compatible with the protein domains and biological function for each MIB1 dimer type was selected. PyMOL v1.4.1 was used for alignment, visualization options and model decoration. 3D models were performed by Dr. F. Martinez de Benito (CNIC).

Isolation of whole mononuclear cells from peripheral blood. EDTA-treated peripheral blood from patients and control subjects was diluted in one volume of PBS and slowly layered over a Ficoll-Hypaque solution. After centrifugation at 900*g* with no brake, the mononuclear cell layer was collected from the top of the Ficoll-Hypaque solution and washed twice with PBS to remove most of the platelets. Pelleted cells were lysed in RIPA buffer and total proteins (25 µg) were separated by SDS-PAGE and transferred to a PVDF membrane. Blots were incubated overnight with the primary antibodies to N1ICD, Mib1 and β-actin described above and under the same conditions.

T cell culture. After isolation from peripheral blood, whole mononuclear cells were seeded at 1–2 x 10^6 cells per ml in RPMI medium containing 10% FBS and 5 µg/ml phytohemagglutinin (PHA, Sigma). After 2 days, cultures were washed with PBS to remove PHA and the cells were stimulated with interleukin-2 (IL-2) (50 U/ml). Density was maintained at 1–2 x 10^6 cells per ml for 7 days.

T cell gene expression analysis. For

qPCR assays, cells were cultured in IL-2–free medium overnight and then collected for RNA extraction with an RNeasy Mini Kit (Qiagen). RNA was reverse transcribed to cDNA using a Superscript III First-Strand kit (Invitrogen). qPCR was performed using the Power SYBR Green system (Applied Biosystems). Relative expression was calculated by the delta cycle threshold (Δ*Ct*) method. The primers used were as follows: *DTX1*: forward, 5′-ACGAGAAAGGCCGGAAGGT-3′; reverse, 5′-GGTGTTGGACGTGCCGATAG-3′; *GATA3*: forward, 5'-TGGGCTCTACTAC AAGCTTCACAATAT-3';reverse, 5′-TTGCTAGACATTTTTCGGTTTCTG-3′; *GUSB*:forward, 5′-CAACGAGCCTGCGTCCCACC-3′; reverse, 5′-ACGGAGCCCCCTTGTCTGCT-2′ (Van de Walle et al., 2009). qPCR assays were also performed with the following NOTCH target genes: *HES1*, *NOTCH3*, *NRARP*, *TCF7*, *HEY1* and *c-MYC*, whose expression was not significantly affected. For primer sequences, see (Van de Walle et al., 2009).

Semiquantitative RT-PCR and qPCR analysis of *MIB1* mutant transcripts. The cDNA generated from T cells of patients was used to analyse the effect of the V943F and R530X mutations on the expression of the corresponding mutant transcripts. An initial estimate of the expression of these mRNAs was achieved by RT-PCR using primers spanning both mutations. For V943F the primers were forward, 5′-AAAGTTCAGAAAGATGCCACTG-3′ and reverse, 5′-CATTCACTCATGCGGTCTC-3′; for R530X, the primers were forward, 5′-TGGCCACACAGCTATGCAAGT-3′ and reverse, 5′-TCCCCTTAGTGCAGCATGATG-3′. The PCR products (266 bp for V943F and 433 bp for R530X) were cloned into the pGEM-T plasmid and 24 clones of each mutation were sequenced to estimate the percentage of WT compared to mutant transcripts.

Mutant transcripts were quantified by qPCR using primers to amplify the *MIB1* cDNA 5′ and 3′ ends of the mutations. The primers used were forward, 5′-CATTGGCATTCGATGGAA-3′ and reverse, 5′-CTCTGGCTGTAATCTTCTTAG-3′, which are common to both mutations. To amplify the 3′ end of R530X, we used the primers forward, 5′-TTAACAGTTCAAGCAATT-3′ and reverse, 5′-GCAGGAATCATTATTAACAAG-3′.
To amplify the 3′ end of V943F, 5′-GATAGGACATTCACTCAT-3′.

Generation and cloning of *MIB1* mutations. Complete cDNA for *MIB1* was obtained from clone IMAGE 40008395. The sequence was amplified with Phusion High-Fidelity DNA Polymerase (NEB) with primers containing BamHI and EcoRI sites, and cloned in frame with an HA epitope into the BglII-EcoRI sites of pCELF (a gift from A. Martín-Pendás). *MIB1* cDNA was also cloned in frame with Flag, CFP and YFP into the BamHI and EcoRI sites of pEF-Flag (Copeland and Treisman, 2002), pEYFP-N1 and pECFP-N1 (Invitrogen), respectively. The constructs were sequenced and HA-MIB1 was then cloned into the BamHI-EcoRI sites of pCS2. Point mutations were introduced into the pCS2-*MIB1* and pECFP-N1-*MIB1* sequence using the QuikChange II XL site-directed mutagenesis kit (Agilent Technologies).

For V943F, we used the primers MIB1 V943F forward (5′-GGACAAGGATAATACCA AT**T**TCAATGCAGATGTGCAA-3′) and MIB1

V943F reverse (5′-TTGCACATCTGCATTG A**A**ATTGGTATTATCCTTGTCC-3′).
For R530X, we used the primers MIB1 R530X forward (5′-GAATGC**T**CGAAACAAGCGCTGACA GACACCACTTCATATTG-3′) and MIB1 R530X reverse (5′-CAATATGAAGTGGTGTCTGTC**A** GCGCTTGTTTCGAGCATTC-3′).
For the zebrafish dominant-negative mutation mib1ta52b (M989R), we used the primers MIB1 M989R forward (5′-TCAACTCTGTGGAGACCGCA**G**GAGT GAATGTCCTATCTGTC-3′)
and MIB1 M989R reverse (5′-GACAGATAGGACATTCACT**C**CTGCGG TCTCCACAGAGTTGA-3′). The mutant nucleotides are bold and underlined. All point mutations were sequence verified.

Transfections and MIB1 functional assays. Functional assays were performed as described (Itoh et al., 2003) with slight modifications. HEK293 cells were co-transfected with 8 µg total DNA (pcDNA3-JAGGED1, pNA3-GFP-ubiquitin and the different pCS2-HA-MIB1 and pCEFL-Flag-MIB1 constructs) using Lipofectamine Plus Reagent (Life Technologies). 24 h after transfection, cells were incubated with 5 µM MG-132 (Calbiochem) for a further 4 h and then lysed in IONIC buffer (50 mM Tris, pH 8, 150 mM NaCl, 0.5% NP40, 0.5% sodium deoxycholate and 0.05% SDS) containing protease inhibitor cocktail (Roche) and 10 µM MG-132. One-fifth of the precleared lysate from a 100-mm dish was immunoprecipitated by overnight incubation at 4 °C with Jag1-specific antibody (SC-6011, Santa Cruz Biotechnology, 1:100) followed by incubation with protein G Sepharose (GE Healthcare Bio-Sciences) for 3 h at 4°C. The Sepharose bead–protein pellets were washed six times with ice-cold IONIC buffer and boiled in 2x SDS-PAGE sample buffer containing 50 mM dithiothreitol (DTT). Immunoprecipitated proteins and total lysates were analyzed by SDS-PAGE and transferred to a PVDF membrane. Blots were incubated overnight with antibodies to GFP (1:400, SC9996, Santa Cruz Biotechnology), HA (Santa Cruz, sc-805, 1:200), Flag (Sigma, F7425, 1:1,000) and Jag1, Mib1 and β-actin under the same conditions described above.

FRET analysis. Pairwise combinations of 0.5 µg pEYFP-C1 plasmid encoding YFP-tagged WT MIB1 and 0.5 µg pECFP-C1 plasmid encoding CFP-tagged WT, V943F or R530X MIB1 were co-transfected in HEK293 cells using Lipofectamine Plus Reagent (Life Technologies). For controls, cells were transfected with plasmids encoding only the fluorescent proteins or with combinations of these plasmids with the plasmid encoding YFP-tagged WT MIB1. FRET acceptor photobleaching analysis was performed with a Leica TCS SP5 confocal microscope.

Coimmunoprecipitation assays. We performed the dimerization assay described in (Zhang et al., 2007b) with slight variations. Briefly, HEK293 cells were transiently co-transfected with 5 µg each of pCS2-HA-MIB1 and pCEFL-Flag-MIB1 constructs using Lipofectamine Plus Reagent (Life Technologies). For the Mib1-Jagged1 interaction assay, HEK293 cells constitutively expressing Jagged1 (Chapman et al., 2006) were transfected with 5 µg of pCEFL-Flag-MIB1 constructs in the same conditions. Cells were harvested 24 h after transfection in IONIC buffer containing protease inhibitor cocktail (Roche) and MG-132. For

coimmunoprecipitation, lysates from 100-mm dishes were centrifuged and incubated with anti-Flag M2 affinity gel (Sigma, A2220) for 4 h at 4 °C with gentle rocking. After six washes with lysis buffer, proteins were eluted with 2x SDS-PAGE sample buffer containing 50 mM DTT and electrophoresed in SDS polyacrylamide gels followed by western blotting. Coimmunoprecipitated HA-MIB1, Flag-MIB1 and Jagged1 were detected as described above.

Luciferase assays. HEK293 cells constitutively expressing Notch1 (Chapman et al., 2006) were co-transfected with the Notch reporter plasmid pGL3-10xCBF1-Luc (Koibuchi and Chin, 2007) and pGL3-*Renilla* luciferase at a 5:1 ratio using Lipofectamine Plus Reagent (Life Technologies). In parallel, Jag1-HEK293 cells (Chapman et al., 2006) were transfected with one of the various MIB1 plasmids. At 24 h after transfection, Notch1-HEK293 and Jag1-HEK293 cells were cocultured in 24-well plates; 48 h later, the firefly and *Renilla* luciferase activities were measured using the Dual Luciferase Assay System (Promega). Data are expressed as ratios of firefly to *Renilla* luciferase. Experiments were performed in quadruplicate samples.

***MIB1* functional assays in zebrafish.** Zebrafish (*Danio rerio*) were maintained and raised under standard conditions at 28 °C. Transgenic *Tg(mlc2a:GFP)* embryos were used to visualize heart development. The *Tg(mlc2a:GFP)*; *mib*$^{ta52b/ta52b}$ line was generated by standard crossing of individual lines and was used to obtain *mib1* mutants for use as phenotype controls. Capped mRNA encoding the human M989R, R530X or V943F *MIB1* mutations were generated by using the mMESSAGE mMACHINE kit (Ambion) from pCS2-MIB mutant variants. Capped mRNAs were microinjected under a range of concentrations into embryos at the one- or two-cell stage. Capped GFP and WT MIB1 mRNAs were used as microinjection controls. Embryos were allowed to develop at 28 °C. Twenty-four hours after fertilization, embryos were incubated in water containing 0.2 mM 1-phenyl-2-thio-urea (Sigma) to prevent pigmentation. The numbers of embryos showing a WT or dysmorphic phenotype were counted at 72 h.p.f. Pictures were taken at 80 h.p.f. using a dissection microscope equipped for epifluorescence (MZF16FA, Leica) and a digital camera (DFC310FX, Leica). At least 100 embryos per condition were analyzed in each experiment.

Zebrafish Notch reporter assay. *Tg(Tp1bglob:eGFP)*^{um14} is a transgenic Notch-responsive zebrafish line harboring a construct with 12 RBPJK binding sites upstream of the β-globin minimal promoter and the *eGFP* reporter gene (Parsons et al., 2009). *Tg(Tp1bglob:eGFP)*^{um14} embryos were injected at the one- or two- cell stage with capped mRNAs encoding the M989R, R530X or V943F *MIB1* mutations and allowed to develop at 28 °C. At 24 h.p.f. Fish embryos were incubated in water containing 0.2 mM 1-phenyl-2-thio-urea (Sigma) to prevent pigmentation. At 32 h.p.f., pictures were taken of groups of 20–25 embryos (three Petri dishes with approximately 75 embryos each; MZF16FA, Leica), and the average intensity in the green channel in at least 12 pictures per experiment was measured with Adobe PhotoShop CS3 Extended (Adobe Systems Incorporated). GFP fluorescence intensity

was compared with that of control uninjected larvae.

Statistics. Statistical analyses were performed using Student's *t* test in Microsoft Excel 14.1.4. Data are presented as means ± s.e.m., unless otherwise indicated. Differences were considered statistically significant at $P < 0.05$.

RESULTS

The Notch signalling pathway and heart development

To study the role of *Mib1* in heart development we bred mice bearing a *Mib1* conditional loss-of-function allele with three specific heart Cre drivers. *Tie2-Cre* active in the endocardium and vascular endothelium from E7.5 onwards (Kisanuki et al., 2001b), *Nkx2.5-Cre* active in the endocardium and the myocardium from E7.5 (Stanley et al., 2002) but with an stronger expression in the SHF, and the myocardium specific *cTnT-Cre* (Jiao et al., 2003) line active from E8.0. This will allow us to interrupt Notch signalling at the beginning of the chain of events allowing us to study the pathway from a "signalling cell" point of view

The Notch signalling pathway shows a complex expression pattern in the heart (Fig. 6). At E9.5, *Mib1* is expressed ubiquitously, and in the heart it can be seen in the valvulogenic regions and in the chambers. Interestingly, it is expressed in both endocardium and myocardium since early developmental stages. This expression in maintained at E11.5 (Fig. 6 A). There are two Notch ligands differentially expressed in the heart; Delta4 is expressed in the endocardium of both the valvulogenic regions, AVC and OFT, and the chambers (Fig. 4 B). Jagged1 is expressed in the myocardium of the chambers and in the endocardium of the valvulogenic regions (Fig. 6 C). The inactivation of *Mib1* in the endocardium or the myocardium would allow us to determine the contribution of each Notch ligand to cardiac chamber and valves development in the heart.

First, we studied the expression and the activity of the pathway in our *Mib1*-cardio-specific mutant mice. At E9.5 Notch1 is active in the valvulogenic regions and in the base of the trabeculae in the ventricle, as revealed by immunostaining using an antibody that recognizes the intracellular domain of the receptor (N1ICD) (Del Monte et al., 2007) (Fig. 6). Later on, at E11.5, N1ICD is detected in the endocardium of the valves but the restriction expression in the trabeculeae is lost, and N1ICD is found throughout the endocardium (Fig. 6 D). N1ICD staining disappears in the heart of E9.5 *Mib1^{flox};Tie2-Cre* embryos (Fig. 6 E). In *Mib1^{flox};cTnT-Cre* mice, Notch1 activity is severely reduced in the endocardium of the chambers but can still be detected in the endocardium of the valvulogenic regions of the heart (Fig. 6 E). In the case of *Mib1^{flox};Nkx2.5-Cre* mice, N1ICD staining is strongly reduced both in the chambers and in the valvulogenic area (Fig. 6 E). The differential effects on Notch1 activity observed in the different mutants genotypes is very likely due to the different tissue specificity of the drivers.

These results identify Notch as an important pathway involved in heart development, being expressed from early on. The different pattern of expression of the Notch ligands present in the heart, and the fact that Mib1 regulates the two of them, will allow us to dissect their role in the distinct areas of the developing heart. But even if ligands or modulators are expressed in the different tissues of the heart, Notch1, and therefore the pathway, is only active in the endocardium. This suggests that the endocardium is the key tissue directing heart development.

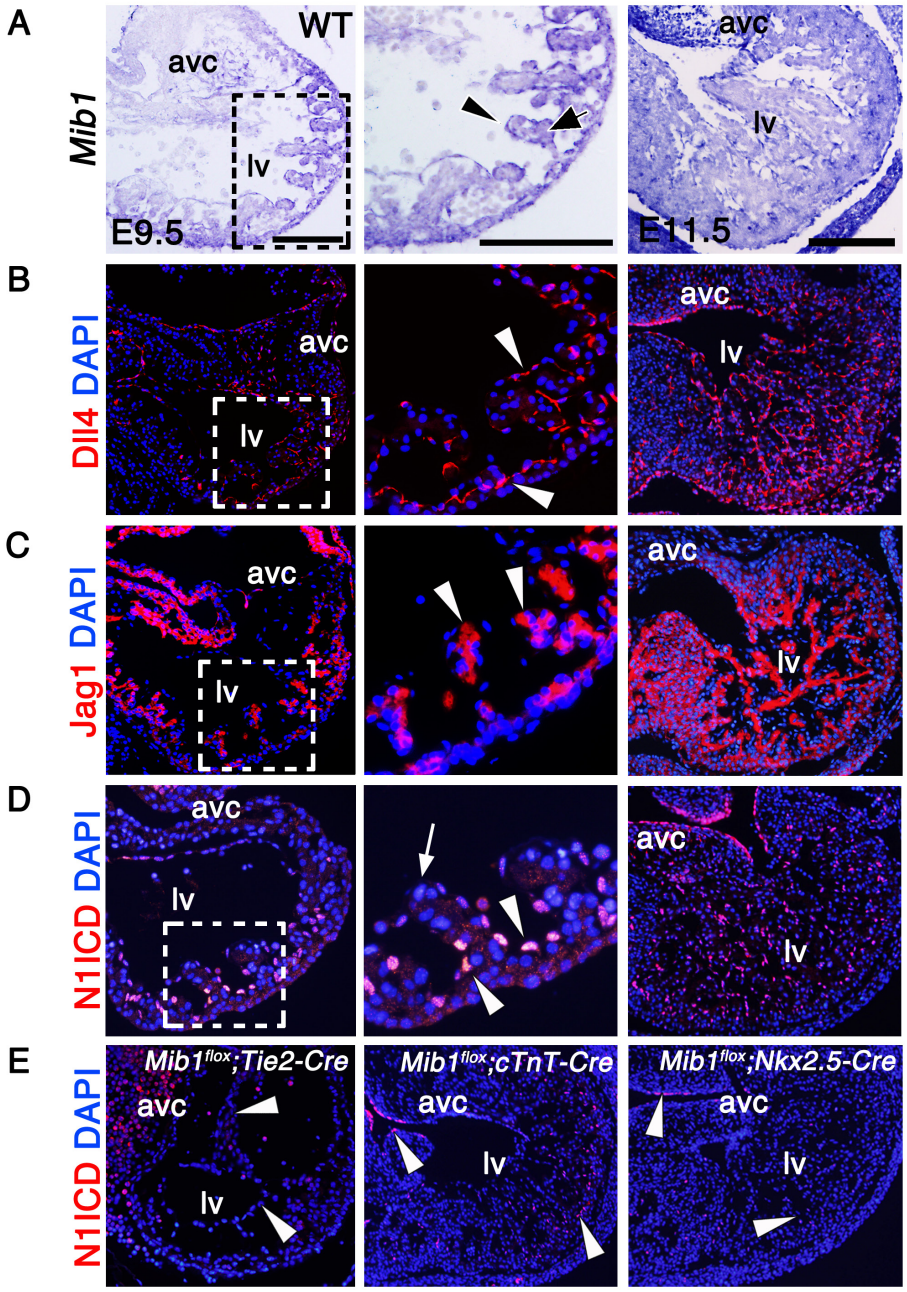

Figure 6 Notch and cardiac development.

Notch elements are expressed at different stages of heart development. (A-F) Transverse sections of E9.5 and E11.5 of wild-type (WT), *Mib1^{flox};Tie2-Cre*, *Mib1^{flox};cTnT-Cre* and *Mib1^{flox};Nkx2.5-Cre* hearts. (A) In situ hybridization (ISH), (B-E) Immunohistochemistry (IHC). High magnification panels show details of the left ventricle (lv) at E9.5. (A) *Mib1* is expressed at E9.5 in the two tissues of the heart, endocardium (arrowhead) and myocardium (arrow). The same expression pattern can be observed at E11.5. (B) Dll4 is expressed in the endocardium at E9.5 and E11.5 (arrowheads). (C) Jagged1 is expressed only in the myocardium at E9.5 and E11.5 (arrowheads). (D) Notch signalling occurs in the base of the trabeculae at E9.5 (arrowheads), there is no N1ICD at the top of the trabeculae at E9.5 (arrow), but the pattern is expanded to the whole trabecular endocardium at E11.5. (E) Upon deletion of *Mib1* in the endocardium with *Tie2-Cre*, in the myocardium with *cTnT-Cre* or in both with *Nkx2.5-Cre* Notch signalling is severely reduced in the heart (arrowheads). avc, atrio ventricular canal; lv, left ventricle. Scale bar = 200um.

Mib1 deletion in the endocardium and vascular endothelium reveals its crucial role for Notch in cardiac development

Targeted inactivation of *Mib1* in the endocardium and vascular endothelium with the *Tie2-Cre* driver line (Kisanuki et al., 2001b) causes lethality at E10.5. General development is delayed and pericardial distension, symptom of cardiac malfunction, can be observed (Fig. 7 A). Histological sections of these embryos at E9.5 show that EMT does not occur, only a few cells are able to transform and invade the endocardial cushions, and trabeculation is reduced (Fig. 7 B). This phenotype is reminiscent of those observed in *Notch1* or *RBPjK* mutants (Timmerman et al., 2004). Immunohistochemical analysis of N1ICD expression revealed a reduction in Notch signalling pathway in the endocardium (Fig. 6). The relative expression of Notch target genes *Hey1*, *Hey2* and *Hey3* was also reduced in *Mib1^{flox};Tie2-Cre* mutant mice hearts (Fig. 7 C)

In situ hybridization analysis indicated that similarly to the phenotype of *Notch1* and *RBPJk* mutant mice, the expression of the cardiac markers Snail 1 (Fig. 8 A, D), Nrg1 (Fig. 8 B, D) and Bmp10 (Fig. 8 C, D) was severely affected in E9.5 *Mib1^{flox};Tie2-Cre* embryos.

Analysis of BrdU incorporation (Fig. 9)

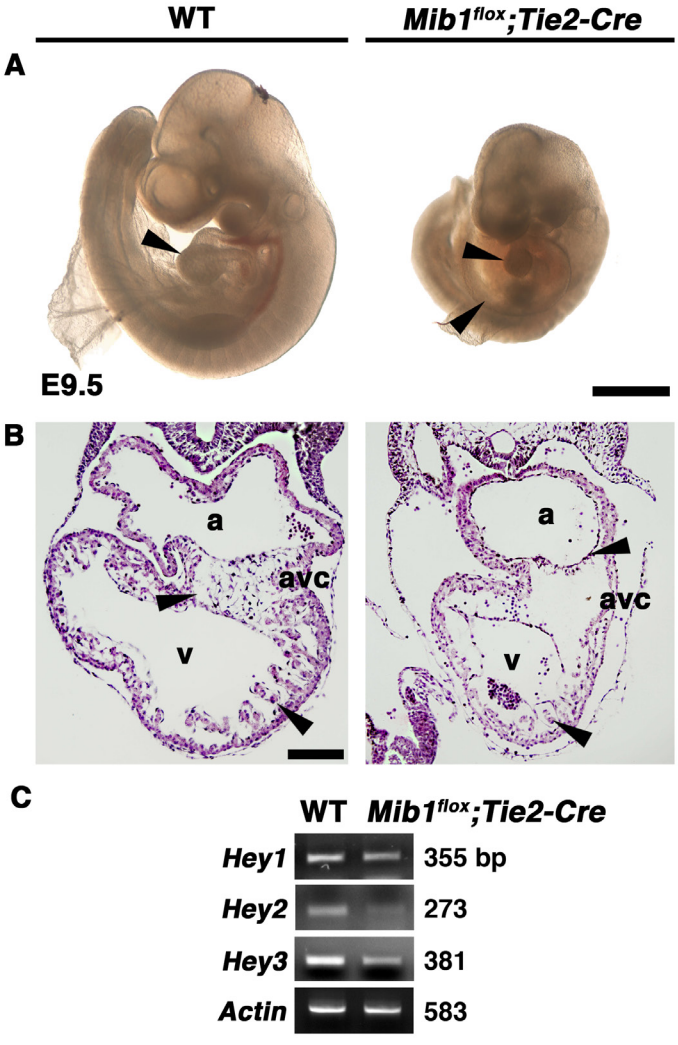

Figure 7. *Mib1* inactivation in the endocardium and vascular endothelium causes a lethal cardiac phenotype.

(A) Whole mount comparison of a wild-type (WT) embryo and a *Mib1^{flox};Tie2-Cre* at E9.5. Delayed development, impaired heart looping and distended pericardium can be observed (arrowheads). Scale bar=500um (B) Transverse sections of WT and *Mib1^{flox};Tie2-Cre* at E9.5, trabeculation and endocardial cushion formation is blocked in transgenic mice (arrowheads). Scale bar=200um. (C) Expression of Notch target genes, *Hey1*, *Hey2* and *Hey3*, is reduced in the heart by RT-PCR. a, atrium; avc, atrioventricular canal; v, ventricle.

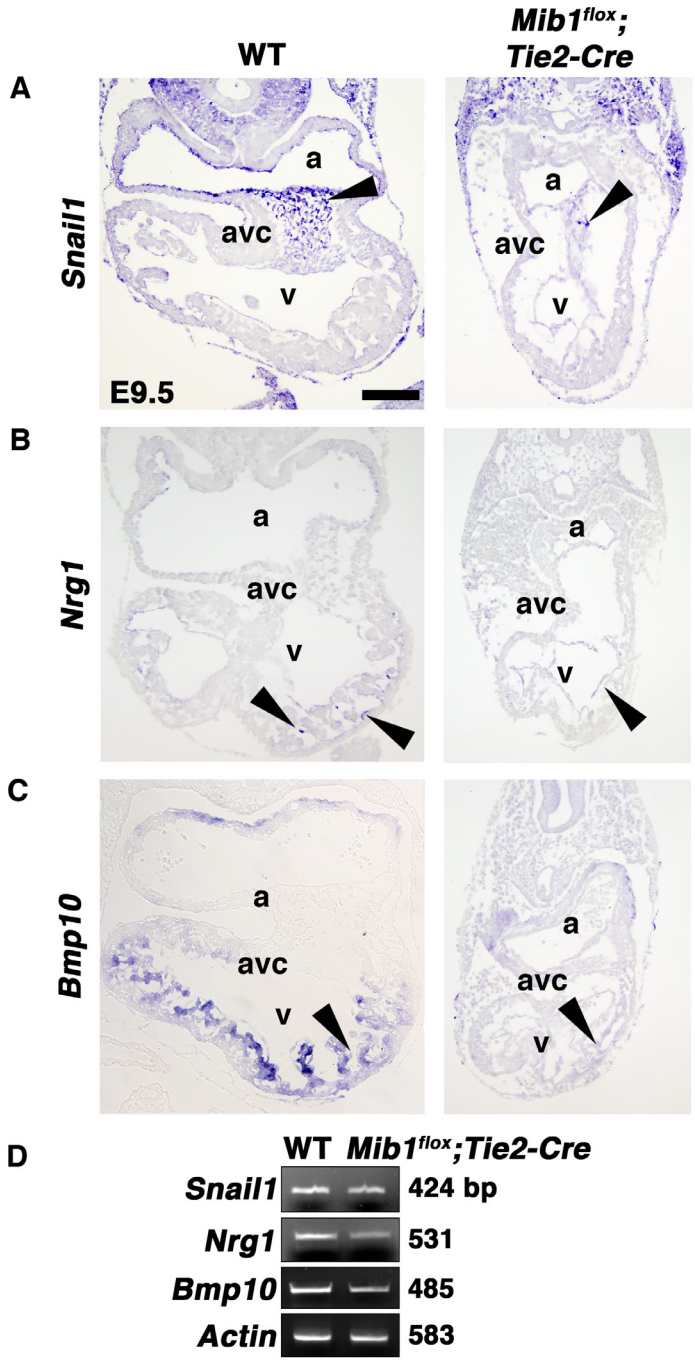

Figure 8. *Tie2-Cre*-mediated *Mib1* inactivation disrupts valvulogenesis and trabeculation.

(A-C) In situ hybridization in transverse sections of wild-type (WT) and *Mib1^{flox};Tie2-Cre* at E9.5 showing a reduced expression of trabeculation and valvulogenesis markers in the transgenic mice. Scale bar=200um. (D) Semi-quantitative RT-PCR. (A) *Snail1* expression is reduced in the AVC (arrowheads). (B) *Nrg1* expression is reduced in the endocardium of the chambers (arrowheads). (C) *Bmp10* expression is reduced in the trabecular myocardium (arrowheads). (D) Expression reduction of *Snail1*, *Nrg1* and *Bmp10* by RT-PCR. a, atrium; avc, atrioventricular canal; v, ventricle.

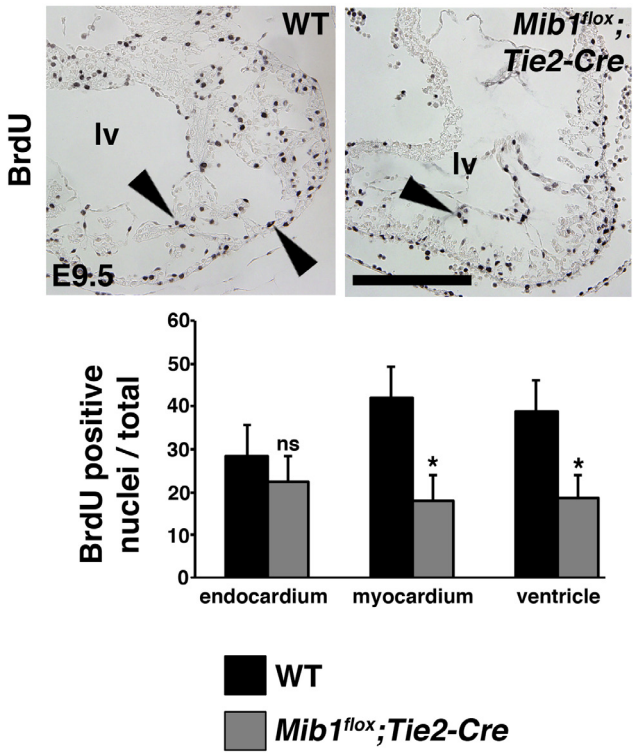

Figure 9. The early ventricular phenotype is due to a reduction of myocardial proliferation.

Transverse sections of wild-type (WT) and *Mib1^{flox};Tie2-Cre* at E9.5. There is a reduction of cellular proliferation in the myocardium of the ventricle as shown by immunostaining of incorporated BrdU after a 1-h pulse at E9.5, with details of the left ventricle shown (top). Arrowheads indicate BrdU-positive nuclei. The ratios of BrdU-positive to total nuclei (bottom) reveal significantly reduced proliferation in the myocardium of *Mib1^{flox};Tie2-Cre* hearts. n = 3 embryos per genotype. *P < 0.05 by Student's t test. Data are the means ± s.e.m. Scale bar=200um. lv, left ventricle.

Mib1 deletion in the heart causes dysmorphic OFT valves

Mib1^{flox};Tie2-Cre mice had defects in the initial steps of valve formation, as EMT is almost abolished and only a few cells are able to transform and invade the cardiac jelly. These few cells express *Snail1* (Fig. 8 A, D). To study the events that take place after EMT during valve development, we bred the *Mib1^{flox}* mice with mice expressing Cre under the control of the *Nkx2.5* promoter (Stanley et al., 2002).

Deleting *Mib1* in both endocardium and myocardium with the *Nkx2.5-Cre* line causes a perinatal lethal cardiac phenotype. Only after birth we stop scoring living mutant mice but until then the percentages are maintained with the expected ranges (Table 1). The difference with the *Tie2-Cre* deletion may be due to the expression of this driver in the vascular endothelium, where Notch plays an important role in early development. On the contrary *Nkx2.5-Cre* is a heart-specific driver.

Analysis of histological sections of *Mib1^{flox};Nkx2.5-Cre* hearts and their 3D episcopic reconstructions (Mohun and Weninger, 2011) showed that the transgenic mice present a dilated ventricle with thin

		Mib1$^{flox/flox}$;Nkx2.5-Cre/+	*Mib1$^{flox/+}$;+/+*	*Mib1$^{flox/+}$;Nkx2.5-Cre/+*	*Mib1$^{flox/flox}$;+/+*
E9.5	56	15 (26.78%)	17 (30.35%)	12 (21.42%)	12 (21.42%)
E10.5	44	4 (9.09%)	9 (20.45%)	11 (25%)	20 (45.45%)
E11.5	99	26 (26.26%)	32 (32.32%)	23 (23.23%)	18 (18.18%)
E12.5	40	7 (17.5%)	5 (12.5%)	16 (40%)	12 (30%)
E14.5	58	16 (27.58%)	12 (20.68%)	15 (25.86%)	15 (25.86%)
E15.5	285	62 (21.75%)	81 (28.42%)	70 (24.56%)	71 (25.26%)
E16.5	124	25 (20.16%)	39 (31.45%)	28 (22.58%)	32 (25.80%)
E17.5	34	8 (23.52%)	7 (20.58%)	8 (23.52%)	11 (32.35%)
P3	36	0 (0%)	14 (38.88%)	13 (36.11%)	9 (25%)
TOTAL	742	155 (20.88%)	209 (28.16%)	188 (25.33%)	190 (25.60%)
Expected		25%	25%	25%	25%

embryos dissected (percentage observed)

Table 1. *Mib1^{flox};Nkx2.5-Cre* lethality table

compact myocardium, defects in the integrity of the interventricular septum and very large trabeculae protruding into the light of the chamber (Fig. 10 A, B). The ventricular phenotype caused by the deletion of *Mib1* in the myocardium will be described later on *Mib1^{flox};cTnT-Cre* mice, that are viable and recapitulate the same ventricular phenotype observed in *Mib1^{flox};Nkx2.5-Cre* mice.

Due to the deletion of *Mib1* also in the endocardium we observed another feature in the heart that was not present in the *Mib1^{flox};cTnT-Cre* mice. *Mib1^{flox};Nkx2.5-Cre* show large leaflets in the two valves of the OFT, the aortic valve (Fig 10 C) and the pulmonary valve (Fig.10 D). After the histological analysis of the valves we performed a 3D reconstruction with Amira software where we could observe that the leaflets of the mutant mice are misaligned forming and aberrant and dysmorphic valve (Fig 10 C).

Deletion of *Mib1* in the endocardium and myocardium but specifically in the SHF using *Islet1-Cre* (Cai et al., 2003) reveals a specific phenotype in SHF derivatives, the right ventricle and the valves of the OFT (Fig. 11). Although trabeculation and compaction occurred normally in the left ventricle, compact myocardium is thinner and there are less trabeculae in the right ventricle of *Mib1^{flox};Isl1-Cre* mice (Fig. 11 A). Leaflets of the aortic valve are enlarged and the valve is dysmorphic similarly to *Mib1^{flox};Nkx2.5-Cre* hearts (Fig. 11 B).

The consequences of *Mlb1* inactivation on ventricular and valvular development is most likely what causes *Mib1^{flox};Nkx2.5-Cre* death at perinatal stages.

Migrating neural crest is present in *Mib1^{flox};Nkx2.5-Cre* mice

Neural crest is crucial for valve cushion formation and septation of the OFT (Kirby et al., 1983, Jiang et al., 2000). It has been described in *DNMAML;Isl1-Cre* mice that the absence of the neural crest-derived mesenchymal cells produces enlarged OFT leaflets similar to those observed in the *Mib1^{flox};Nkx2.5-Cre* mice (High et al., 2009, Jain et al., 2011).

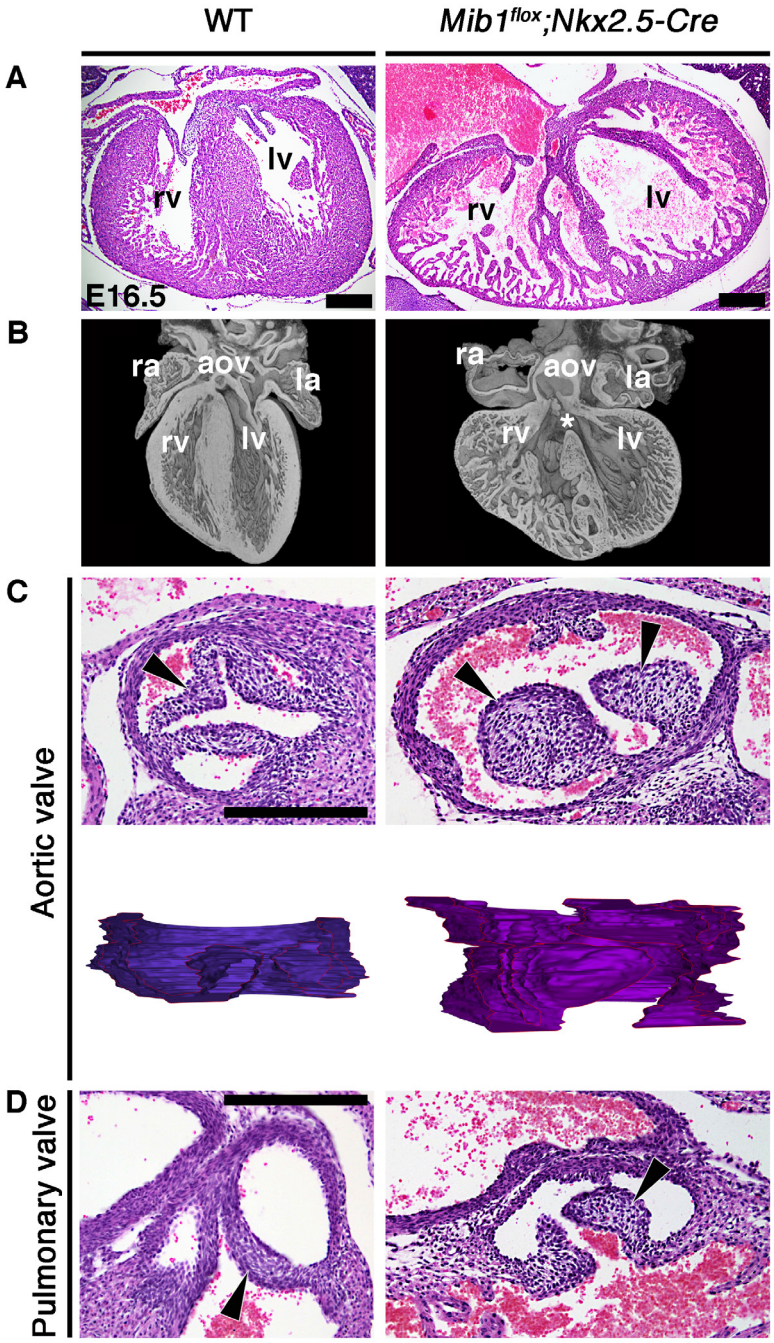

Figure 10. Inactivation of *Mib1* in the endocardium and myocardium with the *Nkx2.5-Cre* line produces dysmorphic OFT valves.

(A, C, D) Transverse sections of wild-type (WT) and *Mib1^{flox};Nkx2.5-Cre* at E16.5, (A) showing the ventricles and (C top, D) details of aortic and pulmonary valve. (B) 3D episcopic reconstruction of the hearts in (A). (C bottom) 3D reconstruction of the transverse sections in (C top). (A, B) *Mib1^{flox};Nkx2.5-Cre* heart is dilated, presents prominent trabeculae in the light of the ventricles, the compact area of the ventricular wall is thinner and show a ventricular septum defect (asterisk). (C, D) aortic and pulmonary valve leaflets are enlarged (arrowheads) and misaligned as shown by the 3D reconstruction in *Mib1^{flox};Nkx2.5-Cre* mice. Scale bar=200um. rv, right ventricle; lv, left ventricle; ra, right atrium; la, left atrium; aov, aortic valve.

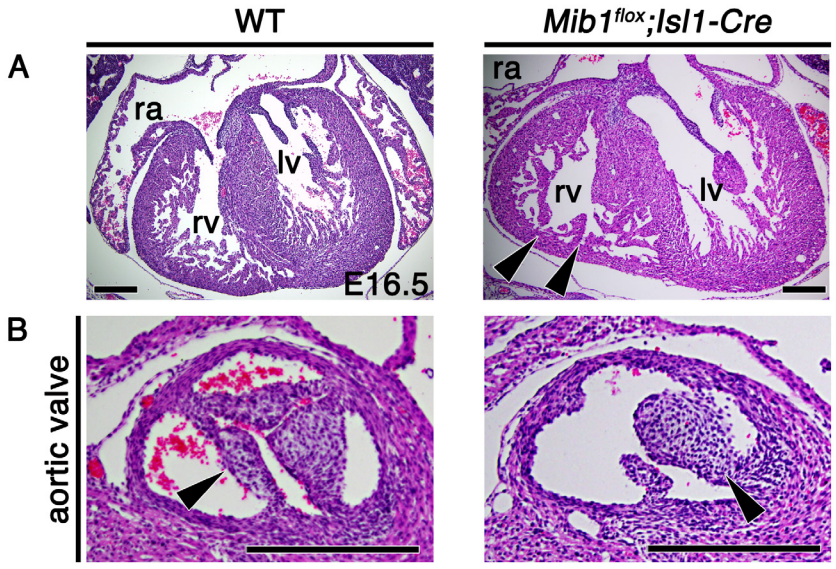

Figure 11. Deletion of *Mib1* in the specifically in the SHF produces dysmorphic OFT valves.

(A, B) Transverse sections of wild-type (WT) and *Mib1^{flox};Isl1-Cre* at E16.5, (A) showing the ventricles and (B) details of aortic valve. (A) *Mib1^{flox};Isl1-Cre* heart shows abnormal trabeculation in the right ventricle (arrowheads). (B) aortic and pulmonary valve leaflets are enlarged (arrowheads) and misaligned. The phenoptype observed in the valves is very similar to that observed in *Mib1^{flox};Nkx2.5-Cre* mice. Scale bar=200um. rv, right ventricle; lv, left ventricle; ra, right atrium.

These mice show a reduction of apoptosis at the time of valve morphogenesis and septation resulting in enlarged leaflets (Jain et al., 2011). Notch plays an important role in the migration of neural crest cells into the heart (High et al., 2007, High et al., 2009) thus we assayed the presence of the migrating neural crest in the OFT of *Mib1^{flox};Nkx2.5-Cre* mice (Fig. 12). Expression of neural crest markers *PlexinA2* (Fig.12 A), *Sema3C* (Fig. 12 B) and AP2α (Fig. 12 C) is present in the endocardial cushions of the OFT of *Mib1^{flox};Nkx2.5-Cre* mice at E11.5, indicating that the neural crest has migrated into the developing cushions of the OFT, and therefore it is not the cause of the dysmorphic OFT valves.

Notch regulates BMP signalling during valve morphogenesis

Bmp6 and *Bmp7* are expressed in the OFT leaflets and are necessary for their formation (Kim et al., 2001). For this reason we analysed the expression of BMP molecules in the maturating OFT (Fig. 13). By *in situ* hybridization we can observe an up-regulation of *Bmp6* in the mesenchyme of the aortic valve (Fig. 13 A) and a down-regulation of *Smad6*, a negative regulator of the BMP signalling pathway (Fig. 13 B). To assess the activation of BMP signalling we used an antibody specific for the phosphorylated proteins Smad1/5/8. Phosphorylation of SMAD proteins is a read-out of BMP signalling activation (Massague et al., 2005, van Dijk et al., 2012) and in the dysmorphic valves of *Mib1^{flox};Nkx2.5-*

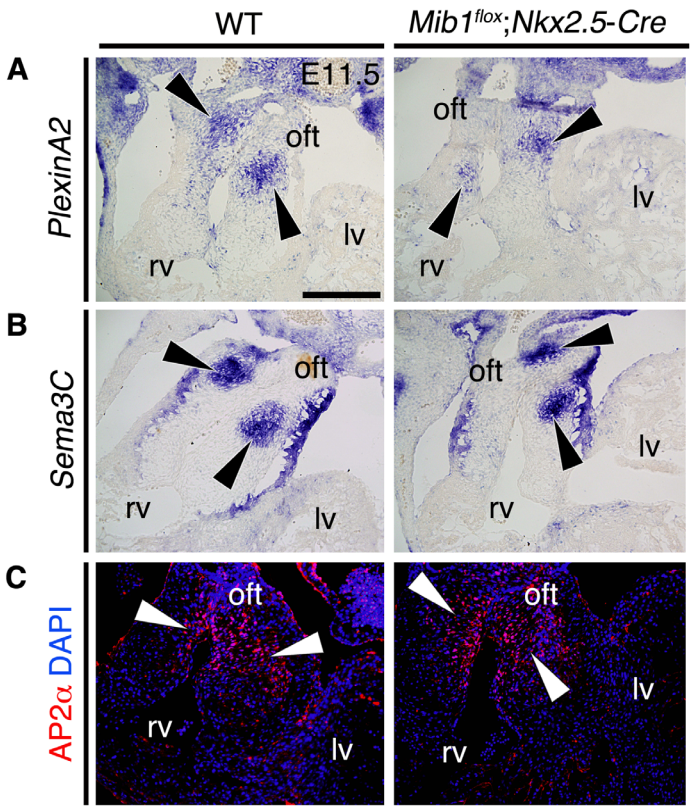

Figure 12. Neural crest is not responsible for the dysmorphic valve phenotype.

(A-C) Transverse sections of wild-type (WT) and *Mib1^{flox};Nkx2.5-Cre* at E11.5 hearts showing details of the OFT. (A,B) In situ hybridization. (C) Immunohistochemistry. Post migratory neural crest is present in *Mib1^{flox};Nkx2.5-Cre* mice as shown by staining of different neural crest markers (arrowheads); (A) *PlexinA2*, (B) *Sema3C* and (C) AP2a. Scale bar=200um. oft, outflow tract; rv, right ventricle; lv, left ventricle.

Cre we observe an increased P-Smad1/5/8 expression in the mesenchyme of the valves (Fig. 13 C). The increase of mesenchymal phosphorylated SMADs confirms the excess of BMP signalling in the *Mib1^{flox};Nkx2.5-Cre* valves.

The increased BMP signalling activity together with the large valve leaflets observed suggested affected cellular proliferation in *Mib1^{flox};Nkx2.5-Cre mice*. BMP signalling has been related to proliferation during heart development (Chen et al., 2004). Analysis of BrdU incorporation in the valves revealed and increased proliferation rate (10%) of the mesenchymal cells in the leaflets of *Mib1^{flox};Nkx2.5-Cre mice* (Fig. 13 D). The larger size of the OFT leaflets is probably due to the increased in mesenchyme cellular proliferation. This larger leaflet size is most likely the reason why they appear misaligned, as they do not fit in the aortic ring.

Notch is active in the endocardium of the maturing OFT valves (Del Monte et al., 2007), but the increased proliferation caused by the up-regulation of BMP signalling occurs in the mesenchyme, suggesting that *Mlb1* inactivation may exert a non-cell autonomous effect in valve mesenchyme.

Together, these results suggest that Notch is crucial for the maturation of OFT valves.

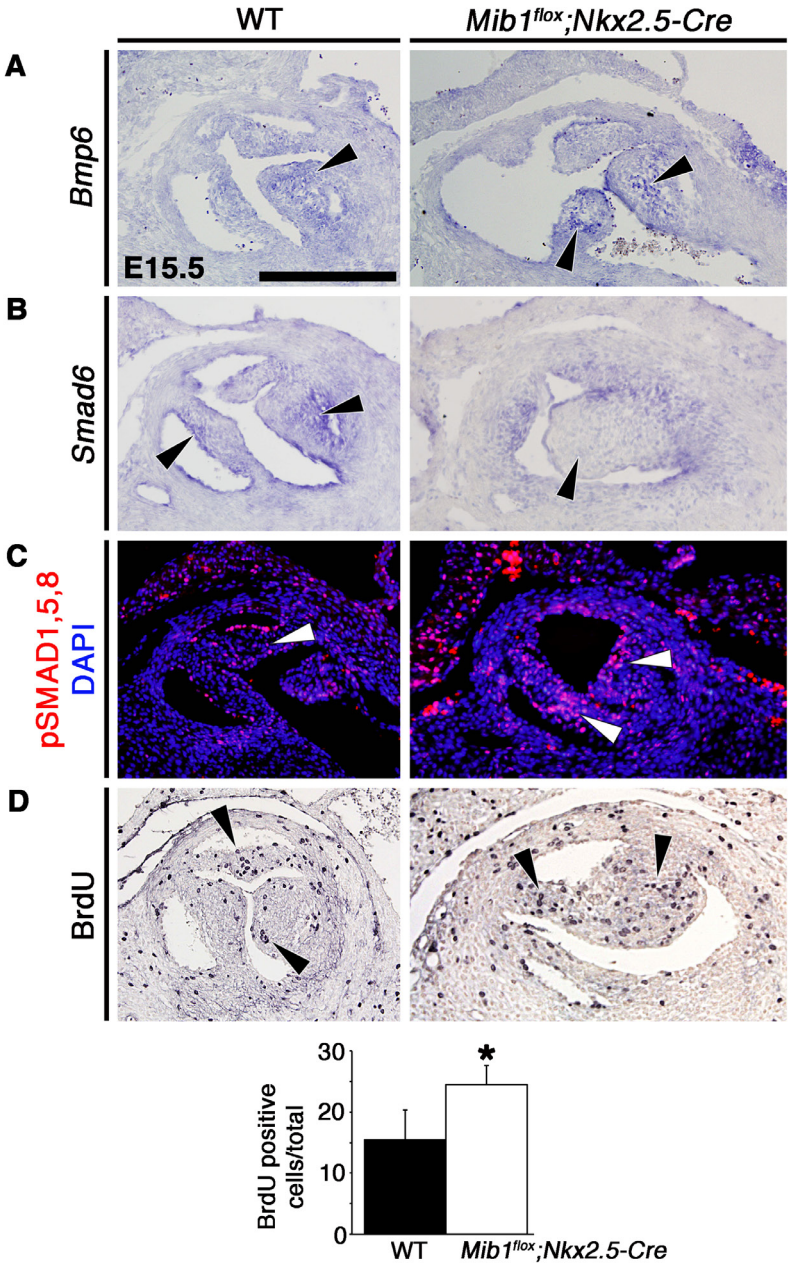

Figure 13. *Mib1* inactivation produces a BMP signalling deregulation and increased cellular proliferation.

(A-D) Transverse sections of wild-type (WT) and *Mib1^{flox};Nkx2.5-Cre* hearts showing details of aortic valve. (A, B) In situ hybridization. (C, D) Immunohistochemistry. BMP signalling is up-regulated in *Mib1^{flox};Nkx2.5-Cre*. (A) *Bmp6* is up-regulated (arrowheads). (B) *Smad6*, a negative regulator, down-regulated (arrowheads). (C) Phosphorylation of SMAD proteins 1, 5 and 8, readout of BMP up-regulation, is increased (arrowheads). (D) There is a reduction of cellular proliferation in the mesenchyme of the valve leaflet as shown by immunostaining of incorporated BrdU after a 1-h pulse at E15.5, with details of the aortic valve shown (top). Arrowheads indicate BrdU-positive nuclei. The ratios of BrdU-positive to total nuclei (bottom) reveal significantly reduced proliferation in the mesenchyme of *Mib1^{flox};Nkx2.5-Cre* OFT valves. n = 3 embryos per genotype. *P < 0.05 by Student's t test. Data are the means ± s.e.m. Scale bar=200um.

Once the endocardial cushions have been formed and they need to be remodelled, Notch regulates BMP signalling and cellular proliferation in a non-cell autonomous fashion.

Jag1 and Dll4 are expressed in the endocardium of the OFT. Deleting Mib1 with the Nkx2.5-Cre driver disrupts signalling of both ligands, so we cannot discard that Dll4 has a role to play after EMT in valve development. In the case of the dysmorphic OFT valves, we cannot dissect if the phenotype is caused by the abrogation of the signal by Dll4 or Jag1 or if both ligands are important for valve maturation.

Mib1 deletion in the myocardium causes LVNC

To determine the role of the ligand (-s) signalling from the myocardium, *Mib1* was deleted in in the myocardium with the *cTnT-Cre* line (Jiao et al., 2003). The ligand expressed in the myocardium is Jag1 (Fig. 6 C). Mib1-mediated genetic inactivation of the myocardial signal produces a reduction of Notch1 activation in the endocardium (Fig. 6 E). *Mib1^{flox};cTnT-Cre* mice are viable but show a striking embryonic foetal phenotype (Fig. 14). Although these mice are viable there is a reduction of survival after E15.5 when the observed mutant percentage goes from around 25% to only around 14% after birth (Table 2).

The histological examination and 3D episcopic reconstruction (Mohun and Weninger, 2011) of the histological sections at E16.5 showed that mutants have a dilated heart with thin compact myocardium and large, non-compacted trabeculae protruding toward the light of the ventricle and defects in the ventricular septum (Fig. 14 A-D). The same features can be observed in newborn mice. WT newborn mice show an already well compacted myocardium while the *Mib1^{flox};cTnT-Cre* littermates have large trabeculae in the left and right ventricles. The defects in the septum can still be observed and fibrotic areas are present around those defects (Fig. 14 D). These mice show the same ventricular phenotype as the *Mib1^{flox};Nkx2.5-Cre* (Fig 10). In the case of the *Mib1^{flox};cTnT-Cre,* only myocardial ligand signalling is compromised and thus, there is no OFT phenotype and mutant mice are viable and reach adulthood, allowing us to study the *Mib1*

		Mib1$^{flox/flox}$; cTnT-Cre/+	***Mib1$^{flox/+}$; +/+***	***Mib1$^{flox/+}$; cTnT-Cre/+***	***Mib1$^{flox/flox}$; +/+***
E9.5	58	16 (27.58%)	13 (22.41%)	16 (27.58%)	13 (22.41%)
E10.5	71	20 (28.16%)	16 (22.53%)	19 (26.76%)	16 (22.53%)
E11.5	193	43 (22.27%)	57 (29.53%)	46 (23.83%)	47 (25.35%)
E13.5	67	11 (16.41%)	19 (28.35%)	19 (28.35%)	18 (26.86%)
E14.5	93	20 (21.50%)	22 (23.65%)	24 (25.80%)	27 (29.03%)
E15.5	168	43 (25.59%)	42 (25%)	47 (27.97%)	36 (21.42%)
E16.5	115	22 (19.13%)	24 (20.86%)	41 (35.65%)	28 (24.34%)
P3	48	7 (14.58%)	15 (31.25%)	12 (25%)	14 (29.16%)
TOTAL	813	182 (22.38%)	208 (25.58%)	224 (27.55%)	199 (24.47%)
Expected		25%	25%	25%	25%

embryos dissected (percentage observed)

Table 2. *Mib1^{flox};cTnT-Cre* lethality table

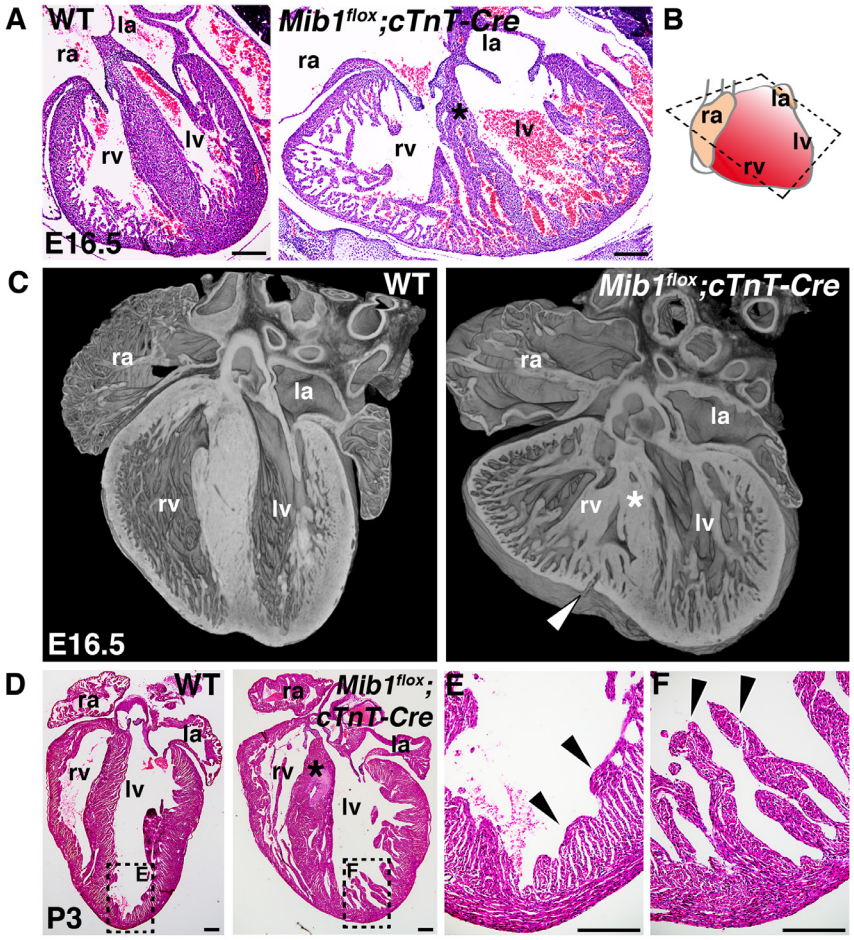

Figure 14. *Mib1* inactivation in the myocardium produces LVNC.

Transverse sections of wild-type (WT) and *Mib1*^{flox}*;cTnT-Cre* hearts. (A) Sections at E16.5. *Mib1*^{flox}*;cTnT-Cre* mutant heart is dilated, has large trabeculae, the compact myocardium is thinner than in the WT and presents abnormal ventricular septum (asterisk). (B) Scheme showing the plane of histological sections in (A, D). (C) Episcopic 3D reconstruction of (A) where the abnormal septum (asterisk) and the very thin compact wall (arrowhead) are very evident. (D) Heart sections from P3 mice. The myocardium in WT mice is almost fully compacted (D, enlarged in E, arrowheads); in contrast, hearts from *Mib1*^{flox}*;cTnT-Cre* mutants have very large trabeculae (D, enlarged in F, arrowheads). Asterisks indicate abnormal ventricular septum in the mutants. Scale bar=200um. ra, right atrium; la, left atrium; rv, right ventricle; lv, left ventricle.

ventricular phenotype. The non-compaction phenotype observed during development in the embryo and after birth in the newborn is maintained and can be observed later in adult mice.

Echocardiographic analysis of adult mice revealed prominent trabeculations and deep intertrabecular recesses in the mutants (Fig. 15 A and Videos 1 and 2. ep, epicardium; en, endocardium, prominent trabecules marked with asterisk). Measuring the ratio of non-compacted myocardium and compacted myocardium revealed that the mutant mice had a non-compaction index of 2.0 (Fig. 15 B). A non-compaction index equal or larger than 2.0 is a diagnostic landmark for LVNC (Jenni et al., 2001, Stollberger et al., 2002). In addition to all the structural defects mentioned above,

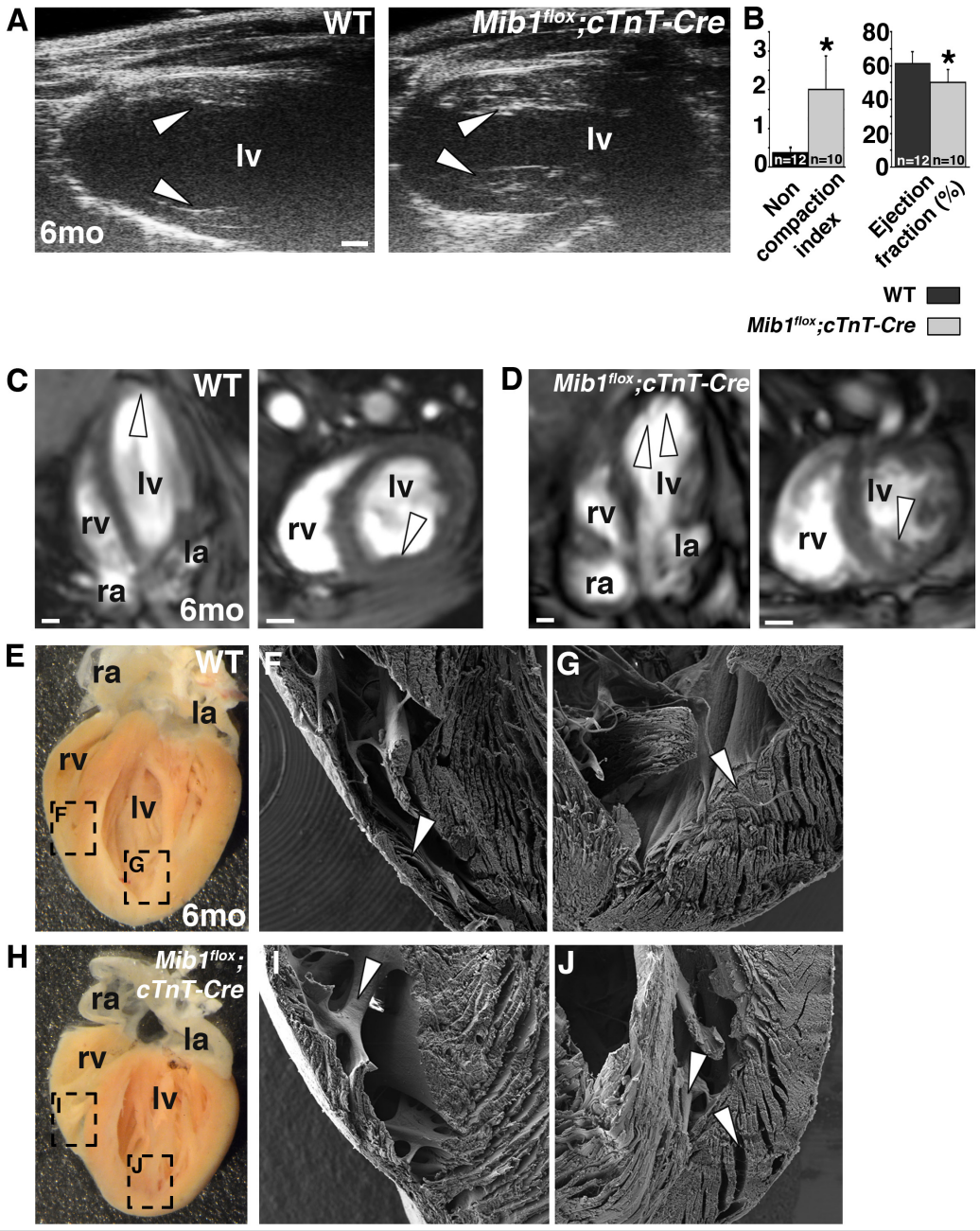

Figure 15. Adult mice LVNC phenotype.

(A) Echocardiography analysis in 6-month-old wild-type (WT) and *Mib1^{flox};cTnT-Cre* mice. Arrowheads indicate the smooth endocardial surface in the WT heart. Note the thickened and irregular endocardial layer in the mutant heart. Scale bar, 1 mm. (B) Non-compaction index and ejection fraction in hearts of 6-month-old WT and *Mib1^{flox};cTnT-Cre* mice. *P < 0.05 determined by Student's t test. Data are the mean ± s.e.m. (C,D) CMRI in 6-month-old WT and *Mib1^{flox};cTnT-Cre* mutant mice. Images show four-chamber (4c) and short axis (sa) views. Scale bars, 1 mm. Arrowheads indicate the smooth ventricular surface (C) or prominent trabeculae in ventricular lumens (D). (E-J) Scanning electron microscopy of 6-month-old WT and *Mib1^{flox};cTnT-Cre* hearts showing details of right ventricle (F, I) and left ventricle (G, J). Arrowheads show the trabeculae in the chamber (I, J) and the compacted myocardium (G) compared to the deep intertrabecular recesses in mutant hearts (J). rv, right ventricle; lv, left ventricle; ra, right atrium; la, left atrium.

myocardium at these stages, suggesting that the Mib1 phenotype was due, at least in part, to impaired Jag1-dependent signalling.

The structural and functional features observed in the *Mib1flox;cTnT-Cre* hearts reproduce the features associated to the human LVNC cardiomyopathy, suggesting that *Mib1^{flox};cTnT-Cre* may be a mouse model to study this disease.

Human *MIB1* mutations cause LVNC

We next examined whether mutations in human *MIB1* are associated with clinical LVNC. Sequencing of the 20 coding exons of *MIB1* in a cohort of 100 individuals of Southern European ancestry (Spanish) with LVNC identified two mutations. The two mutations were found in familial cases of LVNC; in this study 48% of the LVNC cases analysed were familial.

One mutation identified in a proband with inherited LVNC is a heterozygous G>T transversion of nucleotide 2827 in exon 20 of *MIB1,* which predicts a change in amino acid 943 from valine to phenylalanine (V943F, present in proband 1.III.1; Fig. 16 A-E). Val943 is located within a coiled-coil region separating the three ring-finger domains that mediate protein-protein interactions and comprise the site of MIB1 ubiquitin ligase activity (Barsi et al., 2005) (Fig. 16 A) *In silico* modelling with PolyPhen-2 (Adzhubei et al., 2010) of the effect of the V943F mutation on MIB1 structure and function gave out a score of 0.675. This means that the mutation of this residue in the protein would have a potentially deleterious effect. *In silico* reconstruction of the MIB1 protein structure suggested that the phenylalanine aromatic ring could disrupt the tertiary structure of the ring-finger region (Fig. 16 C). Phylogenetic analysis (Fig. 16 D) and the high genetic evolutionary rate profiling (GERP) score (Davydov et al., 2010) of Val943 (5.67) indicated that this amino acid is under selective constraint.

Genotyping of other family members of the proband tracked the mutation back three generations (Fig. 16 E) and showed that it occurred only in LVNC-affected individuals within the family.

The second mutation that we identified is a heterozygous C>T transition of nucleotide 1587 in *MIB1* exon 11, which predicts a premature stop codon instead of arginine at position 530 in the MIB1 ankyrin repeats region (R530X, present in proband 2.II.1; Fig. 16 A, F, G). We tracked this mutation back through two generations of LVNC-affected individuals (Fig. 16 G).

The inheritance pattern observed in both families was autosomal dominant and the disease phenotype was highly penetrant being present in all the members of the families that carried the mutation.

After comparing all the individuals carrying either one or the other mutation and with LVNC to a cohort of healthy volunteers (Table 3) we observed that there is a perfect correlation of genotype and phenotype. All the patients carrying MIB1 mutations fulfilled at least one the criteria to diagnose LVNC. It is interesting to note that there are no differences in these families related to sex or age of the patients.

To rule out the presence of other mutations in the patients we analysed the DNA of the two families and sequenced *MHY7*, *MYBPC3*,

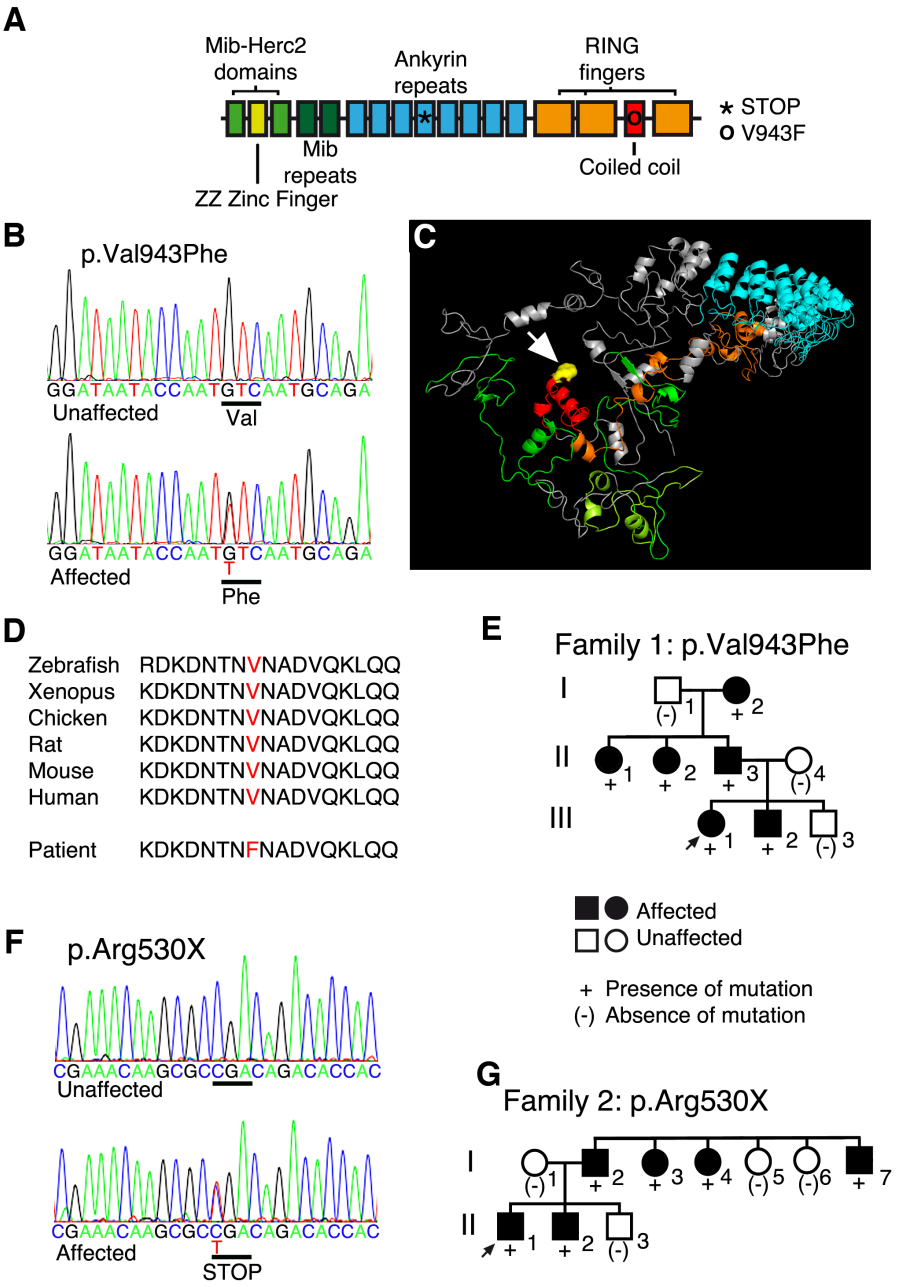

Figure 16. Mutations in human *MIB1* cause LVNC.

(A) Schematic of MIB1 domain structure. A valine-to-phenylalanine missense mutation (V943F) is located in the ring-fingers domain of MIB1 and was found in one patient with LVNC from family 1 (open circle). A premature stop codon mutation (R530X) is located in the ankyrin repeats region and was found in another affected family, family 2 (asterisk). (B) Sequence chromatogram of unaffected and affected members of family 1. Val, valine; Phe, phenylalanine. (C) In silico model of the MIB1 monomer; color code as in (A). The aromatic ring of the phenylalanine residue (yellow, arrow) probably affects the tertiary structure of this domain. (D) Evolutionary conservation of Val943. (E) Occurrence of the V943F mutation and LVNC in family 1 over three generations. Members of each generation are indicated numerically; squares, males; circles, females. The proband is indicated by an arrow. (F) Sequence chromatograms of unaffected and affected members of family 2 showing the position of the R530X mutation. (G) Occurrence of R530X and LVNC in family 2 over two generations.

TNNT2, *TNNI3*, *TPM1*, *ACTC*, *MYL2*, *MYL3*, *TNNC*, *G4.5*, *LDB3* and *LMNA*, candidate genes implicated in LVNC (Captur and Nihoyannopoulos, 2010, Ichida, 2009) and no mutation was found in any of the two families. As a control a group of 263 healthy individuals from Spain was sequenced and none presented any of the two mutations indicating that they were not common single nucleotide polymorphisms (SNPs). The fact that the mutations are not SNPs and that the families only present one gene mutated indicates that this two *MIB1 de novo* mutations are the cause for the LVNC in these patients.

Human LVNC phenotype associated to *MIB1* mutations

The proband with the V943F mutation (1.III.1) underwent heart transplantation, and pathological examination of her heart revealed evident signs of LVNC. The persistent trabeculation is obvious in the two ventricles especially in the left ventricle where the non-compacted layer is almost as thick as the compacted one (Fig. 17 A).

Four- and two-chamber CMRI views of the hearts of the fathers of the two probands (1.II.3 and 2.I.2; Table 3) revealed prominent trabeculations that were not present in the heart of an unaffected subject (Fig. 17 B and Videos 7–12). The short-axis views revealed marked trabeculations in the right ventricles as well (Fig. 17 B and Supplementary Videos 13–15) consistent with the histopathological analysis of the heart of the transplanted individual. The phenotype observed in the human patients of LVNC is similar to the phenotype that we have observed in the *Mib1^{flox}; cTnT-Cre* mice (Fig. 14, 15).

Western blot analysis of peripheral blood from patients 1.II.3 and 2.I.2 revealed approximately 8% and 20% reductions, respectively, in MIB1 expression compared to control samples (Fig. 17 C. D). We did not detect the predicted truncated MIB1 form generated by the R530X mutation (Fig. 16 D) suggesting that the mutant mRNA might be degraded by nonsense-mediated decay (NMD) (Frischmeyer et al., 2002).

We next analysed N1ICD expression in

Figure 17. LVNC patients with *MIB1* mutations have reduced expression of N1ICD, *DTX1* and *GATA3*.

(A) Sections of a structurally normal heart and the heart of the proband from family 1 (1.III.1; Fig. 15), who has the V943F mutation. Arrowheads indicate the compacted myocardium in the control heart and the non-compacted myocardium in the proband's heart. Scale bars, 10 mm. Rv, right ventricle; lv, left ventricle. (B) CMRI sections of hearts showing four-chamber (4c), two-chamber (2c) and short axis (sa) views comparing images of a control heart (in an individual without the *MIB1* mutation) with images of the heart of subject 1.II.3, who has the V943F *MIB1* mutation, and images of the heart of subject 2.I.2, who has the R530X *MIB1* mutation. Arrowheads indicate the trabeculae, which are prominent in the ventricles of the individuals with MIB1 mutations. Scale bars, 50 mm. (C–E) Western blots of MIB1 and N1ICD in lymphocytes from the blood of three healthy donors (C1–C3) and subjects 1.I.2, 1.II.3, 1.III.2, 2.I.4, 2.II.1 and 2.I.7. Densitometric quantification of the protein expression shows low MIB1 expression (C,D) and a parallel reduction in NOTCH activity (E,F). Data are the mean ± s.e.m. (G) Quantitative real-time RT-PCR analysis of the expression of *DTX1* and *GATA3* expression relative to that of *GUSB* in the subjects analyzed in (E). *P < 0.05 determined by Student's t test. Data are the mean ± s.e.m.

peripheral blood samples from groups of three patients carrying the V943F mutation (1.I.2, 1.II.2 and 1.III.2) or the R530X mutation (2.I.4, 2.II.1 and 2.I.7). Both groups showed a significant reduction of about 50% of N1ICD expression compared with unaffected subjects (Fig. 17 E, F). We also analysed white blood cells from these patients for the expression of NOTCH targets specific for developing human T lymphocytes: *DTX1, GATA3, HES1, NOTCH3, NRARP, TCF7, HEY1* and *c-MYC (Van de Walle et al., 2009).* The expression of DTX1 and GATA3 was lower in both groups of patients compared with unaffected subjects (Fig. 17 G) Together these data indicate that both of the *MIB1* mutations affect NOTCH signalling.

To further investigate the effect of the mutations on *MIB1* expression and what happens with the truncated mRNA, we synthesized cDNA from the peripheral blood of patients 1.I.2, 1.II.3 and 1.III.2 (all with

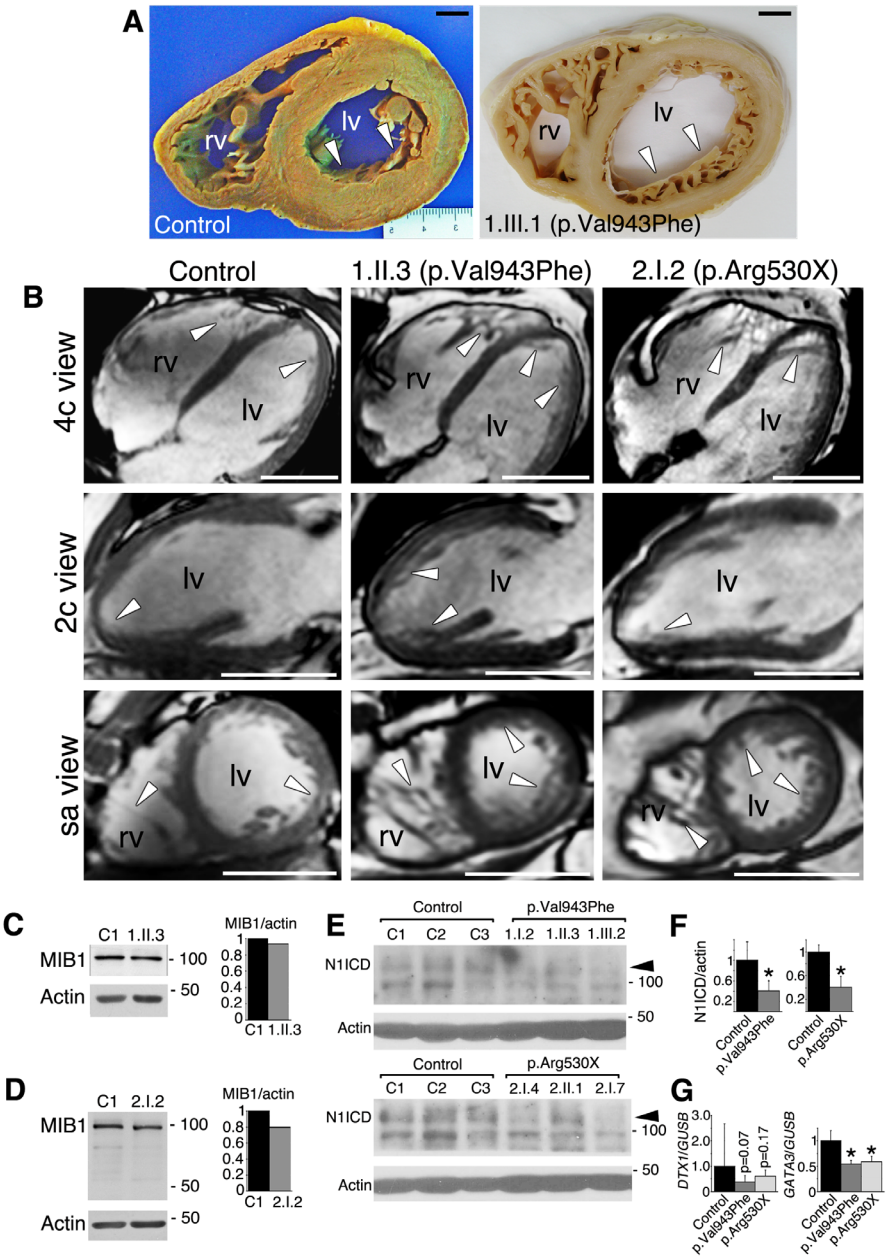

ECHOCARDIOGRAPHY

LVNC								Outcome
Case	Sex	Age	LVEDd	LVEF%	ECG	ECHO VISUAL		
1.I.2	1	70	45(91%)	50	Normal	Mild trabeculations, LV hypertrophy		Under surveillance
1.II.1	1	42	44(100%)	57	Normal	LV apical muscular band		Under surveillance
1.II.2	1	35	45(101%)	57	Normal	Not definitive		Under surveillance
1.II.3	0	48	55(110%)	55	Normal	Trabeculated RV and LV plus small apical pseudoaneurysm		Under surveillance
1.III.1	1	14	59/136%)	25	Abnormal, RBBB, LAH	LVNC		Heart transplant
1.III.2	0	8	37(97%)	59	Normal	LV cleft and striking RV, mild trabeculated LV		Under surveillance
2.I.2	0	55	52(104%)	48	Mild abnormalities (low voltage QRS)	Hypertrabeculated RV, mild trabeculated LV		Under surveillance
2.I.3	0	71	53(108%)	55	Abnormal (AF, RBBB, low voltage QRS)	Borderline LV wall thickness (difficult to evaluate due to severe obesity. CMRI not possible)		Under surveillance
2.I.4	0	65	46(94%)	55	Abnormal	LV hypertrophy (difficult to evaluate due to severe obesity. CMRI not possible)		Under surveillance
2.I.7	0	53	45(91%)	52	Abnormal ((-) T wave V1-V3)	Mild LV hypertrophy		Under surveillance
2.II.1	0	17	71(125%)	29	Abnormal (AF, Q wave V1-V3, rS V5-V6)	LVNC		Severe heart failure
2.II.2	0	23	59(99%)	55	Mild abnormalities (Low voltage QRS)	LV apical muscular band		Under surveillance

LVEDd: left ventricular end-diastolic dimension (mm) and % predicted (Henry formula). LVEF (%): left ventricular ejection fraction (%). AF: atrial fibrillation. RBBB: Right bundle branch block. LAH: left anterior hemi-block.
1.I.2, 1.II.1, 1.II.2, 1.II.3, 1.III.2, 2.I.2, 2.I.7, and 2.II.2 individuals were examined by CMRI. See below.

CMRI

LVNC																										
Case	Sex	BSA	LVEDV	LVEDI	LVESV	LVESI	LVEF	LVSV	C LV mass	C LV mass indexed	G LV mass	T LV mass	T LV mass indexed	% T mass of LV	NC SAX	CSAX	NC/C SAX	medial ST	mid RV WT
1.I.2	1	1,83	83,00	45,46	28,35	15,53	65,84	54,65	65,57	35,91	90,34	24,77	13,57	27,42	9,35	2,74	**3,41**	6,63	7,07
1.II.1	1	1,56	124,93	80,14	46,57	29,87	62,72	78,36	56,53	36,26	86,48	29,95	19,21	34,63	17,00	4,25	**4,00**	6,43	4,39
1.II.2	1	1,56	134,86	86,26	50,50	32,30	62,56	84,36	55,67	35,61	85,50	29,83	19,08	34,89	8,97	4,33	**2,07**	6,31	4,78
1.II.3	0	2,11	148,74	70,49	62,30	29,53	58,12	82,14	114,73	54,37	143,74	29,01	13,75	20,18	8,66	4,01	**2,16**	8,13	5.23
1.III.1	1	TRANSPLANTED																	
1.III.2	0	1,00	101,93	101,68	34,09	34,01	66,57	67,84	50,26	50,13	65,47	15,21	15,17	23,23	5,38	3,87	**1,39**	2,88	11,20
2.I.2	0	2,16	144,21	66,76	59,99	27,77	58,40	84,22	109,19	50,55	159,17	49,98	23,14	31,40	12,82	5,05	**2,54**	6,58	5,25
2.I.7	0	2,10	144,91	69,12	58,63	27,96	59,54	86,28	72,27	34,47	111,92	39,65	18,91	35,43	12,66	4,60	**2,75**	6,98	6,4
2.II.1	0	SEVERE HEART FAILURE																	
2.II.2	0	2,33	184,77	79,17	85,69	36,71	53,62	99,08	99,77	42,75	155,43	55,66	23,85	35,81	11,83	4,03	**2,94**	6,97	6,33

CONTROLS																			
Case	Sex	BSA	LVEDV	LVEDI	LVESV	LVESI	LVEF	LVSV	C LV mass	C LV mass indexed	G LV mass	T LV mass	T LV mass indexed	% T mass of LV	NC SAX	CSAX	NC/C SAX	mid ST	mid RV WT
1	0	2,37	284,60	120,08	105,40	44,47	62,97	179,00	174,08	73,45	205,74	31,66	13,36	15,39	6,76	5,47	**1,24**	9,47	2,28
2	1	1,69	130,77	77,38	46,79	27,69	64,22	83,39	67,79	40,11	82,94	15,15	8,96	18,27	10,25	6,69	**1,53**	7,90	2,45
3	0	1,84	153,68	83,52	57,53	31,27	62,57	96,15	91,75	49,86	101,44	9,69	5,27	9,55	5,44	5,01	**1,09**	9,39	3,46
4	0	1,77	162,35	91,72	57,55	32,51	64,55	104,80	92,69	52,37	103,96	11,27	6,37	10,84	6,95	5,40	**1,29**	8,57	2,34
5	0	2,00	166,93	83,47	57,76	28,88	65,40	109,16	98,10	49,05	110,90	12,80	6,40	11,54	6,79	5,46	**1,24**	9,25	3,99
6	0	1,78	190,24	106,88	74,31	41,75	60,94	115,93	128,11	71,97	142,95	14,84	8,34	10,38	9,03	7,44	**1,21**	8,22	3.90
7	0	2,05	179,36	87,49	67,22	32,79	62,52	112,14	109,10	53,22	130,41	21,31	10,40	16,34	7,79	5,70	**1,37**	8,16	3.67
8	1	1,59	131,14	82,48	44,87	28,22	65,79	86,27	74,99	47,16	87,70	12,71	7,99	14,49	6,74	4,83	**1,40**	7,19	2.67
9	0	1,86	157,38	84,61	54,54	29,32	65,35	102,84	107,87	57,99	129,20	21,33	11,47	16,51	10,32	6,56	**1,57**	8,98	4,02

LEGENDS
Sex: 0 male, 1 female
BSA: Body Surface area (m^2)
LVEDV: Left ventricular end-diastolic volume (ml)
LVEDVI: Left ventricular end-diastolic volume indexed by BSA (ml/m^2)
LVESV:Left ventricular end-sistolic volume (ml)
LVESI:Left ventricular end-sistolic volume indexed by BSA (ml/m^2)
LVEF: Left ventricular ejection fraction (%)
LVSV: Left ventricular stroke volume (ml)
Compacted LV mass: LV mass including papillary muscles an excluding trabeculations (g)
Compacted LV mass Indexed: Compacted LV mass indexed by BSA (g/m^2)
Global LV mass: LV mass including papillary muscles and trabeculations (g)
Trabeculated LV mass: Global LV mass - Compacted LV mass (g)
Trabeculated LV mass Indexed: Trabeculated LV mass indexed by BSA (g/m^2)
% Trabeculated mass of LV: (Global LV mass-Compacted LV mass)/Global LV mass * 100
NC: Measurement of non compaction myocardium (mm)
C: Measurement of compacted myocardium (mm)
NC/C Ratio. **Non compaction index**
SAX: Short axis plane
RV: Right ventricle
Mid ST: medial septum thickness (mm)
Mid RV WT: Medial right ventricle wall thickness (mm)

Table 3. Features of LVNC patients harbouring *MIB1* mutations

V943F), patients 2.I.4, 2.II.1 and 2.I.7 (all with R530X) and control samples and performed quantitative real-time PCR (qPCR) using two primer pairs targeting regions 5′and 3′ to the mutation sites (Fig. 18 A). This is a common strategy used to determine the stability of mRNAs carrying premature stop codons. In the case of the V943F mutation, the two primer pairs did not detect statistically significant differences in expression of 3' and 5' PCRs compared to control *MIB1* cDNA (Fig. 17 A-C). In contrast, in the case of the R530X mutation, the 3′ primers detected significantly lower mRNA expression (Fig. 18 A, D, E) suggesting that a nonsense mediated decay (NMD) mechanism might be responsible for degrading R530X mutant mRNA. NMD is a surveillance pathway which function is to reduce errors in gene expression by eliminating mRNA with premature stop codons (Chang et al., 2007). We next amplified the cDNA regions spanning both mutations by RT-PCR and cloned the

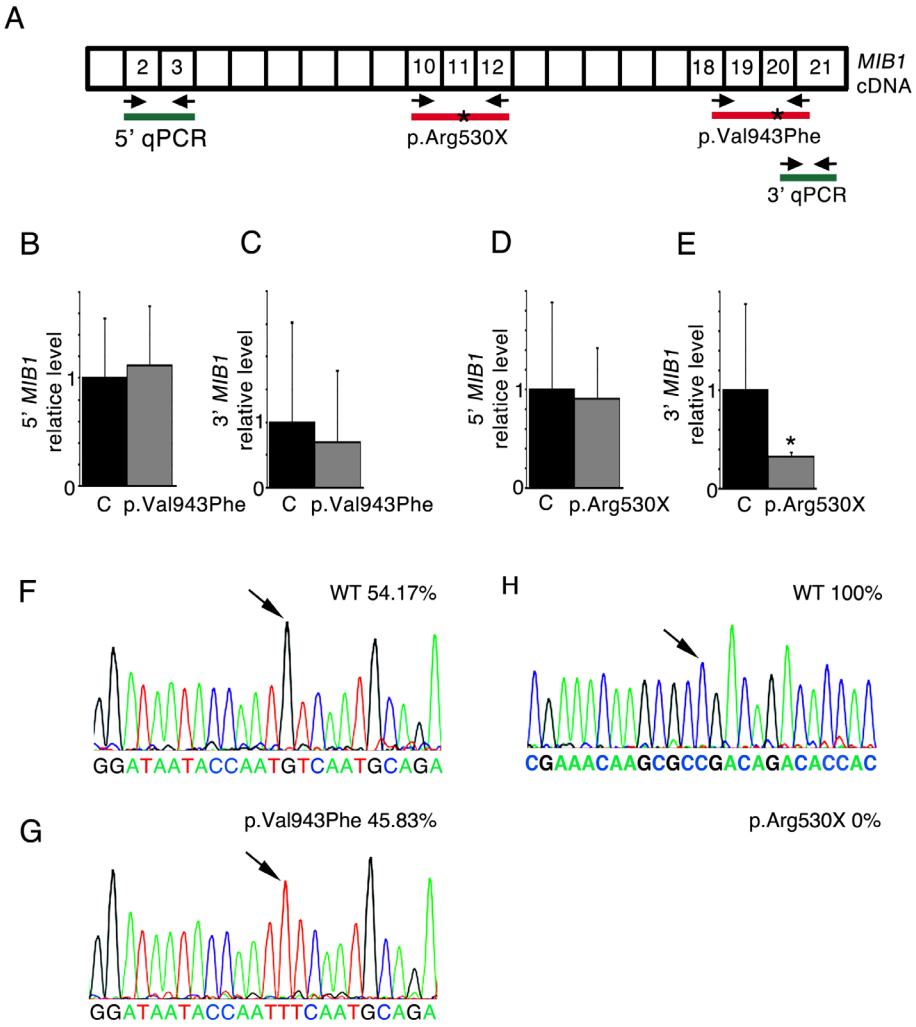

Figure 18. Effect of p.Val943Phe and p.Arg530X mutations on *MIB1* mRNA expression.

(A) Scheme of *MIB1* cDNA. PCR-amplified exons are numbered. The arrows indicate the PCR primers, green colouring the regions amplified by qPCR, and red the regions spanning the *MIB1* mutations (*) that were amplified by RT-PCR, cloned and sequenced. (B-E) qPCR analysis of lymphocytes from three control subjects and three patients. (B,C) The 5' and 3' regions of the *MIB1* cDNA are amplified at similar levels in control and patient samples, suggesting that the p.Val943Phe mutation does not significantly affect *MIB1* transcription. (D,E) In patients with the p.Arg530X mutation, the 5' region of *MIB1* is expressed at normal levels (D) but the 3' region is not (E), suggesting that the mRNA is being degraded. (F,G) Sequence chromatogram of the PCR fragments spanning the p.Val943Phe mutation. 54.17% (13 out of 24) of the clones analyzed contained a wild-type (WT) G nucleotide (F) and 45.83% (11 out of 24) a T (G), suggesting that the mutant and WT mRNA are expressed at similar levels. (H) Sequence chromatogram of the PCR fragments spanning the p.Arg530X mutation. Only the WT gene was amplified (100%).

266-bp (V943F) and 433-bp (R530X) PCR products en masse and sequenced them. Whereas V943F mutant and WT cDNAs were cloned at similar frequencies, the cDNA containing the R530X mutation was never amplified (Fig. 18 A, F-G). These confirm our hypothesis that the truncated mRNA resulting from the R530X allele is degraded by NMD.

Identified mutations disrupt MIB1 and NOTCH activity

In silico modelling supports the idea that MIB1 is a homodimer (Fig. 19 A). This modelling also indicated that the V943F mutant would alter the alignment of the ring-finger domains in heterodimers formed by WT and V943F mutant MIB1 (Fig. 19 B). The dimerization would happen anti-pairwise and situate the active domain of the monomers, responsible for the ubiquitylation of Notch ligands, close to each other. Furthermore, modelling of the docking of the MIB1-dimer ring fingers with JAG1 indicates that formation of V943F-WT dimers would distort the angle of interaction with JAG1 and thus interfere with the signalling (Fig. 19 C-F).

To test whether MIB1 forms a homodimer, we carried out co-immunoprecipitation (coIP) assays with hemagglutinin (HA)-tagged WT MIB1 and various Flag-tagged MIB1 variants: WT, V943F, R530X and a previously characterized dominant-negative mutant (M989R) (Zhang et al., 2007b). We co-transfected these tagged cDNAs in pair-wise combinations with the HA-tagged WT MIB1 cDNA into HEK293 cells. Immunoprecipitation with antibodies to Flag and western blotting with antibodies to HA detected a 100-kDa band corresponding to WT MIB1 in all immunoprecipitates, and western blotting with an antibody to Flag confirmed the presence of all Flag-tagged MIB1 variants, even the short form corresponding to the R530X mutation (Fig. 20 A). These results indicate that MIB1 forms homodimers and even the mutant forms are able to interact. Interaction between the monomers probably occurs through ankyrin repeats, as has been established for other proteins containing this domain (Sedgwick and Smerdon, 1999). Detection in the immunoprecipitate of the truncated MIB1 protein encoded by the R530X mutant cDNA is probably a result of its expression from a cDNA construct that does not undergo splicing, thereby escaping NMD. We confirmed these findings by fluorescence resonance energy transfer (FRET) using the acceptor photobleaching technique (Rodighiero et al., 2008).

Similarly to the co-IP experiments, we co-transfected HEK293 cells in pairwise combinations with the pEYFP-C1 plasmid encoding yellow fluorescent protein (YFP)-tagged WT MIB1 and the pECFP-C1 plasmid encoding cyan fluorescent protein (CFP)-tagged WT MIB1 or V943F or R530X mutant MIB1. We found that both MIB1 mutant proteins interacted with the WT protein (Fig. 21). We then transfected the various Flag-tagged mutant *MIB1* variants into HEK293 cells stably expressing murine Jag1 (Chapman et al., 2006) and carried out coIP assays. Western blot analysis with antibodies to JAG1 detected this protein in immunoprecipitates of all mutant variants (V943F, R530X and M989R) using antibodies to Flag (Fig. 20 B). The MIB1 heterodimers are able to bind normally to the Notch ligands and thus interfere with the normal signalling.

Then we tested the effect of the *MIB1* mutations on JAG1 ubiquitylation, because that is the biochemical function of MIB1 in the signalling cells of the pathway. We co-transfected HEK293 cells with JAG1, eGFP-tagged ubiquitin (Hansson et al., 2010), WT HA-tagged MIB1 and the Flag-tagged MIB1 variants (V943F, R530X or M989R). JAG1

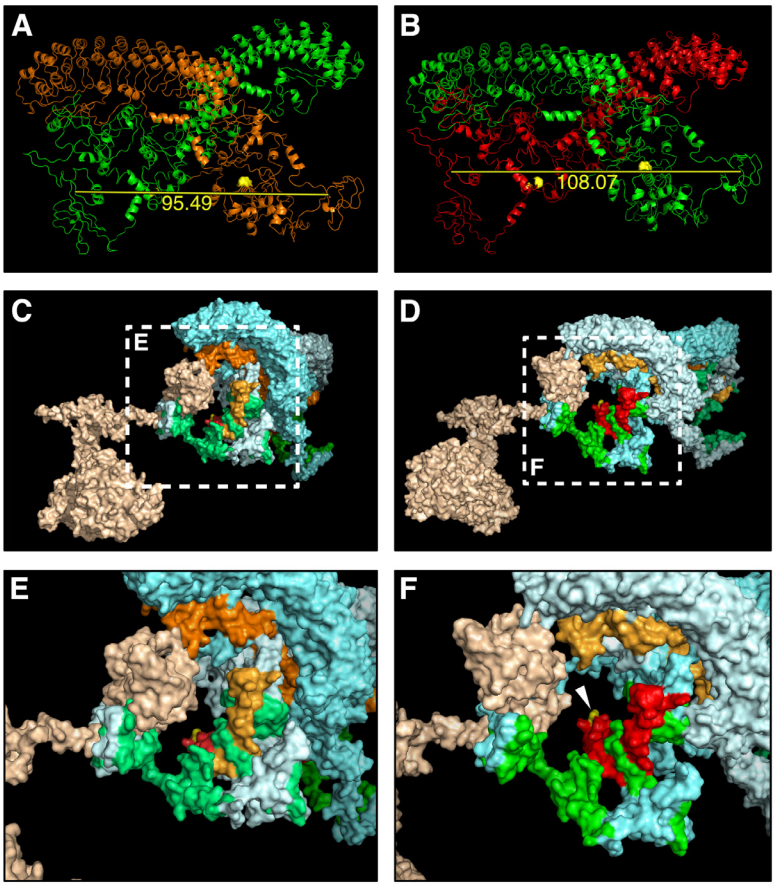

Figure 19. In silico modelling predicts that MIB1 functions as a dimer.

(A,B) Theoretical MIB1-MIB1 dimer models predicted with the Hex server. (C-F) JAG1-MIB1 docking models predicted with the ClusPro server. All protein structures were predicted with iTASSER. (A) MIB1 homodimer formed by two WT chains (green and orange). (B) MIB1 heterodimer formed by one WT MIB1 chain (green) and one p.Val943Phe MIB1 mutant chain (red). Yellow indicates 943V or 943F. The yellow bar indicates relative distance between the MIB/herc2 domains which is greater in the WT-V943 heterodimer. (C,E) Docking model for JAG1 and WT MIB1 (wheat, JAG1; cyan, MIB1; green, MIB/herc2 domains; orange, ring finger domains; red, coiled-coil domain; yellow, 943V). (D,F) Docking model for JAG1 and p.Val943Phe MIB1, showing a distorted JAG1-MIB1 angle (arrowhead) caused by the increased distance between the MIB/herc2 domains of the mutant heterodimer. (Wheat, JAG1; cyan, WT MIB1; light cyan p.Val943Phe MIB1; green, MIB/herc2 domains; orange, ring finger domains; red, coiled-coil domain; yellow, 943F).

ubiquitylation was strongly induced in cells transfected with WT MIB1 plus empty vector, but was markedly lower in cells co-transfected with WT MIB1 plus V934F or WT MIB1 plus the R530X mutant (Fig. 20 C). Thus, in this setting, the V934F and R530X mutants seem to impair MIB1 function in a dominant-negative fashion. Co-transfection of WT MIB1 and the M989R mutant cDNA yielded similarly low amounts of JAG1 ubiquitylation as the other mutations (Fig. 20 C).

To study the effect of these mutant *MIB1* variants *in vivo,* we microinjected the mutant mRNAs into *Tg(mlc2a:GFP)* zebrafish embryos, which express eGFP in cardiomyocytes in the developing heart. We compared the outcomes from these zebrafish with the reference

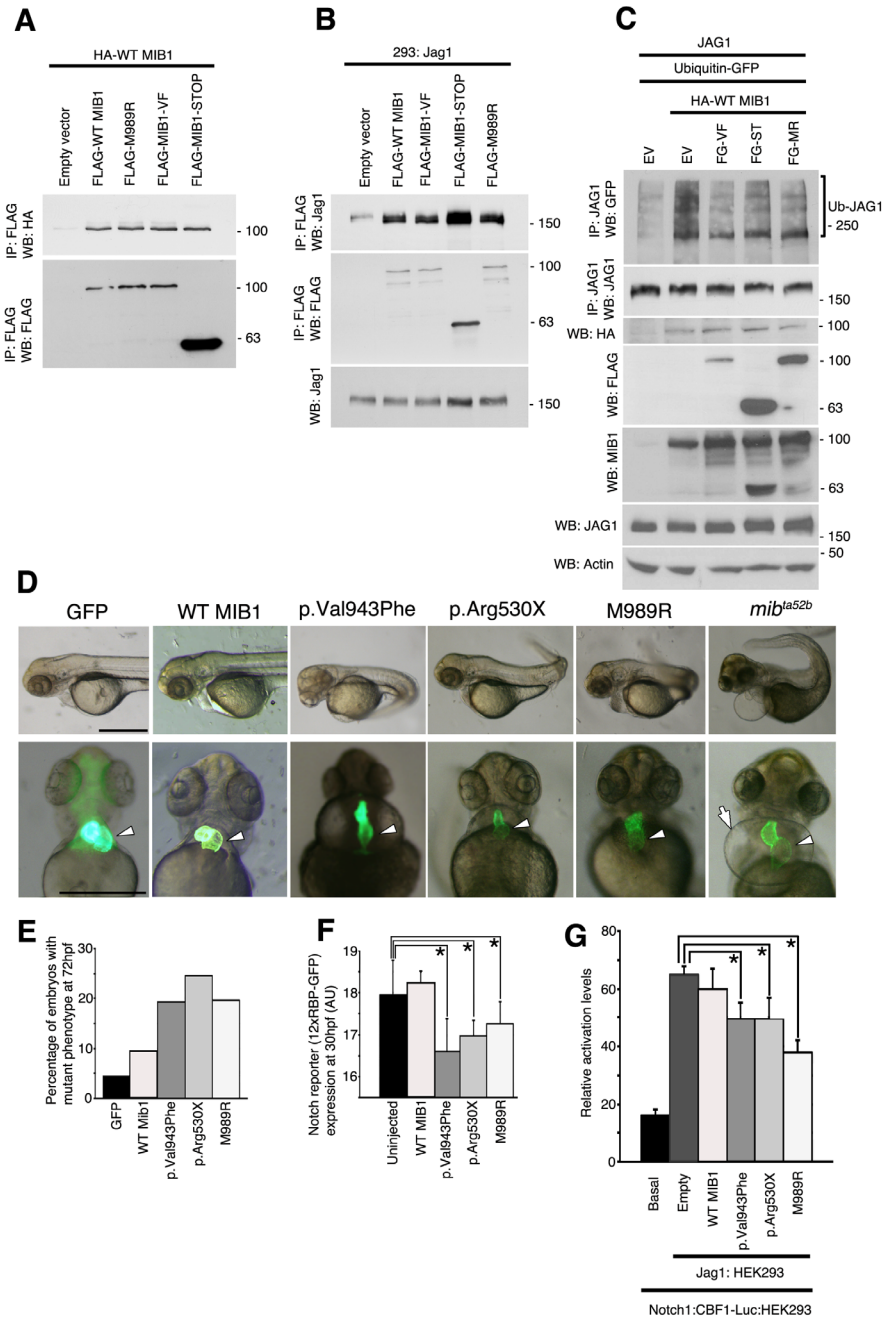

phenotype of zebrafish homozygous for the *mib1ta52b* allele, equivalent to the dominant-negative M989R mutation (Zhang et al., 2007b), which show severely defective cardiovascular development. Examination of larvae at 72 h post fertilization (h.p.f.) injected at the one- to two-cell stage with control *eGFP* mRNA revealed normal leftward looping of the two-chambered heart and transgene expression delineating the ventricle (Fig. 20 D, E). Development was similarly unaffected by microinjection with WT *MIB1* mRNA (Fig. 20 D, E). In contrast, when injecting the different *Mib1* variants we observe not only a cardiac phenotype but also a general developmental phenotype characteristic of abrogated Notch signalling. Microinjection with V943F mutant mRNA severely disrupted embryonic development, impairing cardiac looping and generating a kinked tail (Fig. 20

Figure 20. MIB1 is a homodimer whose ubiquitin ligase activity is impaired by the identified mutations.

(A) HA and Flag blotting in Flag immunoprecipitates of HEK293 cells co-transfected with WT HA-tagged MIB1 (Flag-WT MIB1) and various Flag-tagged MIB1 variants (Flag-M989R, Flag-tagged M989R MIB1; Flag-MIB1-VF, Flag-tagged V943F MIB1; Flag-MIB1-STOP, Flag-tagged R530X MIB1). IP, immunoprecipitation; WB, western blotting. (B) Flag and Jag1 blotting in Flag immunoprecipitates of Jag1-expressing HEK293 cells co-transfected with Flag-tagged WT MIB1 or Flag-tagged MIB1 variants. (C) GFP, JAG1, HA, Flag and MIB1 blotting in JAG1 immunoprecipitates of HEK293 cells co-transfected with JAG1, ubiquitin-GFP and empty vector (EV) or JAG1, ubiquitin-GFP and HA-tagged WT MIB1 plus one of the various forms of Flag-tagged (FG) MIB1 (VF, V943F mutation; ST, R530X mutation; MR, M989R mutation) or the empty vector. JAG1 immunoprecipitation was followed by western blotting for GFP-tagged ubiquitin to reveal ubiquitination (top). Western blotting with antibodies to HA and Flag revealed expression of WT and mutant MIB1 variants (middle). MIB1 western blotting revealed basal expression in non-transfected cells and similar expression levels in transfected cells. JAG1 was present in all immunoprecipitates (bottom). Actin was used as a loading control (D,E) Effect of *MIB1* variant mRNAs on zebrafish development. Lateral and ventral views are shown. Left, 72 h.p.f. Tg(mlc2a:eGFP) transgenic zebrafish larva microinjected with control GFP mRNA. The heart appears normal and looped towards the left (arrowhead). The remaining images show results of microinjection of mRNAs encoding WT, V943F, R530X and M989R *MIB1*. Note the kinked tail and the straight heart tube (arrowheads). The *mib1*^{ta52b} mutant shows a similar phenotype to that of embryos microinjected with mutant forms of *MIB1*. Note also the pericardial dystension (arrow). Scale bars, 0.5 mm. (e) Percentage of larvae with a mutant phenotype at 72 h.p.f. after microinjection of the *MIB1* mRNAs. (F) Notch reporter expression in *Tg(Tp1bglob:eGFP)*^{um14} larvae at 30 h.p.f. after microinjection of *MIB1* mutant mRNAs. Activity was measured by quantification of GFP luminescence. The solid black bar shows basal reporter activity in uninjected larvae. AU, arbitrary units. (G) Notch signaling activity measured by 10xCBF1-Luc reporter assay. The solid black bar shows basal reporter activity in NOTCH1-expressing HEK293 cells. Data are means from quadriplicate measures of each coculture; error bars represent standard deviations (*P < 0.05 determined by Student's t test).

D, E). Microinjection of R530X mutant mRNA produced a similar phenotype (Fig. 20 D, E) as did microinjection of the control M989R mutant mRNA (Fig. 20 D, E). The cardiac and tail defects in each group were similar to those in *Tg(mlc2a:GFP); mib*$^{ta52b/ta52b}$ mutants, which also showed a marked pericardial distension (Fig. 20 D), suggesting abnormal cardiac function. Moreover, microinjection of the various *MIB1* mutant mRNAs into the zebrafish Notch reporter line *Tg(Tp1bglob:eGFP)*^{um14} (Parsons et al., 2009) strongly attenuated reporter expression (Fig. 20 F). These data indicate that the V943F and R530X *MIB1* mutations severely impair Notch activity *in vivo.*

To complement these findings, we co-cultured HEK293 cells stably expressing Jag1 transfected with the various MIB1 variants with Notch1-expressing HEK293 cells (Chapman et al., 2006) co-transfected with the Notch signalling reporter 10xCBF1-Luc (McKenzie et al., 2005) and *Renilla* luciferase. This reporter contains ten repetitions of the RBPjK binding site in front of the luciferase gene that will be expressed upon Notch activation. Jag1-HEK293 cells expressing WT *MIB1* increased the activity of the 10xCBF1-Luc reporter, whereas the V934F, R530X and M989R

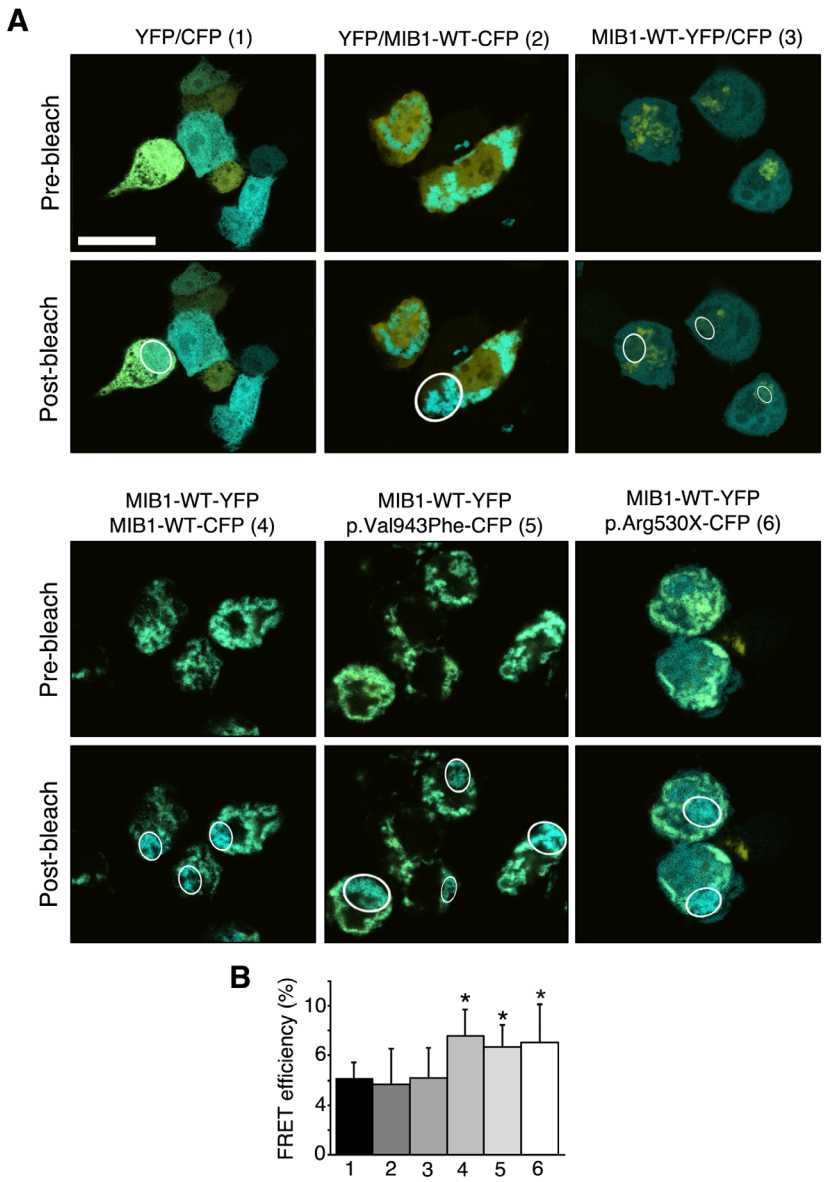

Figure 21. MIB1-dimer analysis by FRET.

(A) For negative controls, HEK293T cells were co-transfected with empty pEYFP-C1 plus empty pECFP-C1, empty pEYFP-C1 plus pECFP-C1 encoding CFP-tagged WT MIB1, or pEYFP-C1 encoding YFP-tagged WT MIB1 plus pECFP-C1. For a positive control, HEK293T cells were co-transfected with pEYFP-C1 encoding YFP-tagged WT MIB1 and pECFP-C1 encoding CFP-tagged WT MIB1. HEK293 cells were co-transfected in pair-wise combinations with pEYFP-C1, WT MIB1 plus pECFP-C1 encoding CFP-tagged p.Val943Phe or p.Arg530X. Images are shown before and after photobleaching of the acceptor within the indicated region. FRET efficiency was determined by the acceptor (YFP) photobleaching method and was measured only in the (acceptor) bleached area. Scale bar=20µm. (B) Quantification of FRET efficiency. Differences were significant when comparing the different MIB1 combinations to all three negative controls. $p<0.05$.

MIB1 mutant forms reduced the activity of the reporter (Fig. 20 G) indicating that both human mutations disrupt Notch signalling.

Mib1 regulates cardiac development and disease genes

After analysing the biochemical effects of the *MIB1* mutations we wanted to study the effect that deletion of *Mib1* in the myocardium has in ventricular development and maturation.

Analysis of chamber markers in E15.5 *Mib1^{flox};cTnT-cre* mice revealed expansion of the compact myocardium markers *Hey2* (Koibuchi and Chin, 2007), *Tbx20* (Singh et al., 2005) and *n-Myc* (Moens et al., 1993) to the trabeculae (Fig. 21 A) and reduced expression of the trabecular markers *Anf* (also known as *Nppa*) (Zeller et al., 1987)*, Bmp10* (Chen et al., 2004) and *Cx40* (also known as *Gja5)* (Van Kempen et al., 1996) (Fig. 22 A). We confirmed these observations by qPCR showing an increase of relative expression of the compact zone genes and a reduction of the trabecular genes (Fig. 22 B). Analysis of BrdU incorporation revealed increased proliferation of in between 10% and 15% of trabecular cardiomyocytes in the hearts of E15.5 *Mib1^{flox};cTnT-cre* embryos (Fig. 22 C, D) suggesting increased cardiomyocyte proliferation as the cause of the enlarged, non-compacted trabeculae in these mutants. Interestingly there were no differences in proliferation in the compact zone of mutant ventricles. The altered gene expression at E15.5 suggests that maintenance of trabecular maturation and patterning is impaired in *Mib1^{flox};cTnT-Cre* mutant mice. All the markers mentioned above were normally expressed in E11.5 *Mib1^{flox};cTnT-Cre* mutant mice (Fig. 23 A-E). The same happened at postnatal day 3 (P3). At postnatal stages not only the expression of *Hey2*, *Anf*, *Bmp10* and *Cx40* became normalized again (Fig. 24 A-D), but also the proliferation rate is normalized as well at this stage (Fig. 24 E). Suggesting that LVNC is a developmental disease with a very specific time window. Compaction starts after the trabeculae have been formed at E11.5 and finishes before birth.

Coronary artery development also seemed to be defective, as indicated by lost or reduced expression of *Hey1*, *Hey3* and *Efnb2* (*ephrinB2*) in the vessels of the compact myocardium (Fig. 25 A, B, D). Whether the absence of proper coronary vessels in the compact myocardium is a consequence of the non-compaction of the myocardium or is causal to this phenotype is not yet clear and it would be a very interesting question to address.

Expression of endocardial markers such as *Nrg1* or *Irx5* and myocardial markers such as *Irx4*, *MyH7* and *Nkx2.5* remains unaltered in the non-compacted hearts of *Mib1^{flox};cTnT-Cre* mice (Fig. 25 C. E-H). These results suggest that the non-compaction phenotype is a chamber maturation defect that does not affect lineage identity.

Global gene expression a analysis of E14.5 *Mib1^{flox};cTnT-Cre* mutant ventricles by RNA sequencing (RNA-seq) identified altered expression of 315 genes ($P \leq 0.05$); 132 of these genes were up-regulated and 183 were down-regulated (Complete data of the RNA-seq is supplied with the supplementary files). This experiment confirms the initial marker analysis; *Tbx20* and *Hey2* were up-regulated, whereas *Anf, Bmp10* and *Cx40* were down-regulated in the mutant ventricles. We also detected alterations in the expression of genes involved in the differentiation of cardiac endothelium and endocardium (Vwf,

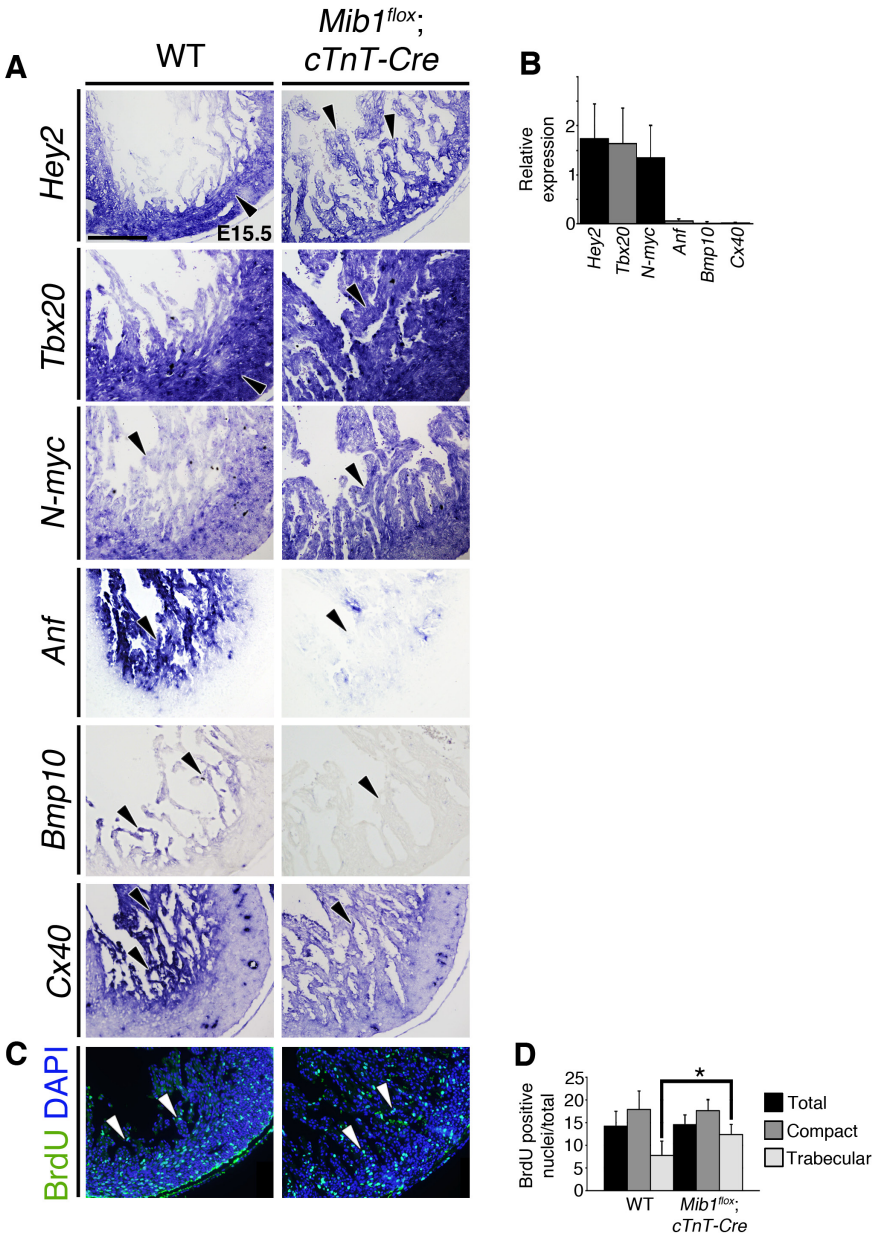

Figure 22. Defective ventricular maturation and cardiac gene expression in E15.5 *Mib1^{flox};cTnT-Cre* mice.

(A) In situ hybridization in E15.5 hearts showing that the compact myocardium markers *Hey2*, *Tbx20* and *n-Myc* expand to the trabeculae, whereas the trabecular markers *Anf*, *Bmp10* and *Cx40* are downregulated in *Mib1^{flox};cTnT-Cre* mutant mice. Arrowheads indicate where the gene is expressed. Scale bar, 50 µm. (B) qPCR analysis of the markers shown in (A). Data are the means ± s.e.m. from four sets of independent WT and mutant samples relative to *β-actin*. WT expression was normalized to 1. (C) Trabeculae remain proliferative in *Mib1^{flox};cTnT-Cre* hearts, as shown by immunostaining of incorporated BrdU in WT and *Mib1^{flox};cTnT-Cre* hearts after a 1-h pulse at E15.5, with details of the left ventricle shown. Arrowheads indicate BrdU-positive nuclei. (D) The ratios of BrdU-positive to total nuclei reveal significantly elevated proliferation in the trabeculae of *Mib1^{flox};cTnT-Cre* hearts. n = 3 embryos per genotype. *P < 0.05 by Student's t test. Ratios shown were calculated for both ventricles, and the images are from the left ventricles. Data are the means ± s.e.m.

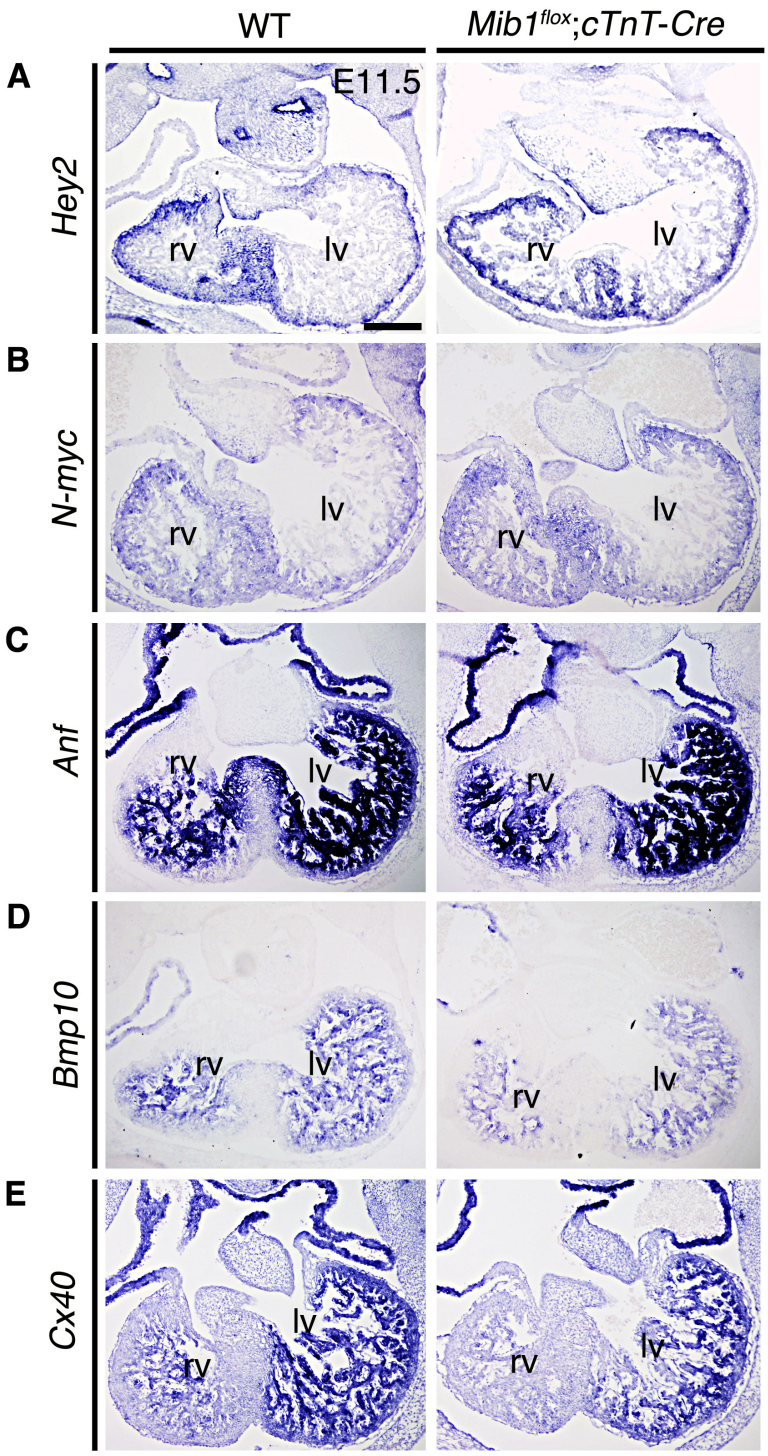

Figure 23. Compact zone and trabecular markers are normally expressed at E11.5.

In situ hybridization (A) *Hey2*, (B) *n-myc*, (C) *Anf*, (D) *Bmp10*, (E) *Cx40* in wild-type (WT) and *Mib1^{flox};cTnT-Cre* E11.5 hearts showing normal expression of trabecular and compact zone markers. All sections are transverse. None of the markers shows evident changes in overall expression levels or expression patterns. Note that the phenotype seen at later stages of development in *Mib1^{flox};cTnT-Cre* hearts is not apparent at E11.5. Scale bar=200µm. rv, right ventricle; lv, left ventricle.

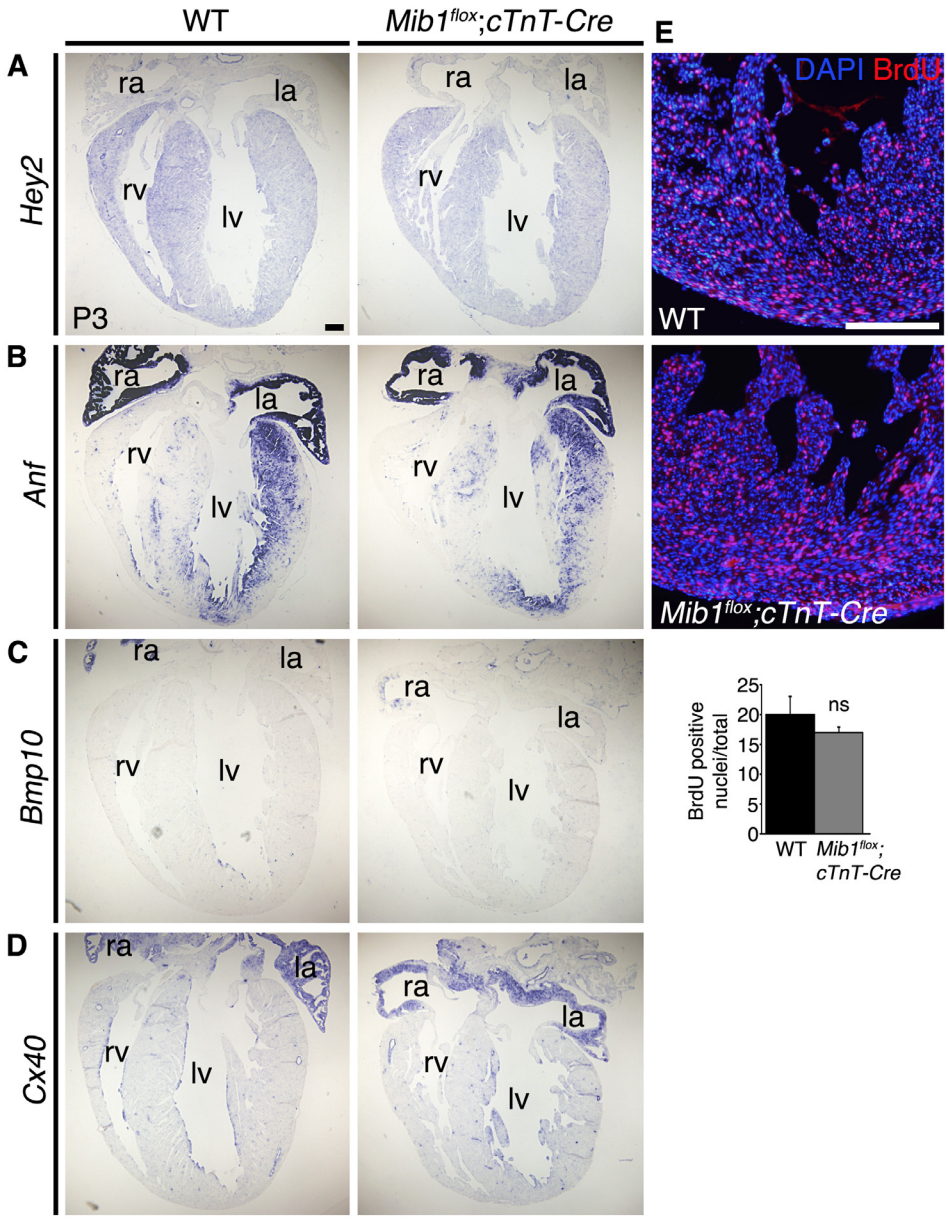

Figure 24. Chamber gene expression and cell proliferation are normal in *Mib1^{flox};cTnT-Cre* postnatal hearts.

Transverse sections of postnatal-day-3 wild-type (WT) and *Mib1^{flox};cTnT-Cre* hearts. In situ hybridization of (A) *Hey2*, (B) *Anf*, (C) *Bmp10* and (D) *Cx40* show similar expression patterns in WT and mutants. (E) Cardiac cell proliferation measured by BrdU incorporation is also similar as shown by immunostaining of incorporated BrdU in WT and *Mib1^{flox};cTnT-Cre* hearts after a 1-h pulse at P3, with details of the left ventricle shown. The ratios of BrdU-positive to total nuclei reveal no statistical difference. n = 3 embryos per genotype. *P < 0.05 by Student's t test. Ratios shown were calculated for both ventricles, and the images are from the left ventricles. Data are the means ± s.e.m. Scale bar=200µm. rv, right ventricle; lv, left ventricle; ra, right atrium; la, left atrium.

Hif1a, Epha4 and *Irx1)* and cardiomyocytes (Irx4, *Myl2, Tnnt2, Myo3b* and *Bmp5).* Genes involved in coronary vasculogenesis (Epas1, *Adam19, Foxc1, Sema3a* and *Angpt1)* were also down-regulated, reflecting the markedly reduced coronary vasculature of *Mib1^{flox};cTnT-*

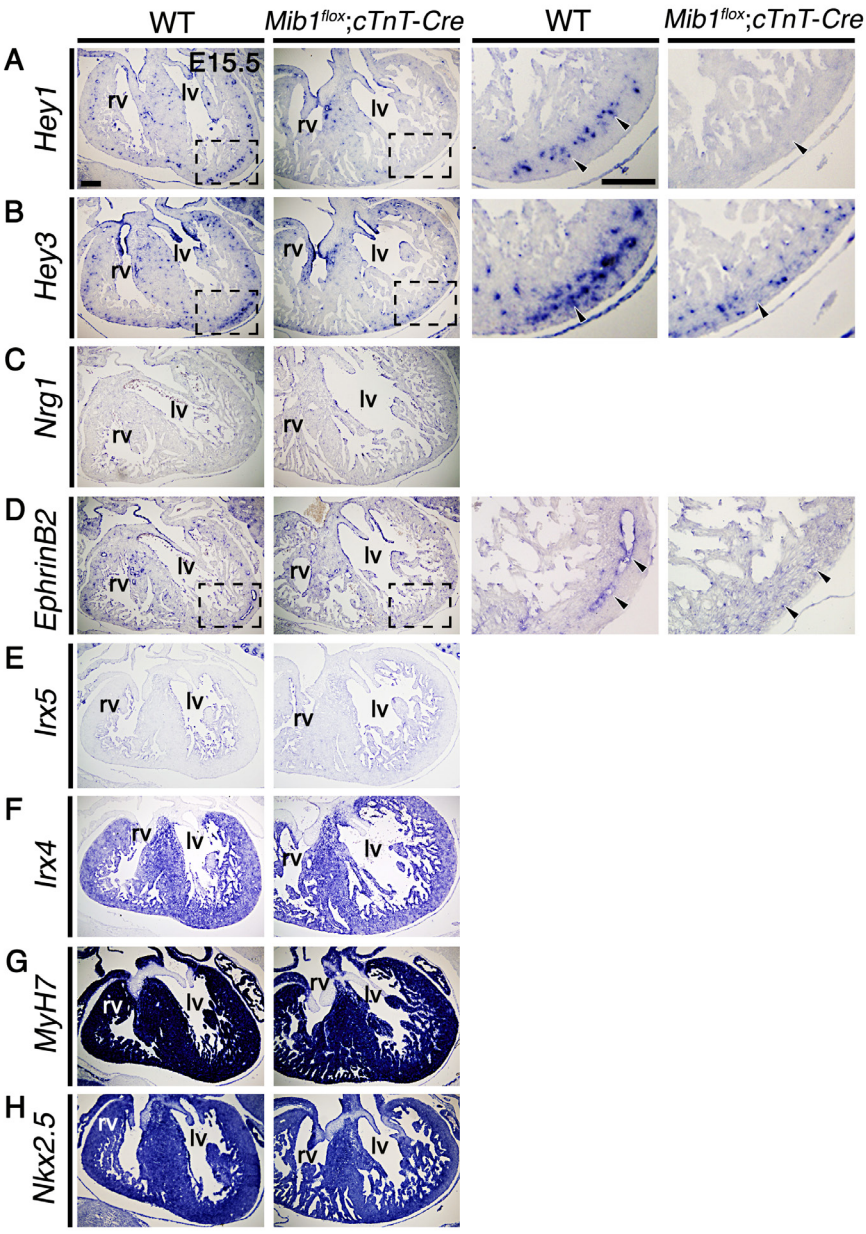

Figure 25. The identity of chamber endocardium and myocardium is not altered in E15.5 *Mib1^{flox};cTnT-Cre* mice.

Transverse sections of wild-type (WT) and *Mib1^{flox};cTnT-Cre* heart at E15.5. In situ hybridization of chamber endocardium, myocardium and coronary vessels markers; (A) *Hey1*, (B) *Hey3*, (C) *Nrg1*, (D) *EphrinB2*, (E) *Irx5*, (F) *Irx4*, (G) *MyH7* and (H) *Nkx2.5*. None of the markers shows evident changes in overall expression levels. Arrowheads (insets A, B, C) mark the coronary vessels in the compact myocardium, which appear small in *Mib1^{flox};cTnT-Cre* hearts, consistent with the loss of *Hey1*, *Hey3* and *EphrinB2* expression. Scale bar=200μm. rv, right ventricle; lv, left ventricle.

Cre mutant mice (Fig. 26 A).

Gene Ontology classification showed that several genes deregulated in *Mib1^{flox};cTnT-cre* ventricles encode cardiac developmental regulators and signalling pathways mediating cardiac hypertrophy (Fig. 26 B). The RNA-seq data confirmed our *in situ* hybridization analysis and demonstrated that *Mib1* inactivation in the myocardium disrupts the differentiation

and maturation of cardiomyocytes and the formation and development of the vascular coronary plexus (Fig. 26 B). This would in turn affect the process of ventricular maturation and compaction.

Deletion of *Mib1* in the myocardium on *Mib1^{flox};cTnT-Cre* mice leads to LVNC cardiomyopathy by arresting the maturation and compaction of the trabeculae that maintain a proliferative status during foetal stages.

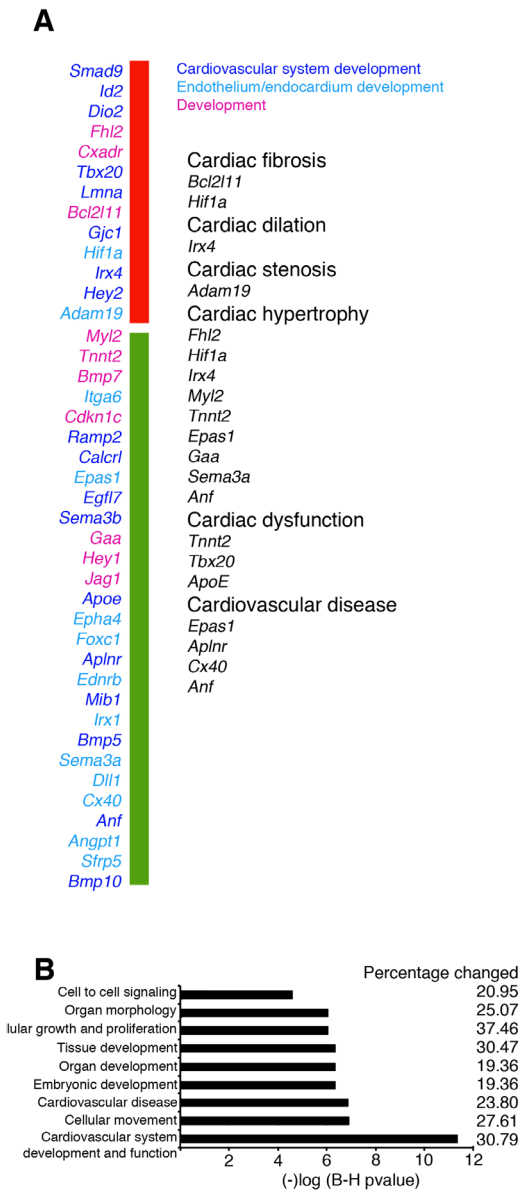

Figure 26. Global expression analysis of E14.5 *Mib1^{flox};cTnT-Cre* hearts.

(A) List of selected dysregulated genes identified by RNA-seq and ordered by fold change from wild-type, with red indicating up-regulated genes and green indicating down-regulated genes. Color codes indicate the biological functions of the genes. The column on the right lists the subset of dysregulated genes that are developmental genes related to cardiovascular disease. (B) Analysis of functional categories for the dysregulated genes in *Mib1^{flox};cTnT-Cre* hearts. B-H P value, Benjamini-Hochberg–adjusted P value. The percentage changed indicates the percentage of genes involved in the listed biological functions that changed in comparison to WT. The total percentage changed is over 100% because a given gene can be involved in more than one biological function.

DISCUSSION

The *Mib1*^{flox} mouse is an excellent tool to study the role of the Notch ligands in cardiac development

The Notch pathway elements are widely expressed during heart development. Mib1, the E3 ubiquitin ligase responsible for the endocytosis of ligands and the activation of the pathway, is expressed ubiquitously in the embryo during development and in the heart, in particular in the two earliest differentiating tissues, the endocardium and myocardium. MIb1 regulates signalling of the Notch ligands Dll4 and Jag1 that are differentially expressed in the heart. Both ligands are expressed in the endocardium of the valvular regions, but in the chambers, Dll4 is expressed in the endocardium and Jag1 in the myocardium.

Notch1, the main receptor in the heart, is expressed throughout the whole endocardium (Timmerman et al., 2004) but the protein is only active in the endocardium of AVC, OFT and trabeculae suggesting that the endocardium is a key tissue for Notch signalling in the heart.

Targeted inactivation of *Mib1* in the heart with different tissue-specific drivers allows us not only to study the role of Mib1 as a regulator of Notch signalling during heart development, but also in the case of the chambers, where the ligands are differentially expressed, to dissect their role (-s). Standard targeted inactivation of *Mib1* produces phenotypes similar to those observed in *Notch1* null mutants (Koo et al., 2005a).

Mib1 deletion in the endocardium disrupts early heart development

The results observed using the *Mib1*^{flox}*;Tie2-Cre* mice indicate that Mib1 plays an important role during early heart development. Dll4 is the only ligand with endocardial expression at this stage, thus being a potential Mib1 substrate, suggesting that the phenotype of Mib1 endocardial inactivation reflects an impairment of Dll4 signalling. At E9.5, the *Mib1*^{flox}*;Tie2-Cre* mutant phenotype consists in a developmental delay and pericardial dilation. Molecularly, there is a marked reduction in Notch1 activity and the cardiac expression of the Notch target genes, *Hey1*, *Hey2* and *HeyL* is diminished. Histologically, we observe that *Mib1*^{flox}*;Tie2-Cre* mice fail to undergo cardiac looping, a severely reduced EMT, trabeculation is impaired and there is a reduction in cellular proliferation.

This phenotype results to be lethal at around E11. At E9.5 what we observe is that *Mib1*^{flox}*;Tie2-Cre* mice fail to undergo cardiac looping and that EMT and trabeculation are impaired. These phenotypes prove the crucial role of Mib1 in the endocardium during these important events that take place during early heart development. It also identifies Dll4 as the ligand responsible Notch activation during early heart development. Cardiac phenotypes observed in standard *Notch1* and *RBPJK* knock-outs or endocardial-vascular conditional *Notch1* mutants (Timmerman et al., 2004, Grego-Bessa et al., 2007) are similar to the ones observed upon *Mib1* endocardial-vascular deletion, suggesting that there is a MIb1-Dll4-Notch1 signalling cascade necessary for early heart development.

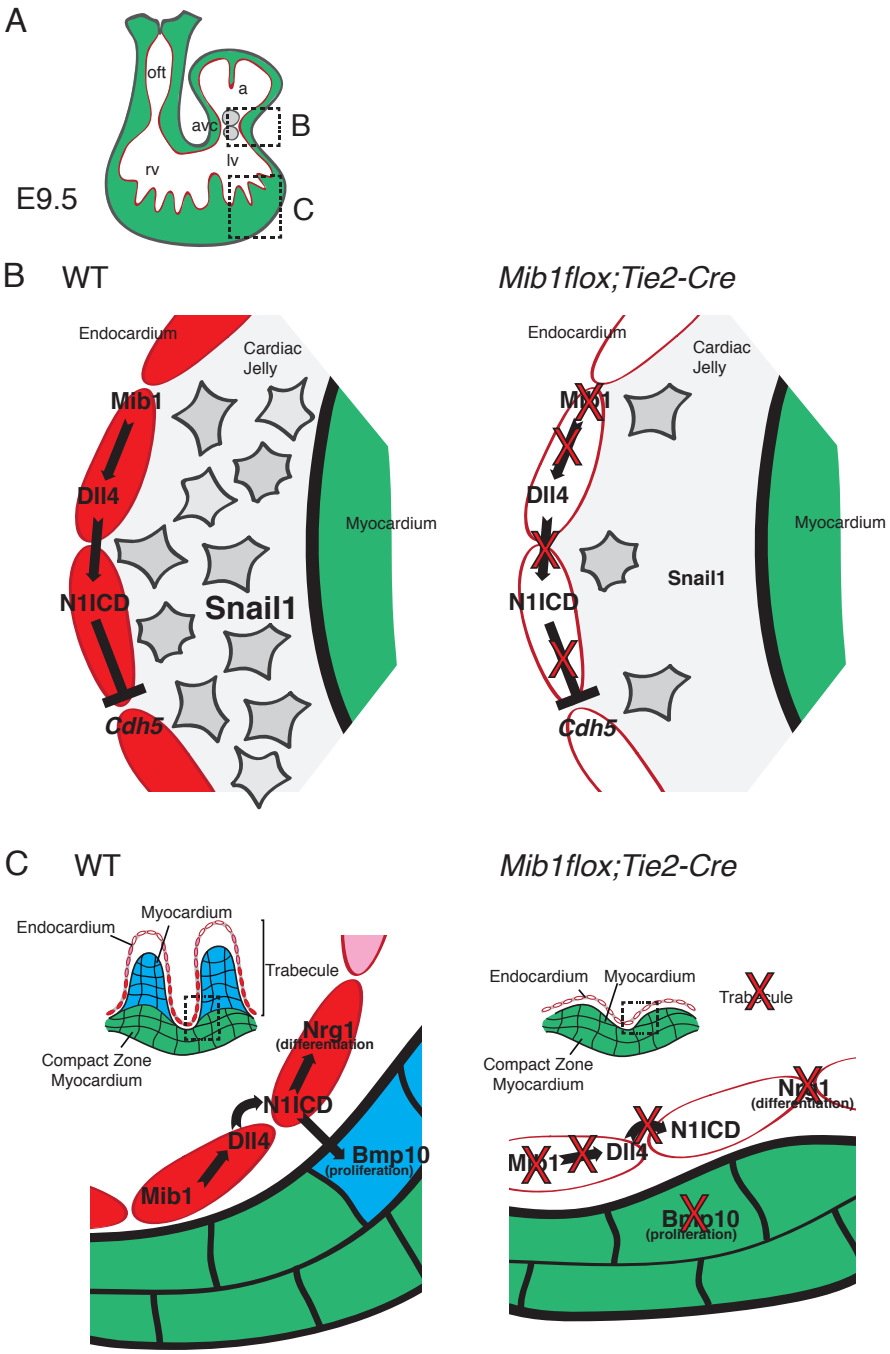

Abrogation of Mib1-Dll4-Notch1 signalling disrupts trabeculation (Fig. 27 B, C) and the formation of the endocardial cushions by EMT; it leads to a poor heart function that can be observed by the dilation of the pericardium in the mutant embryo at E9.5. This Mib1-Notch phenotype is not caused by any of the other Notch E3 ubiquitin ligases that are dispensable for development (Vollrath et al., 2001, Ruan et al., 2001, Koo et al., 2007), suggesting that there are no functional redundancies of Mib1 with Mib2, Neurl1 or Neurl2 during development.

Thus, we suggest that during early heart development, Notch1 activation is driven by Dll4. Our data also identify the endocardium as a key signalling tissue during early heart

Figure 27. Proposed mechanism of Notch regulation of early heart development.

(A) Schematic wild-type (WT) heart at E9.5. (B) In WT embryos, ubiquitylation of Dll4 allows Notch activation in the endocardium of the valves. N1ICD is required for the repression of *Cdh5*. This will allow the endocardial cells to undergo EMT, invade the cardiac jelly and form the valve primordia. In *Mib1^{flox};Tie2-Cre* embryos the absence of Mib1 inhibits the activation of N1ICD that is not able to supress *Cdh5*, thus only some endoccardial cells undergo EMT and invade the cardiac jelly. There is no formation of the valve primordia. (C) In WT embryos ubiquitylation of Dll4 allows Notch activation at the base of the trabecules. N1ICD activation is required for the expression of *Nrg1* and *Bmp10* that are required for the differentiation and maturation of the ventricles. In *Mib1^{flox};Tie2-Cre* embryos the absence of Mib1 inhibits the activation of N1ICD by Dll4 so that *Bmp10* and *Nrg1* are not expressed and the ventricle fails to develop.

development. Signals emanating from the endocardium (ie: Nrg1, TGFβ2) are necessary for the crucial events that take place during this time, such as trabeculation or valvulogenesis. In the case of the trabeculae, the myocardium responds to these signals (Fig. 27). Our results leave an open question of what is the temporal specificity of Jag1, the ligand expressed in the myocardium that we think is involved in the LVNC phenotype observed.

Mib1 deletion causes dysmorphic OFT valves

The early lethality of Notch mutant mice has not allowed us until now to study the development of the heart beyond mid-gestation. At E9.5, valvulogenesis and trabeculation are already underway but the morphogenetic processes that transform an embryonic heart into a mature adult heart have not yet started. Endocardial cushions have to form the valves and the trabeculae will contribute to the compacted ventricular wall. Deletion of *Mib1* with *Nkx2.5-Cre* has allowed us to study the role of Notch signalling pathway in valve development beyond EMT and trabeculation.

Nkx2.5 is expressed in the endocardium similarly to *Tie2*, but it is not expressed in the vascular endothelium. Although we have not performed a precise time-course of activation of these two Cre drivers, bot have been described to be active from E7.5 onwards (Kisanuki et al., 2001b, Stanley et al., 2002). The observation that *Tie2-Cre*-mediated *Mib1* inactivation causes lethality at E10.5 and Nkx2.5-Cre prior to birth, suggests that Mib1 function in the vasculature is crucial for embryonic viability. These differences in viability have allowed us to study the role of Mib1-Notch signalling in valve morphogenesis.

Standard inactivation of *Dll4* causes lethality in a haplo-insuficient manner and produces a severe vascular phenotype (Krebs et al., 2004, Duarte et al., 2004). *Mlb1*, *Dll4* (D'Amato, unpublished), and *Notch1* inactivation in the endocardium is recessive lethal, indicating the importance of using endocardial-specific drivers to study the role of Notch in the heart.

Mib1^{flox};Nkx2.5-Cre mice show dysmorphic OFT valves due to increased cellular proliferation in the valve mesenchyme. After EMT, the large endocardial cushions undergo a morphogenetic process leading to the mature functional valves. Program cell death or apoptosis in the mesenchyme of the valve primordial in involved in the morphogenesis of

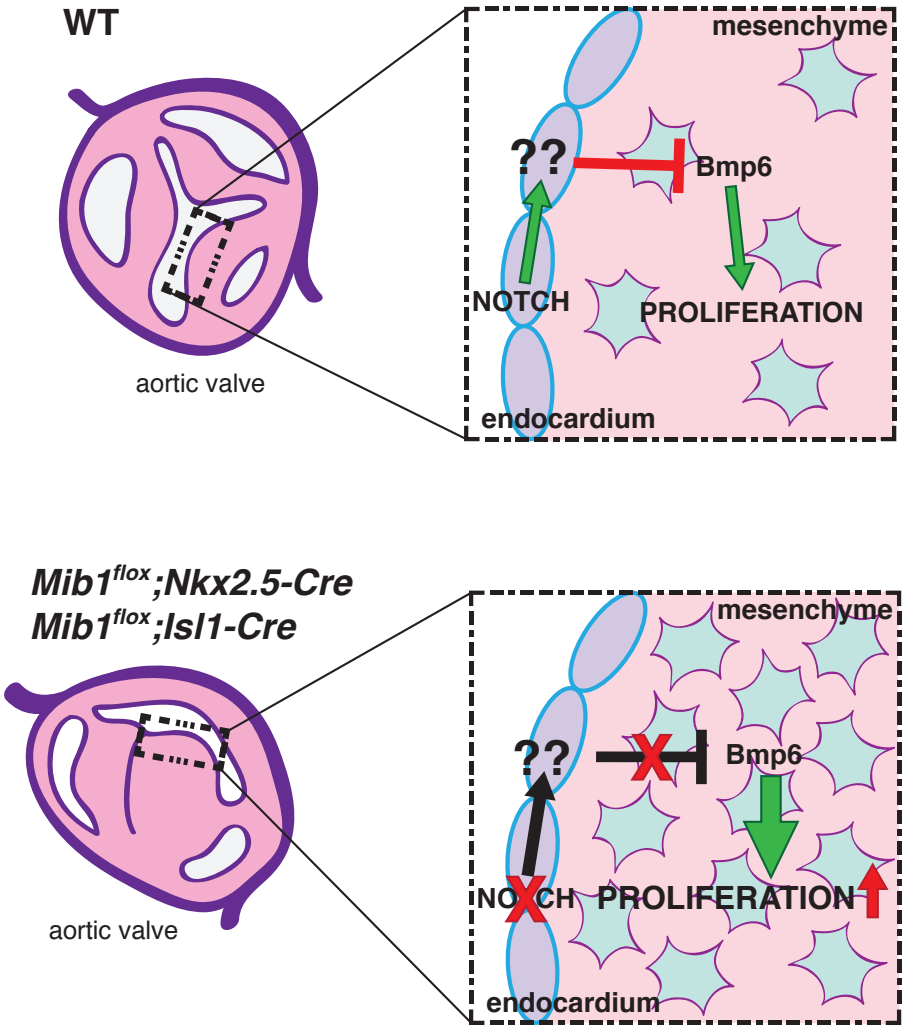

Figure 28. Proposed mechanism of Notch pathway function in OFT valve leaflet morphogenesis and maturation.

(A) In wild-type (WT) embryos, ubiquitination of either Jag1 or Delta4 allows Notch activation in the endocardium of the valves. N1ICD is required for the expression of a still unknown non-cell autonomous regulator of BMP signalling in the mesenchyme of the leaflet. This will negatively regulate BMP and cellular proliferation will stop so that the leaflet can undergo the morphogenesis process required for valve maturation. (B) In *Mib1^{flox};Nkx2.5-Cre* valves, Notch1 activity is impaired so the unknown regulator of BMP might not be expressed producing a deregulation of BMP and an increased cellular proliferation in the mesenchyme of the maturing valve that will form large leaflets resulting in dysmorphic OFT valves.

the valves (Hinton and Yutzey, 2011). On this context, Notch has been described as being required for the migration of the neural crest-derived mesenchyme that is crucialllly involved in the apoptosis of the cushion mesenchyme (Jain et al., 2011). Our findings indicating the presence of neural crest-derived mesenchyme and the observation of normal apoptosis in the cushions of *Mib1^{flox};Nkx2.5-Cre* mice, rules out apoptosis as a mechanism responsible for the enlarged leaflets observed in these mutants.

Our data show that Notch signalling abrogation in the endocardium of the leaflets produces an up-regulation of *Bmp6* and a down-regulation of its negative regulator

Smad6. Not only the expression of BMP genes is up-regulated, but also the activation of the pathway is up-regulated, as indicates the increased expression of phospho-Smad 1/5/8 proteins in the mesenchyme of the OFT leaflets. *Bmp6; Bmp7* double knockout mice have hypoplastic OFT cushions (Kim et al., 2001). Although both BMP proteins appear to be required for the development of the cushions, our results suggest that Bmp6 regulates the proliferation of cushion mesenchyme. Thus, we suggest that the enlarged leaflets are caused by increased proliferation of the mesenchymal cells due to the up-regulated BMP. The mutant leaflets are so large that they cannot align at the same level in the valve, thus being the likely cause of valve dysmorphology and incompetence.

Our results suggest that endocardial Notch regulates BMP signalling and mesenchymal cell proliferation in a non-cell autonomous fashion (Fig 28 A). In the endocardium, Notch would regulate the expression of a diffusible molecule that signals to the mesenchyme where it negatively regulates BMP and cellular proliferation. In the *Mib1^{flox};Nkx2.5-Cre* mutant (Fig. 28 B), devoid of Notch activation in the valvulogenic territory, there would be no expression of this diffusible molecule and thus BMP and proliferation would be dysregulated, leading to a dysmorphic OFT valve. The perinatal lethality of *Mib1^{flox};Nkx2.5-Cre* mice is likely due to the valve dysmorphology that severely disrupts cardiac function and causes death at a very demanding time point in terms of cardiac function: birth.

Jagged1 and Dll4 are both expressed in the OFT, thus the deletion of *Mib1* does not allow us to dissect the specific-role of these ligands in valve morphogenesis. Nevertheless, the severe phenotype of Mib1 strongly suggests an important role for these ligands in valve maturation. The similarities of the phenotypes observed in *Mib1^{flox};Nkx2.5-Cre* and *Mib1^{flox};Isl1-Cre* mice suggest that the phenotypes are heart specific. *Islet1* derivatives in the heart are both neural crest and second heart filed origin (Engleka et al., 2012) but *Nkx2.5* is only expressed in the heart. The regulation of mesenchyme proliferation by Notch from the endocardium during the maturation of the valves occurs after the migration of the other lineages in the heart. This suggests that they are two temporally separated processes, first EMT and migration of neural crest and then maturation and sculption of the leaflets.

Valve dysmorphology, either AV or OFT valves, is one the most common valve CHD and it is one of the leading causes in adult heart disease (Goldbarg et al., 2007). Notch has been demonstrated to be crucial not only for early valve development (Timmerman et al., 2004, Luna-Zurita et al., 2010) but also to have an impact on adult valve disease (Garg et al., 2005, Nus et al., 2011). This work reveals the importance of Mib1 (and in s.l. of Notch) in valve development and its potential implication in human valve disease.

MIB1 mutations cause LVNC

The results obtained with the *Mib1^{flox};cTnT-Cre* mice identify NOTCH as the first signalling pathway to our knowledge whose dysfunction has a causal role in LVNC. Until this moment the genes related to this cardiomyopathy were heterogeneous, mutations in structural genes of the cardiac fibers, mitochondrial genes or

in *G4.5* that is located in the X chromosome have been shown to cause LVNC (Oechslin and Jenni, 2011). We think that this research opens a new avenue into our understanding of this cardiomyopathy, especially from the mechanistic point of view.

Sequencing of the *MIB1* coding exons in a cohort of 100 patients with LVNC (48% of which were familial cases) identified two germline mutations (V943F and R530X) in two probands. The two mutant families do not present mutations in the other genes that have already been associated with LVNC. These *MIB1* mutations were associated with LVNC in an autosomal-dominant fashion. Image analysis of the hearts of the fathers of the two probands as well as those of family members with inherited *MIB1* mutations showed the presence of prominent trabeculations in both ventricles, and most of these individuals also showed reduced cardiac performance. Analysis of peripheral blood from these patients revealed low N1ICD and target-gene expression. In the two families the mutations segregated perfectly with the LVNC phenotype.

Additional evidence demonstrated that the V943F and R530X *MIB1* mutations disrupt Notch signalling: (I) microinjection of the corresponding *MIB1* mutant mRNAs into zebrafish embryos produces an embryonic and cardiac Notch-like phenotype; and (II) the activity of the Notch-RBP reporter 10xCBF1-Luc is attenuated *in vivo* and *in vitro* as a result of expression of either of the *MIB1* mutant mRNAs

Taking together all these data demonstrates that the two *MIB1* mutations affect NOTCH signalling both *in vivo* and *in vitro* but more importantly this affection of the pathway is what causes the disease.

Our findings indicate that MIB1 functions as a homodimer. *In silico* modelling suggests that WT MIB1 monomers form a head-to-tail homodimer that interacts with JAG1 through the Herc2 domain. Moreover, FRET signal measurements and co-immunoprecipitation studies showed that WT MIB1 monomers dimerize and that dimers are also formed between WT and mutant MIB1 monomers or between mutant monomers.

We were unable to detect expression of the predicted truncated protein produced by the R530X mutation in blood samples of patients with LVNC. qPCR and sequencing analyses of PCR products generated from the lymphocytes of these patients indicated that expression of the mutant mRNA harbouring the R530X mutation is almost completely abolished, probably by NMD. We suggest that in the settings of transfected HEK293 cells or microinjected zebrafish embryos, the R530X mutant protein expressed from a cDNA construct and not subject to NMD has a dominant-negative effect on MIB1 function through heterodimerization with the WT MIB1 protein. In contrast, the LVNC phenotype in patients with the R530X mutation would result from MIB1 haploinsufficiency. Expression of the mutant mRNA encoded by the V943F mutation was not affected in the lymphocytes of patients with LVNC and thus may give rise to an abnormal MIB1 monomer that is able to interact with a WT monomer, disrupting the function of the MIB1 heterodimer in a dominant-negative manner. This dominant-negative effect has been described for the zebrafish mutant *mib1ta52b,* which behaves

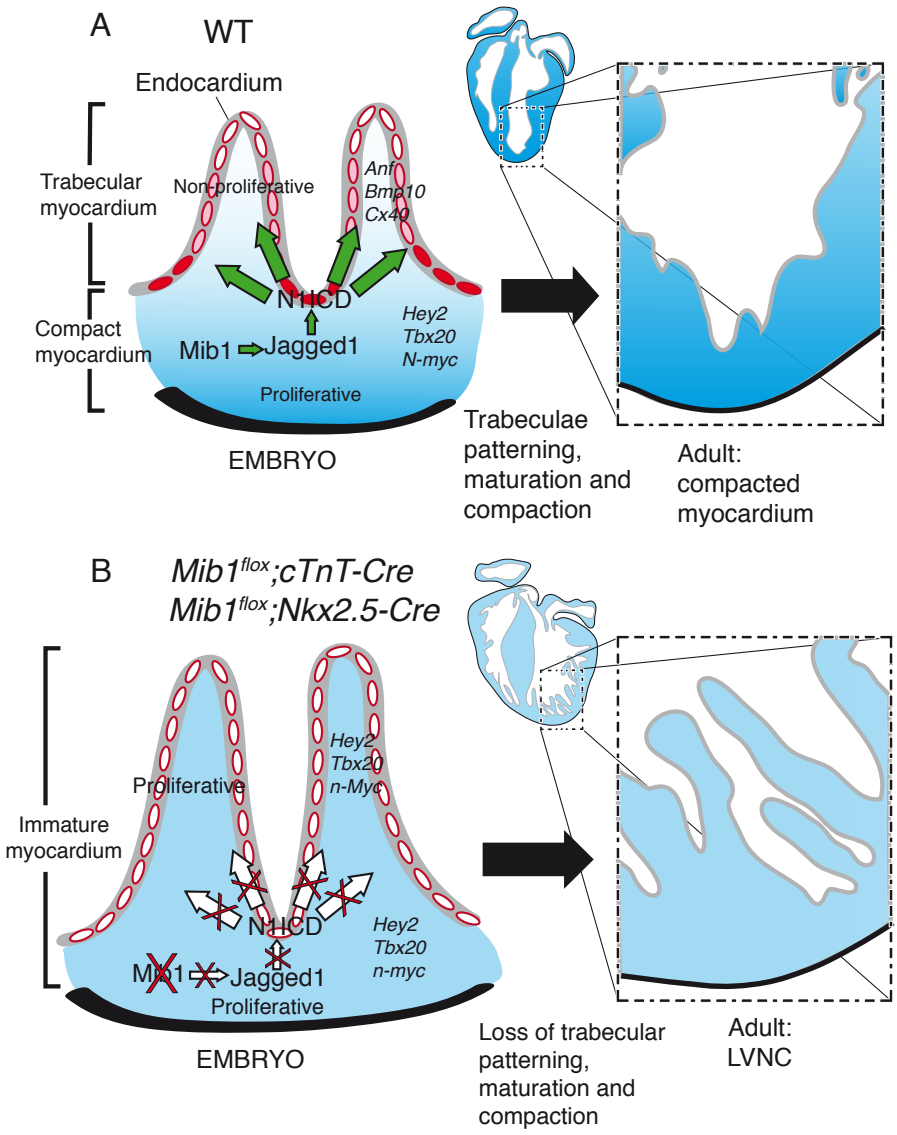

Figure 29. Proposed mechanism of Notch pathway function in trabecular maturation and compaction.

(A) In wild-type (WT) embryos, ubiquitylation of Jag1 by Mib1 in the myocardium allows Notch1 activation in the endocardium at the base of the developing trabeculae (red-filled cells). N1ICD is required to sustain trabecular patterning, maturation and compaction. The compact myocardium (positive for *Hey2*, *Tbx20* and *n-Myc*) proliferates actively, unlike the trabecular myocardium (positive for *Anf*, *Bmp10* and *Cx40*). Notch-dependent chamber maturation leads to compacted ventricular myocardium in the adult mouse. (B) In *Mib1^{flox};cTnT-Cre* embryos, Notch1 activity is impaired and compact myocardium markers (*Hey2*, *Tbx20* and *n-Myc*) are consequently expanded to the trabeculae, which remain abnormally proliferative. The resulting disruption of trabecular patterning, maturation and compaction manifests as LVNC.

similarly in ubiquitylation assays and harbours a missense mutation (M989R) in the C-terminal ring finger of mib1 (Zhang et al., 2007a), which is very close to the location of the *MIB1* V943F mutation.

Thus, we propose that both mutations result in loss of MIB1 WT function. In the

case of R530X, this would be due to haplo-insufficiency caused by insufficient synthesis of WT MIB1 protein; in the case of V943F, this would be due to a dominant-negative effect of the mutant protein, titrating down the amount of functional WT MIB1 dimers through heterotypic or homotypic interactions. In both cases, loss of MIB1 function leads to disease inherited in an autosomal-dominant fashion.

Endocardial-vascular inactivation of *Mib1* showed that Notch signalling is essential for the first events of ventricular chamber development. Similarly systemic or endocardial-specific inactivation of mouse *Notch1* or *Rbpj* disrupts trabeculation, leading to the formation of an anomalous 'spongy' myocardial wall. During this early stage of trabeculation, the ligand Dll4 is the main Notch activator in the endocardium (Grego-Bessa et al., 2007). We found that inactivation of *Mib1* in the myocardium gives rise to a dilated heart with enlarged ventricular trabeculae and a thin compact myocardium. Echocardiographic and CMRI analyses indicated that this phenotype persists in the adult heart, which had a reduced ejection fraction and a non-compaction index of 2.0. These features are all strongly reminiscent of LVNC, establishing *Mib1^{flox};cTnT-Cre* mice as the first animal model of LVNC, to our knowledge. Although *Mib1^{flox};Nkx2.5-Cre* show the same phenotype observed in the LVNC model their perinatal lethality caused by the valve maturation arrest disqualifies these mice as a model for LVNC.

We propose that myocardial Mib1 activity enables Jag1-dependent activation of Notch1 in the endocardium, triggering downstream signalling events that sustain normal trabecular patterning, maturation and myocardial compaction processes occurring in the mouse embryo, well after mid-gestation (>E11.5; Fig. 29). This hypothesis is consistent with the RNA-seq data showing that a set of differentiation genes for endothelium, endocardium and trabecular cardiomyocytes was down-regulated in *Mib1^{flox};cTnT-cre* mutant embryos. The expansion of compact zone markers to the trabeculae of E15.5 *Mib1^{flox}; cTnT-cre* mutant mice further suggests that trabecular patterning and maturation is impaired. In addition, the disruption of coronary vessel markers in *Mib1^{flox};cTnT-Cre* mutants indicates correct compaction of the ventricular wall is required for the coronary plexus formation. Notch signalling inactivation indirectly impairs coronary vessel formation.

The expression of the maturation and differentiation markers that are disrupted at E15.5 is unaffected at E11.5. The same occurs with the proliferation. At P3, when analysed in newborn mice markers expression and cellular proliferation are normal, suggesting that the MIb1-dependent processes leading to myocardial compaction are over. These observations suggest that the NOTCH-related LVNC has a developmental basis and that the process of compaction happens within a precise time window.

The abrogation of myocardial-endocardial Mib1-Jag1-Notch1 is crucial for the ventricular maturation. It is also required for compaction of the ventricular walls and for coronary plexus formation. These findings suggest that Jag1 is the ligand responsible for chamber maturation in the chamber, while Dll4 would be required for early chamber development.

NOTCH signalling alterations are involved in a range of human congenital heart disease

with autosomal-dominant inheritance, suggesting a high sensitivity of normal heart development to NOTCH dosage (High and Epstein, 2008, MacGrogan et al., 2010, Gridley, 2010). The complexity of NOTCH function in the human heart becomes evident from the specificity of the disease phenotypes associated with NOTCH alteration. Our current data establish the causal role of NOTCH dysregulation in LVNC, a congenital cardiomyopathy that results from a developmental arrest in ventricular maturation and myocardial compaction. These findings have the potential to improve diagnosis and risk stratification, allowing timely intervention in LVNC-associated complications (Sarma et al., 2010). In addition, as other NOTCH pathway elements may be involved in LVNC, our findings may help identify new diagnostic or therapeutic disease targets.

Mib1 is crucial for heart development

The different phenotypes observed upon deletion of *Mib1* in the endocardium and in the myocardium indicate that consecutive endocardial-myocardial Notch signalling is crucial for the progression of cardiomyocyte differentiation in the ventricles and cardiac valve cushion morphogenesis. The key role of Notch signalling in the heart is reflected in the consecutive implication of the ligands Dll4 and Jag1, differentially expressed in the heart. In the chambers, at an early stage of ventricular development, Dll4 is the ligand activating Notch1 (Mib1- mediating) within the endocardium, while myocardial Jagged1 does not seems to be functionally relevant, as there is not an early mutant phenotype for *Mib1^{flox};cTnT-Cre* mutants. One intriguing observation is that at this early stage of chamber development (E9.0-E10.5), chamber endocardium is only in close apposition with the myocardium at the base of the developing trabeculae. As development proceeds, Jagged1 expressed in the myocardium would be able to activate Notch1 in the endocardium because ventricular growth has lead to a close apposition of trabecular endocardium and myocardium. At this developmental stage (E13.5) is when *Mib1^{flox};cTnT-Cre* mutants begin to show a severe foetal and later adult LVNC phenotype. Our results could be further elaborated by the recently observed expression of a modulator of the Notch receptor, Manic fringe (G. D'Amato, unpublished data) that selects spatio-temporally the signaling specificity of the ligands. In conclusion, Notch ligands play different roles during ventricular chamber development. Dll4 is more important during early development, while Jag1 in the later but crucial processes of chamber maturation and compaction. We suggest that during ventricular development there is sequential activation of the ligands (G. D'Amato, unpublished data). Whether this phenomenon is only spatially regulated or there is also a time component remains undetermined.

In the valves, although Dll4 is also required for EMT and the early events of valvulogenesis, there is no a spatial difference between Dll4 and Jag1 endocardial expression. This makes impossible to dissect with Mib1 the influence of the two ligands in valve maturation and morphogenesis. It becomes clear that Notch is crucial not only for triggering valve development by EMT, but also for the maturation and homeostasis of the structure.

Tissue-specific *Mib1* deletion disrupts Notch signaling in the endocardium. Endocardial Notch activity regulates cardiac valve and chamber development and maturation. In these processes, endocardial Notch acts in a non-cell autonomous manner to regulate valve morphogenesis and cardiac chamber maturation.

CONCLUSIONS / CONCLUSIONES

1. The Notch ligands are differentially expressed in the heart. In the ventricles Dll4 is expressed in the endocardium, and Jagged1 in the myocardium. In the valves, both ligands are expressed in the endocardium. Genetic manipulation of *Mib1* is an excellent approach to genetically dissect the role of the ligands Dll4 and Jagged1 in heart development, as its inactivation allows us to study the full effect of Notch ligands signalling abrogation.

2. Notch activation in the endocardium orchestrates the non-cell autonomous effects in the myocardium essential for trabecular development and myocardial compaction, and thus is crucial for heart development.

3. Genetic inactivation of *Mib1* in the endocardium-endothelium disrupts heart development. Trabeculae and endocardial cushions are not formed. Delta4 is the ligand responsible for this early Notch phenotype.

4. Genetic inactivation of *Mib1* in the endocardium and in the myocardium blocks OFT valve maturation producing dysmorphic valve leaflets. We have been unable of fully dissecting which of the ligands is responsible for this phenotype, although our data suggest an early role only for Dll4 in endocardial EMT but we cannot discard that both Dll4 and Jag1 participate in valve morphogenesis.

5. During valve morphogenesis, Notch regulates BMP signalling in a non-cell autonomous manner modulating mesenchymal cellular proliferation in the leaflets. The deregulation of BMP signalling is responsible for the increased size of the OFT valve leaflets of *Mib1^{flox};Nkx2.5-Cre* mice.

6. Genetic inactivation of *Mib1* in the myocardium causes a severe ventricular phenotype that resembles the human LVNC cardiomyopathy. *MIb1* myocardial inactivation impairs the maturation of the myocardium, and the trabeculae express compact myocardium markers and remain proliferative. This phenotype is likely caused by the abrogation of Jag1 signalling from the myocardium.

7. Mutations in human *MIB1* cause LVNC cardiomyopathy, the third most important cardiomyopathy. LVNC *MIB1* pedigrees show a perfect correlation of phenotype and genotype and the mutations are inherited in an autosomal dominant manner.

8. V943F *MIB1* mutation has a dominant negative effect on the WT protein causing the cardiomyopathy; on the other hand the R530X mutation produces the cardiomyopathy by haplo-insufiency of the MIB1 protein.

9. NOTCH-dependent LVNC has a developmental basis making NOTCH a new diagnostic tool for the cardiomyopathy.

1. Los ligandos de Notch se expresan diferencialmente en el corazón. En los ventrículos Dll4 se expresa en el endocardio y Jag1 en el endocardio. En las válvulas ambos se expresan en el endocarido. La manipulación genética de *Mib1* es una abordaje excelente para diseccionar el papel de los ligandos Dll4 y Jag1 durante el desarrollo cardiaco.

2. La activación de Notch en el endocardio tiene efectos no autónomo celulares en el micoardio que son esenciales para el desarrollo trabecular y la compactación del ventrículo, y por ello son cruciales para el desarrollo del corazón.

3. La inactivación genética de *Mib1* en el endocardio y el endotelio interrumpe el desarrollo del corazón. Las trabéculas y los colchones del endocardio no se forman. Dll4 es el ligando responsable de este fenotipo temprano de Notch.

4. La inactivación genética de *Mib1* en el endocardio y en el miocardio bloquea la maduración de las válvulas del OFT produciendo valvas dismórficas. No hemos podido determinar que ligando es responsable de este fenotipo, aunque nuestros datos sugieren un papel temprano de Dll4 en la EMT del endocardio, no podemos descartar que Dll4 y Jag1 participen conjuntamente en la morfogénesis de las válvulas.

5. Durante la morfogénesis de las válvulas, Notch regula la señalización por BMP de una manera no autónoma celular, modulando la proliferación celular en las valvas. La desregulación de la señalización por BMP es responsable del incremento de tamaño de las valvas en las válvulas del OFT en los ratones *Mib1^{flox};Nkx2.5-Cre*.

6. La eliminación de *Mib1* en el miocardio cause un severo fenotipo ventricular similar a la cardiomiopatía humana LVNC. La inactivación de *Mib1* en el miocardio impide la maduración del miocardio, las trabéculas expresan marcadores de miocardio compacto y mantienen el estado proliferativo. Este fenotipo parece ser causado por la eliminación de la señalización dependiente de Jag1 desde el miocardio.

7. Mutaciones en *MIB1* humano causan la cardiomiopatía LVNC., que es la tercera cardiomiopatía más importante. Los pedigríes de LVNC producidos por mutaciones en *MIB1* presentan una correlación perfecta entre fenotipo y genotipo, y las mutaciones en *MIB1* se

heredan de manera autosómica dominante.

8. En caso de la mutación V943F la proteína MIB1 mutante tiene un efecto dominante negativo causante de la enfermedad, mientras que en el caso de la R530X la cardiomiopatía se produce por haplo insuficiencia de MIB1.

9. La LVNC dependiente de NOTCH tiene una base de desarrollo. Esto transforma a NOTCH en una nueva herramienta de diagnostico para la cardiomiopatía.

BIBLIOGRAPHY

A

AANHAANEN, W. T., MOORMAN, A. F. & CHRISTOFFELS, V. M. 2011. Origin and development of the atrioventricular myocardial lineage: insight into the development of accessory pathways. *Birth Defects Res A Clin Mol Teratol,* 91, 565-77.

ADAMS, R. H., WILKINSON, G. A., WEISS, C., DIELLA, F., GALE, N. W., DEUTSCH, U., RISAU, W. & KLEIN, R. 1999. Roles of ephrinB ligands and EphB receptors in cardiovascular development: demarcation of arterial/venous domains, vascular morphogenesis, and sprouting angiogenesis. *Genes Dev,* 13, 295-306.

ADZHUBEI, I. A., SCHMIDT, S., PESHKIN, L., RAMENSKY, V. E., GERASIMOVA, A., BORK, P., KONDRASHOV, A. S. & SUNYAEV, S. R. 2010. A method and server for predicting damaging missense mutations. *Nat Methods,* 7, 248-9.

ALFIERI, C. M., CHEEK, J., CHAKRABORTY, S. & YUTZEY, K. E. 2010. Wnt signaling in heart valve development and osteogenic gene induction. *Dev Biol,* 338, 127-35.

ARNOLD, K., BORDOLI, L., KOPP, J. & SCHWEDE, T. 2006. The SWISS-MODEL workspace: a web-based environment for protein structure homology modelling. *Bioinformatics,* 22, 195-201.

ARTAVANIS-TSAKONAS, S. & MUSKAVITCH, M. A. 2010. Notch: the past, the present, and the future. *Curr Top Dev Biol,* 92, 1-29.

ARTAVANIS-TSAKONAS, S., RAND, M. D. & LAKE, R. J. 1999. Notch signaling: cell fate control and signal integration in development. *Science,* 284, 770-6.

B

BARSI, J. C., RAJENDRA, R., WU, J. I. & ARTZT, K. 2005. Mind bomb1 is a ubiquitin ligase essential for mouse embryonic development and Notch signaling. *Mech Dev,* 122, 1106-17.

BEN-SHACHAR, G., ARCILLA, R. A., LUCAS, R. V. & MANASEK, F. J. 1985. Ventricular trabeculations in the chick embryo heart and their contribution to ventricular and muscular septal development. *Circ Res,* 57, 759-66.

BENEDITO, R., ROCA, C., SORENSEN, I., ADAMS, S., GOSSLER, A., FRUTTIGER, M. & ADAMS, R. H. 2009. The notch ligands Dll4 and Jagged1 have opposing effects on angiogenesis. *Cell,* 137, 1124-35.

BETTENHAUSEN, B., HRABE DE ANGELIS, M., SIMON, D., GUENET, J. L. & GOSSLER, A. 1995. Transient and restricted expression during mouse embryogenesis of Dll1, a murine gene closely related to Drosophila Delta. *Development,* 121, 2407-18.

BI, W., DRAKE, C. J. & SCHWARZ, J. J. 1999. The transcription factor MEF2C-null mouse exhibits complex vascular malformations and reduced cardiac expression of angiopoietin 1 and VEGF. *Dev Biol,* 211, 255-67.

BILLIARD, F., KIRSHNER, J. R., TAIT, M., DANAVE, A., TAHERI, S., ZHANG, W., WAITE, J. C., OLSON, K., CHEN, G., COETZEE, S., HYLTON, D., MURPHY, A. J., YANCOPOULOS, G. D., THURSTON, G. & SKOKOS, D. 2011. Ongoing Dll4-Notch signaling is required for T-cell homeostasis in the adult thymus. *Eur J Immunol,* 41, 2207-16.

BIONE, S., D'ADAMO, P., MAESTRINI, E., GEDEON, A. K., BOLHUIS, P. A. & TONIOLO, D. 1996. A novel X-linked gene, G4.5. is responsible for Barth syndrome. *Nat Genet,* 12, 385-9.

BLAIR, S. S. 2000. Notch signaling: Fringe really is a glycosyltransferase. *Curr Biol,* 10, R608-12.

BLAUMUELLER, C. M., QI, H., ZAGOURAS, P. & ARTAVANIS-TSAKONAS, S. 1997. Intracellular cleavage of Notch leads to a heterodimeric receptor on the plasma membrane. *Cell,* 90, 281-91.

BUCKINGHAM, M., MEILHAC, S. & ZAFFRAN, S.

2005. Building the mammalian heart from two sources of myocardial cells. *Nat Rev Genet,* 6, 826-35.

C

CAI, C. L., LIANG, X., SHI, Y., CHU, P. H., PFAFF, S. L., CHEN, J. & EVANS, S. 2003. Isl1 identifies a cardiac progenitor population that proliferates prior to differentiation and contributes a majority of cells to the heart. *Dev Cell,* 5, 877-89.

CAPOCCIA, B. J., JIN, R. U., KONG, Y. Y., PEEK, R. M., JR., FASSAN, M., RUGGE, M. & MILLS, J. C. 2013. The ubiquitin ligase Mindbomb 1 coordinates gastrointestinal secretory cell maturation. *J Clin Invest,* 123, 1475-91.

CAPTUR, G. & NIHOYANNOPOULOS, P. 2010. Left ventricular non-compaction: genetic heterogeneity, diagnosis and clinical course. *Int J Cardiol,* 140, 145-53.

CHANG, Y. F., IMAM, J. S. & WILKINSON, M. F. 2007. The nonsense-mediated decay RNA surveillance pathway. *Annu Rev Biochem,* 76, 51-74.

CHAPMAN, G., LIU, L., SAHLGREN, C., DAHLQVIST, C. & LENDAHL, U. 2006. High levels of Notch signaling down-regulate Numb and Numblike. *J Cell Biol,* 175, 535-40.

CHEN, H., SHI, S., ACOSTA, L., LI, W., LU, J., BAO, S., CHEN, Z., YANG, Z., SCHNEIDER, M. D., CHIEN, K. R., CONWAY, S. J., YODER, M. C., HANELINE, L. S., FRANCO, D. & SHOU, W. 2004. BMP10 is essential for maintaining cardiac growth during murine cardiogenesis. *Development,* 131, 2219-31.

CHEN, W. & CASEY CORLISS, D. 2004. Three modules of zebrafish Mind bomb work cooperatively to promote Delta ubiquitination and endocytosis. *Dev Biol,* 267, 361-73.

COMBS, M. D. & YUTZEY, K. E. 2009. Heart valve development: regulatory networks in development and disease. *Circ Res,* 105, 408-21.

COMEAU, S. R., GATCHELL, D. W., VAJDA, S. & CAMACHO, C. J. 2004. ClusPro: an automated docking and discrimination method for the prediction of protein complexes. *Bioinformatics,* 20, 45-50.

COPELAND, J. W. & TREISMAN, R. 2002. The diaphanous-related formin mDia1 controls serum response factor activity through its effects on actin polymerization. *Mol Biol Cell,* 13, 4088-99.

CRUZ-ADALIA, A., JIMENEZ-BORREGUERO, L. J., RAMIREZ-HUESCA, M., CHICO-CALERO, I., BARREIRO, O., LOPEZ-CONESA, E., FRESNO, M., SANCHEZ-MADRID, F. & MARTIN, P. 2010. CD69 limits the severity of cardiomyopathy after autoimmune myocarditis. *Circulation,* 122, 1396-404.

D

DAVYDOV, E. V., GOODE, D. L., SIROTA, M., COOPER, G. M., SIDOW, A. & BATZOGLOU, S. 2010. Identifying a high fraction of the human genome to be under selective constraint using GERP++. *PLoS Comput Biol,* 6, e1001025.

DE LA POMPA, J. L. & EPSTEIN, J. A. 2012. Coordinating tissue interactions: Notch signaling in cardiac development and disease. *Dev Cell,* 22, 244-54.

DE LANGE, F. J., MOORMAN, A. F., ANDERSON, R. H., MANNER, J., SOUFAN, A. T., DE GIER-DE VRIES, C., SCHNEIDER, M. D., WEBB, S., VAN DEN HOFF, M. J. & CHRISTOFFELS, V. M. 2004. Lineage and morphogenetic analysis of the cardiac valves. *Circ Res,* 95, 645-54.

DE VLAMING, A., SAULS, K., HAJDU, Z., VISCONTI, R. P., MEHESZ, A. N., LEVINE, R. A., SLAUGENHAUPT, S. A., HAGEGE, A., CHESTER, A. H., MARKWALD, R. R. & NORRIS, R. A. 2012. Atrioventricular valve development: new perspectives on an old

theme. *Differentiation,* 84, 103-16.

DEBLANDRE, G. A., LAI, E. C. & KINTNER, C. 2001. Xenopus neuralized is a ubiquitin ligase that interacts with XDelta1 and regulates Notch signaling. *Dev Cell,* 1, 795-806.

DEL AMO, F. F., SMITH, D. E., SWIATEK, P. J., GENDRON-MAGUIRE, M., GREENSPAN, R. J., MCMAHON, A. P. & GRIDLEY, T. 1992. Expression pattern of Motch, a mouse homolog of Drosophila Notch, suggests an important role in early postimplantation mouse development. *Development,* 115, 737-44.

DEL MONTE, G., CASANOVA, J. C., GUADIX, J. A., MACGROGAN, D., BURCH, J. B., PEREZ-POMARES, J. M. & DE LA POMPA, J. L. 2011. Differential Notch signaling in the epicardium is required for cardiac inflow development and coronary vessel morphogenesis. *Circ Res,* 108, 824-36.

DEL MONTE, G., GREGO-BESSA, J., GONZALEZ-RAJAL, A., BOLOS, V. & DE LA POMPA, J. L. 2007. Monitoring Notch1 activity in development: evidence for a feedback regulatory loop. *Dev Dyn,* 236, 2594-614.

DEVGAN, V., MAMMUCARI, C., MILLAR, S. E., BRISKEN, C. & DOTTO, G. P. 2005. p21WAF1/Cip1 is a negative transcriptional regulator of Wnt4 expression downstream of Notch1 activation. *Genes Dev,* 19, 1485-95.

DUARTE, A., HIRASHIMA, M., BENEDITO, R., TRINDADE, A., DINIZ, P., BEKMAN, E., COSTA, L., HENRIQUE, D. & ROSSANT, J. 2004. Dosage-sensitive requirement for mouse Dll4 in artery development. *Genes Dev,* 18, 2474-8.

DUNWOODIE, S. L., HENRIQUE, D., HARRISON, S. M. & BEDDINGTON, R. S. 1997. Mouse Dll3: a novel divergent Delta gene which may complement the function of other Delta homologues during early pattern formation in the mouse embryo. *Development,* 124, 3065-76.

E

EISENBERG, L. M. & MARKWALD, R. R. 1995. Molecular regulation of atrioventricular valvuloseptal morphogenesis. *Circ Res,* 77, 1-6.

ENGBERDING, R. & BENDER, F. 1984. Identification of a rare congenital anomaly of the myocardium by two-dimensional echocardiography: persistence of isolated myocardial sinusoids. *Am J Cardiol,* 53, 1733-4.

ENGLEKA, K. A., MANDERFIELD, L. J., BRUST, R. D., LI, L., COHEN, A., DYMECKI, S. M. & EPSTEIN, J. A. 2012. Islet1 derivatives in the heart are of both neural crest and second heart field origin. *Circ Res,* 110, 922-6.

F

FEHON, R. G., KOOH, P. J., REBAY, I., REGAN, C. L., XU, T., MUSKAVITCH, M. A. & ARTAVANIS-TSAKONAS, S. 1990. Molecular interactions between the protein products of the neurogenic loci Notch and Delta, two EGF-homologous genes in Drosophila. *Cell,* 61, 523-34.

FINSTERER, J. 2009. Cardiogenetics, neurogenetics, and pathogenetics of left ventricular hypertrabeculation/ noncompaction. *Pediatr Cardiol,* 30, 659-81.

FRISCHMEYER, P. A., VAN HOOF, A., O'DONNELL, K., GUERRERIO, A. L., PARKER, R. & DIETZ, H. C. 2002. An mRNA surveillance mechanism that eliminates transcripts lacking termination codons. *Science,* 295, 2258-61.

G

GARG, V., MUTH, A. N., RANSOM, J. F., SCHLUTERMAN, M. K., BARNES, R., KING, I. N., GROSSFELD, P. D. & SRIVASTAVA, D. 2005.

Mutations in NOTCH1 cause aortic valve disease. *Nature,* 437, 270-4.

GOLDBARG, S. H., ELMARIAH, S., MILLER, M. A. & FUSTER, V. 2007. Insights into degenerative aortic valve disease. *J Am Coll Cardiol,* 50, 1205-13.

GOLSON, M. L., LE LAY, J., GAO, N., BRAMSWIG, N., LOOMES, K. M., OAKEY, R., MAY, C. L., WHITE, P. & KAESTNER, K. H. 2009. Jagged1 is a competitive inhibitor of Notch signaling in the embryonic pancreas. *Mech Dev,* 126, 687-99.

GREENWAY, S. C., PEREIRA, A. C., LIN, J. C., DEPALMA, S. R., ISRAEL, S. J., MESQUITA, S. M., ERGUL, E., CONTA, J. H., KORN, J. M., MCCARROLL, S. A., GORHAM, J. M., GABRIEL, S., ALTSHULER, D. M., QUINTANILLA-DIECK MDE, L., ARTUNDUAGA, M. A., EAVEY, R. D., PLENGE, R. M., SHADICK, N. A., WEINBLATT, M. E., DE JAGER, P. L., HAFLER, D. A., BREITBART, R. E., SEIDMAN, J. G. & SEIDMAN, C. E. 2009. De novo copy number variants identify new genes and loci in isolated sporadic tetralogy of Fallot. *Nat Genet,* 41, 931-5.

GREGO-BESSA, J., LUNA-ZURITA, L., DEL MONTE, G., BOLOS, V., MELGAR, P., ARANDILLA, A., GARRATT, A. N., ZANG, H., MUKOUYAMA, Y. S., CHEN, H., SHOU, W., BALLESTAR, E., ESTELLER, M., ROJAS, A., PEREZ-POMARES, J. M. & DE LA POMPA, J. L. 2007. Notch signaling is essential for ventricular chamber development. *Dev Cell,* 12, 415-29.

GRIDLEY, T. 2010. Notch signaling in the vasculature. *Curr Top Dev Biol,* 92, 277-309.

GRIESKAMP, T., RUDAT, C., LUDTKE, T. H., NORDEN, J. & KISPERT, A. 2011. Notch signaling regulates smooth muscle differentiation of epicardium-derived cells. *Circ Res,* 108, 813-23.

GUY, T. S. & HILL, A. C. 2012. Mitral valve prolapse. *Annu Rev Med,* 63, 277-92.

H

HANSSON, E. M., LANNER, F., DAS, D., MUTVEI, A., MARKLUND, U., ERICSON, J., FARNEBO, F., STUMM, G., STENMARK, H., ANDERSSON, E. R. & LENDAHL, U. 2010. Control of Notch-ligand endocytosis by ligand-receptor interaction. *J Cell Sci,* 123, 2931-42.

HARTMANN, D., DE STROOPER, B., SERNEELS, L., CRAESSAERTS, K., HERREMAN, A., ANNAERT, W., UMANS, L., LUBKE, T., LENA ILLERT, A., VON FIGURA, K. & SAFTIG, P. 2002. The disintegrin/metalloprotease ADAM 10 is essential for Notch signalling but not for alpha-secretase activity in fibroblasts. *Hum Mol Genet,* 11, 2615-24.

HARVEY, R. P. 2002. Patterning the vertebrate heart. *Nat Rev Genet,* 3, 544-56.

HERMIDA-PRIETO, M., MONSERRAT, L., CASTRO-BEIRAS, A., LAREDO, R., SOLER, R., PETEIRO, J., RODRIGUEZ, E., BOUZAS, B., ALVAREZ, N., MUNIZ, J. & CRESPO-LEIRO, M. 2004. Familial dilated cardiomyopathy and isolated left ventricular noncompaction associated with lamin A/C gene mutations. *Am J Cardiol,* 94, 50-4.

HERTIG, C. M., KUBALAK, S. W., WANG, Y. & CHIEN, K. R. 1999. Synergistic roles of neuregulin-1 and insulin-like growth factor-I in activation of the phosphatidylinositol 3-kinase pathway and cardiac chamber morphogenesis. *J Biol Chem,* 274, 37362-9.

HIGH, F. A. & EPSTEIN, J. A. 2008. The multifaceted role of Notch in cardiac development and disease. *Nat Rev Genet,* 9, 49-61.

HIGH, F. A., JAIN, R., STOLLER, J. Z., ANTONUCCI, N. B., LU, M. M., LOOMES, K. M., KAESTNER, K. H., PEAR, W. S. & EPSTEIN, J. A. 2009. Murine Jagged1/Notch signaling in the second heart field orchestrates Fgf8 expression and tissue-tissue interactions during outflow tract development. *J Clin Invest,* 119, 1986-96.

HIGH, F. A., ZHANG, M., PROWELLER, A., TU, L., PARMACEK, M. S., PEAR, W. S. & EPSTEIN, J. A. 2007. An essential role for Notch in neural crest during cardiovascular development and smooth muscle differentiation. *J Clin Invest,* 117, 353-63.

HINTON, R. B. & YUTZEY, K. E. 2011. Heart valve structure and function in development and disease. *Annu Rev Physiol,* 73, 29-46.

HORN, S., KOBBERUP, S., JORGENSEN, M. C., KALISZ, M., KLEIN, T., KAGEYAMA, R., GEGG, M., LICKERT, H., LINDNER, J., MAGNUSON, M. A., KONG, Y. Y., SERUP, P., AHNFELT-RONNE, J. & JENSEN, J. N. 2012. Mind bomb 1 is required for pancreatic beta-cell formation. *Proc Natl Acad Sci U S A,* 109, 7356-61.

I

ICHIDA, F. 2009. Left ventricular noncompaction. *Circ J,* 73, 19-26.

ICHIDA, F., TSUBATA, S., BOWLES, K. R., HANEDA, N., UESE, K., MIYAWAKI, T., DREYER, W. J., MESSINA, J., LI, H., BOWLES, N. E. & TOWBIN, J. A. 2001. Novel gene mutations in patients with left ventricular noncompaction or Barth syndrome. *Circulation,* 103, 1256-63.

ISO, T., KEDES, L. & HAMAMORI, Y. 2003. HES and HERP families: multiple effectors of the Notch signaling pathway. *J Cell Physiol,* 194, 237-55.

ISO, T., SARTORELLI, V., CHUNG, G., SHICHINOHE, T., KEDES, L. & HAMAMORI, Y. 2001. HERP, a new primary target of Notch regulated by ligand binding. *Mol Cell Biol,* 21, 6071-9.

ITOH, M., KIM, C. H., PALARDY, G., ODA, T., JIANG, Y. J., MAUST, D., YEO, S. Y., LORICK, K., WRIGHT, G. J., ARIZA-MCNAUGHTON, L., WEISSMAN, A. M., LEWIS, J., CHANDRASEKHARAPPA, S. C. & CHITNIS, A. B. 2003. Mind bomb is a ubiquitin ligase that is essential for efficient activation of Notch signaling by Delta. *Dev Cell,* 4, 67-82.

IWAMOTO, R., YAMAZAKI, S., ASAKURA, M., TAKASHIMA, S., HASUWA, H., MIYADO, K., ADACHI, S., KITAKAZE, M., HASHIMOTO, K., RAAB, G., NANBA, D., HIGASHIYAMA, S., HORI, M., KLAGSBRUN, M. & MEKADA, E. 2003. Heparin-binding EGF-like growth factor and ErbB signaling is essential for heart function. *Proc Natl Acad Sci U S A,* 100, 3221-6.

J

JACQUIER, A., THUNY, F., JOP, B., GIORGI, R., COHEN, F., GAUBERT, J. Y., VIDAL, V., BARTOLI, J. M., HABIB, G. & MOULIN, G. 2010. Measurement of trabeculated left ventricular mass using cardiac magnetic resonance imaging in the diagnosis of left ventricular non-compaction. *Eur Heart J,* 31, 1098-104.

JAIN, R., ENGLEKA, K. A., RENTSCHLER, S. L., MANDERFIELD, L. J., LI, L., YUAN, L. & EPSTEIN, J. A. 2011. Cardiac neural crest orchestrates remodeling and functional maturation of mouse semilunar valves. *J Clin Invest,* 121, 422-30.

JENNI, R., OECHSLIN, E., SCHNEIDER, J., ATTENHOFER JOST, C. & KAUFMANN, P. A. 2001. Echocardiographic and pathoanatomical characteristics of isolated left ventricular non-compaction: a step towards classification as a distinct cardiomyopathy. *Heart,* 86, 666-71.

JENNI, R., OECHSLIN, E. N. & VAN DER LOO, B. 2007. Isolated ventricular non-compaction of the myocardium in adults. *Heart,* 93, 11-5.

JEONG, H. W., JEON, U. S., KOO, B. K., KIM, W. Y., IM, S. K., SHIN, J., CHO, Y., KIM, J. & KONG, Y. Y. 2009. Inactivation of Notch signaling in the renal collecting duct causes nephrogenic diabetes insipidus in mice. *J Clin Invest,* 119, 3290-300.

JEONG, H. W., KIM, J. H., KIM, J. Y., HA, S. J. &

KONG, Y. Y. 2012. Mind bomb-1 in dendritic cells is specifically required for Notch-mediated T helper type 2 differentiation. *PLoS One,* 7, e36359.

JIANG, X., ROWITCH, D. H., SORIANO, P., MCMAHON, A. P. & SUCOV, H. M. 2000. Fate of the mammalian cardiac neural crest. *Development,* 127, 1607-16.

JIAO, K., KULESSA, H., TOMPKINS, K., ZHOU, Y., BATTS, L., BALDWIN, H. S. & HOGAN, B. L. 2003. An essential role of Bmp4 in the atrioventricular septation of the mouse heart. *Genes Dev,* 17, 2362-7.

JIN, Y., BLUE, E. K., DIXON, S., SHAO, Z. & GALLAGHER, P. J. 2002. A death-associated protein kinase (DAPK)-interacting protein, DIP-1, is an E3 ubiquitin ligase that promotes tumor necrosis factor-induced apoptosis and regulates the cellular levels of DAPK. *J Biol Chem,* 277, 46980-6.

JONES, D. T., TAYLOR, W. R. & THORNTON, J. M. 1994. A model recognition approach to the prediction of all-helical membrane protein structure and topology. *Biochemistry,* 33, 3038-49.

K

KANG, K., LEE, D., HONG, S., PARK, S. G. & SONG, M. R. 2013. The E3 ligase Mind bomb-1 (Mib1) modulates Delta-Notch signaling to control neurogenesis and gliogenesis in the developing spinal cord. *J Biol Chem,* 288, 2580-92.

KANZLER, B., KUSCHERT, S. J., LIU, Y. H. & MALLO, M. 1998. Hoxa-2 restricts the chondrogenic domain and inhibits bone formation during development of the branchial area. *Development,* 125, 2587-97.

KELLY, R. G. & BUCKINGHAM, M. E. 2002. The anterior heart-forming field: voyage to the arterial pole of the heart. *Trends Genet,* 18, 210-6.

KERN, C. B., TWAL, W. O., MJAATVEDT, C. H., FAIREY, S. E., TOOLE, B. P., IRUELA-ARISPE, M. L. & ARGRAVES, W. S. 2006. Proteolytic cleavage of versican during cardiac cushion morphogenesis. *Dev Dyn,* 235, 2238-47.

KIEFER, F., ARNOLD, K., KUNZLI, M., BORDOLI, L. & SCHWEDE, T. 2009. The SWISS-MODEL Repository and associated resources. *Nucleic Acids Res,* 37, D387-92.

KIM, R. Y., ROBERTSON, E. J. & SOLLOWAY, M. J. 2001. Bmp6 and Bmp7 are required for cushion formation and septation in the developing mouse heart. *Dev Biol,* 235, 449-66.

KIM, T. H. & SHIVDASANI, R. A. 2011. Notch signaling in stomach epithelial stem cell homeostasis. *J Exp Med,* 208, 677-88.

KIMBLE, J. & CRITTENDEN, S. L. 2007. Controls of germline stem cells, entry into meiosis, and the sperm/oocyte decision in Caenorhabditis elegans. *Annu Rev Cell Dev Biol,* 23, 405-33.

KIRBY, M. L., GALE, T. F. & STEWART, D. E. 1983. Neural crest cells contribute to normal aorticopulmonary septation. *Science,* 220, 1059-61.

KISANUKI, Y. Y., HAMMER, R. E., MIYAZAKI, J., WILLIAMS, S. C., RICHARDSON, J. A. & YANAGISAWA, M. 2001a. Tie2-Cre transgenic mice: a new model for endothelial cell-lineage analysis in vivo. *Dev Biol,* 230, 230-42.

KISANUKI, Y. Y., HAMMER, R. E., MIYAZAKI, J., WILLIAMS, S. C., RICHARDSON, J. A. & YANAGISAWA, M. 2001b. Tie2-Cre transgenic mice: a new model for endothelial cell-lineage analysis in vivo. *Dev Biol,* 230, 230-42.

KLAASSEN, S., PROBST, S., OECHSLIN, E., GERULL, B., KRINGS, G., SCHULER, P., GREUTMANN, M., HURLIMANN, D., YEGITBASI, M., PONS, L., GRAMLICH, M., DRENCKHAHN, J. D., HEUSER, A., BERGER, F., JENNI, R. & THIERFELDER, L. 2008. Mutations in sarcomere protein genes in left ventricular noncompaction. *Circulation,* 117, 2893-901.

KOIBUCHI, N. & CHIN, M. T. 2007. CHF1/Hey2 plays a pivotal role in left ventricular maturation through suppression of ectopic atrial gene expression. *Circ Res,* 100, 850-5.

KOKUBO, H., LUN, Y. & JOHNSON, R. L. 1999. Identification and expression of a novel family of bHLH cDNAs related to Drosophila hairy and enhancer of split. *Biochem Biophys Res Commun,* 260, 459-65.

KOKUBO, H., MIYAGAWA-TOMITA, S., NAKAZAWA, M., SAGA, Y. & JOHNSON, R. L. 2005. Mouse hesr1 and hesr2 genes are redundantly required to mediate Notch signaling in the developing cardiovascular system. *Dev Biol,* 278, 301-9.

KOKUBO, H., MIYAGAWA-TOMITA, S., TOMIMATSU, H., NAKASHIMA, Y., NAKAZAWA, M., SAGA, Y. & JOHNSON, R. L. 2004. Targeted disruption of hesr2 results in atrioventricular valve anomalies that lead to heart dysfunction. *Circ Res,* 95, 540-7.

KOO, B. K., LIM, H. S., SONG, R., YOON, M. J., YOON, K. J., MOON, J. S., KIM, Y. W., KWON, M. C., YOO, K. W., KONG, M. P., LEE, J., CHITNIS, A. B., KIM, C. H. & KONG, Y. Y. 2005a. Mind bomb 1 is KOO, B. K., YOON, K. J., YOO, K. W., LIM, H. S., SONG, R., SO, J. H., KIM, C. H. & KONG, Y. Y. 2005b. Mind bomb-2 is an E3 ligase for Notch ligand. *J Biol Chem,* 280, 22335-42.

KOO, B. K., YOON, M. J., YOON, K. J., IM, S. K., KIM, Y. Y., KIM, C. H., SUH, P. G., JAN, Y. N. & KONG, Y. Y. 2007. An obligatory role of mind bomb-1 in notch signaling of mammalian development. *PLoS One,* 2, e1221.

KOPAN, R. 2002. Notch: a membrane-bound transcription factor. *J Cell Sci,* 115, 1095-7.

KOZAKOV, D., BRENKE, R., COMEAU, S. R. & VAJDA, S. 2006. PIPER: an FFT-based protein docking program with pairwise potentials. *Proteins,* 65, 392-406.

KOZAKOV, D., HALL, D. R., BEGLOV, D., BRENKE, R., COMEAU, S. R., SHEN, Y., LI, K., ZHENG, J., VAKILI, P., PASCHALIDIS, I. & VAJDA, S. 2010. Achieving reliability and high accuracy in automated protein docking: ClusPro, PIPER, SDU, and stability analysis in CAPRI rounds 13-19. *Proteins,* 78, 3124-30.

KREBS, L. T., DEFTOS, M. L., BEVAN, M. J. & GRIDLEY, T. 2001. The Nrarp gene encodes an ankyrin-repeat protein that is transcriptionally regulated by the notch signaling pathway. *Dev Biol,* 238, 110-9.

KREBS, L. T., SHUTTER, J. R., TANIGAKI, K., HONJO, T., STARK, K. L. & GRIDLEY, T. 2004. Haploinsufficient lethality and formation of arteriovenous malformations in Notch pathway mutants. *Genes Dev,* 18, 2469-73.

KRUITHOF, B. P., KRAWITZ, S. A. & GAUSSIN, V. 2007. Atrioventricular valve development during late embryonic and postnatal stages involves condensation and extracellular matrix remodeling. *Dev Biol,* 302, 208-17.

LAMAR, E., DEBLANDRE, G., WETTSTEIN, D., GAWANTKA, V., POLLET, N., NIEHRS, C. & KINTNER, C. 2001. Nrarp is a novel intracellular component of the Notch signaling pathway. *Genes Dev,* 15, 1885-99.

LARDELLI, M., DAHLSTRAND, J. & LENDAHL, U. 1994. The novel Notch homologue mouse Notch 3 lacks specific epidermal growth factor-repeats and is expressed in proliferating neuroepithelium. *Mech Dev,* 46, 123-36.

L

LI, B. & DEWEY, C. N. 2011. RSEM: accurate transcript quantification from RNA-Seq data with or without a reference genome. *BMC Bioinformatics,* 12, 323.

LINDSELL, C. E., SHAWBER, C. J., BOULTER, J. & WEINMASTER, G. 1995. Jagged: a mammalian ligand that activates Notch1. *Cell,* 80, 909-17.

LOGEAT, F., BESSIA, C., BROU, C., LEBAIL, O., JARRIAULT, S., SEIDAH, N. G. & ISRAEL,

A. 1998. The Notch1 receptor is cleaved constitutively by a furin-like convertase. *Proc Natl Acad Sci U S A,* 95, 8108-12.

LUNA-ZURITA, L., PRADOS, B., GREGO-BESSA, J., LUXAN, G., DEL MONTE, G., BENGURIA, A., ADAMS, R. H., PEREZ-POMARES, J. M. & DE LA POMPA, J. L. 2010. Integration of a Notch-dependent mesenchymal gene program and Bmp2-driven cell invasiveness regulates murine cardiac valve formation. *J Clin Invest,* 120, 3493-507.

M

MACGROGAN, D., NUS, M. & DE LA POMPA, J. L. 2010. Notch signaling in cardiac development and disease. *Curr Top Dev Biol,* 92, 333-65.

MACINDOE, G., MAVRIDIS, L., VENKATRAMAN, V., DEVIGNES, M. D. & RITCHIE, D. W. 2010. HexServer: an FFT-based protein docking server powered by graphics processors. *Nucleic Acids Res,* 38, W445-9.

MARON, B. J., TOWBIN, J. A., THIENE, G., ANTZELEVITCH, C., CORRADO, D., ARNETT, D., MOSS, A. J., SEIDMAN, C. E., YOUNG, J. B., AMERICAN HEART, A., COUNCIL ON CLINICAL CARDIOLOGY, H. F., TRANSPLANTATION, C., QUALITY OF, C., OUTCOMES, R., FUNCTIONAL, G., TRANSLATIONAL BIOLOGY INTERDISCIPLINARY WORKING, G., COUNCIL ON, E. & PREVENTION 2006. Contemporary definitions and classification of the cardiomyopathies: an American Heart Association Scientific Statement from the Council on Clinical Cardiology, Heart Failure and Transplantation Committee; Quality of Care and Outcomes Research and Functional Genomics and Translational Biology Interdisciplinary Working Groups; and Council on Epidemiology and Prevention. *Circulation,* 113, 1807-16.

MASSAGUE, J., SEOANE, J. & WOTTON, D. 2005. Smad transcription factors. *Genes Dev,* 19, 2783-810.

MCKENZIE, G. J., STEVENSON, P., WARD, G., PAPADIA, S., BADING, H., CHAWLA, S., PRIVALSKY, M. & HARDINGHAM, G. E. 2005. Nuclear Ca2+ and CaM kinase IV specify hormonal- and Notch-responsiveness. *J Neurochem,* 93, 171-85.

MIYAZAKI, Y., NAKANISHI, Y. & HIEDA, Y. 2004. Tissue interaction mediated by neuregulin-1 and ErbB receptors regulates epithelial morphogenesis of mouse embryonic submandibular gland. *Dev Dyn,* 230, 591-6.

MOENS, C. B., STANTON, B. R., PARADA, L. F. & ROSSANT, J. 1993. Defects in heart and lung development in compound heterozygotes for two different targeted mutations at the N-myc locus. *Development,* 119, 485-99.

MOHR, O. L. 1919. Character Changes Caused by Mutation of an Entire Region of a Chromosome in Drosophila. *Genetics,* 4, 275-82.

MOHUN, T. J. & WENINGER, W. J. 2011. Imaging heart development using high-resolution episcopic microscopy. *Curr Opin Genet Dev,* 21, 573-8.

MOHUN, T. J. & WENINGER, W. J. 2012a. Embedding embryos for high-resolution episcopic microscopy (HREM). *Cold Spring Harb Protoc,* 2012, 678-80.

MOHUN, T. J. & WENINGER, W. J. 2012b. Episcopic three-dimensional imaging of embryos. *Cold Spring Harb Protoc,* 2012, 641-6.

MOHUN, T. J. & WENINGER, W. J. 2012c. Generation of volume data by episcopic three-dimensional imaging of embryos. *Cold Spring Harb Protoc,* 2012, 681-2.

MOORMAN, A. F. & CHRISTOFFELS, V. M. 2003. Cardiac chamber formation: development, genes, and evolution. *Physiol Rev,* 83, 1223-67.

MOORMAN, A. F., CHRISTOFFELS, V. M., ANDERSON, R. H. & VAN DEN HOFF, M. J. 2007. The heart-forming fields: one or multiple? *Philos Trans R Soc Lond B Biol Sci,* 362, 1257-65.

MUMM, J. S. & KOPAN, R. 2000. Notch signaling: from the outside in. *Dev Biol,* 228, 151-65.

MUSTARD, D. & RITCHIE, D. W. 2005. Docking essential dynamics eigenstructures. *Proteins,* 60, 269-74.

N

NEMIR, M., CROQUELOIS, A., PEDRAZZINI, T. & RADTKE, F. 2006. Induction of cardiogenesis in embryonic stem cells via downregulation of Notch1 signaling. *Circ Res,* 98, 1471-8.

NIESSEN, K., FU, Y., CHANG, L., HOODLESS, P. A., MCFADDEN, D. & KARSAN, A. 2008. Slug is a direct Notch target required for initiation of cardiac cushion cellularization. *J Cell Biol,* 182, 315-25.

NORRIS, R. A., MORENO-RODRIGUEZ, R., HOFFMAN, S. & MARKWALD, R. R. 2009. The many facets of the matricelluar protein periostin during cardiac development, remodeling, and pathophysiology. *J Cell Commun Signal,* 3, 275-86.

NUS, M., MACGROGAN, D., MARTINEZ-POVEDA, B., BENITO, Y., CASANOVA, J. C., FERNANDEZ-AVILES, F., BERMEJO, J. & DE LA POMPA, J. L. 2011. Diet-induced aortic valve disease in mice haploinsufficient for the Notch pathway effector RBPJK/CSL. *Arterioscler Thromb Vasc Biol,* 31, 1580-8.

O

OECHSLIN, E. & JENNI, R. 2011. Left ventricular non-compaction revisited: a distinct phenotype with genetic heterogeneity? *Eur Heart J,* 32, 1446-56.

OECHSLIN, E. N., ATTENHOFER JOST, C. H., ROJAS, J. R., KAUFMANN, P. A. & JENNI, R. 2000. Long-term follow-up of 34 adults with isolated left ventricular noncompaction: a distinct cardiomyopathy with poor prognosis. *J Am Coll Cardiol,* 36, 493-500.

OKOCHI, M., STEINER, H., FUKUMORI, A., TANII, H., TOMITA, T., TANAKA, T., IWATSUBO, T., KUDO, T., TAKEDA, M. & HAASS, C. 2002. Presenilins mediate a dual intramembranous gamma-secretase cleavage of Notch-1. *EMBO J,* 21, 5408-16.

P

PALOMERO, T., LIM, W. K., ODOM, D. T., SULIS, M. L., REAL, P. J., MARGOLIN, A., BARNES, K. C., O'NEIL, J., NEUBERG, D., WENG, A. P., ASTER, J. C., SIGAUX, F., SOULIER, J., LOOK, A. T., YOUNG, R. A., CALIFANO, A. & FERRANDO, A. A. 2006. NOTCH1 directly regulates c-MYC and activates a feed-forward-loop transcriptional network promoting leukemic cell growth. *Proc Natl Acad Sci U S A,* 103, 18261-6.

PANIN, V. M., PAPAYANNOPOULOS, V., WILSON, R. & IRVINE, K. D. 1997. Fringe modulates Notch-ligand interactions. *Nature,* 387, 908-12.

PARKS, A. L., KLUEG, K. M., STOUT, J. R. & MUSKAVITCH, M. A. 2000. Ligand endocytosis drives receptor dissociation and activation in the Notch pathway. *Development,* 127, 1373-85.

PARSONS, M. J., PISHARATH, H., YUSUFF, S., MOORE, J. C., SIEKMANN, A. F., LAWSON, N. & LEACH, S. D. 2009. Notch-responsive cells initiate the secondary transition in larval zebrafish pancreas. *Mech Dev,* 126, 898-912.

PETERSEN, S. E., SELVANAYAGAM, J. B., WIESMANN, F., ROBSON, M. D., FRANCIS, J. M., ANDERSON, R. H., WATKINS, H. & NEUBAUER, S. 2005. Left ventricular non-compaction: insights from cardiovascular magnetic resonance imaging. *J Am Coll Cardiol,* 46, 101-5.

R

RAND, M. D., GRIMM, L. M., ARTAVANIS-TSAKONAS, S., PATRIUB, V., BLACKLOW, S. C., SKLAR, J. & ASTER, J. C. 2000.

Calcium depletion dissociates and activates heterodimeric notch receptors. *Mol Cell Biol,* 20, 1825-35.

RANGARAJAN, A., TALORA, C., OKUYAMA, R., NICOLAS, M., MAMMUCARI, C., OH, H., ASTER, J. C., KRISHNA, S., METZGER, D., CHAMBON, P., MIELE, L., AGUET, M., RADTKE, F. & DOTTO, G. P. 2001. Notch signaling is a direct determinant of keratinocyte growth arrest and entry into differentiation. *Embo J,* 20, 3427-36.

REBAY, I., FLEMING, R. J., FEHON, R. G., CHERBAS, L., CHERBAS, P. & ARTAVANIS-TSAKONAS, S. 1991. Specific EGF repeats of Notch mediate interactions with Delta and Serrate: implications for Notch as a multifunctional receptor. *Cell,* 67, 687-99.

RECHSTEINER, M. 1988. Regulation of enzyme levels by proteolysis: the role of pest regions. *Adv Enzyme Regul,* 27, 135-51.

RENTSCHLER, S., ZANDER, J., MEYERS, K., FRANCE, D., LEVINE, R., PORTER, G., RIVKEES, S. A., MORLEY, G. E. & FISHMAN, G. I. 2002. Neuregulin-1 promotes formation of the murine cardiac conduction system. *Proc Natl Acad Sci U S A,* 99, 10464-9.

RICHARDSON, P., MCKENNA, W., BRISTOW, M., MAISCH, B., MAUTNER, B., O'CONNELL, J., OLSEN, E., THIENE, G., GOODWIN, J., GYARFAS, I., MARTIN, I. & NORDET, P. 1996. Report of the 1995 World Health Organization/International Society and Federation of Cardiology Task Force on the Definition and Classification of cardiomyopathies. *Circulation,* 93, 841-2.

RITCHIE, D. 2005. High-order analytic translation matrix elements for real-space six-dimensional polar Fourier correlations. *Journal of Applied Crystallography,* 38, 808-818.

RITCHIE, D. W. 2003. Evaluation of protein docking predictions using Hex 3.1 in CAPRI rounds 1 and 2. *Proteins,* 52, 98-106.

RITCHIE, D. W. & KEMP, G. J. 2000. Protein docking using spherical polar Fourier correlations. *Proteins,* 39, 178-94.

RITCHIE, D. W., KOZAKOV, D. & VAJDA, S. 2008. Accelerating and focusing protein-protein docking correlations using multi-dimensional rotational FFT generating functions. *Bioinformatics,* 24, 1865-73.

RITCHIE, D. W. & VENKATRAMAN, V. 2010. Ultra-fast FFT protein docking on graphics processors. *Bioinformatics,* 26, 2398-405.

RITTER, M., OECHSLIN, E., SUTSCH, G., ATTENHOFER, C., SCHNEIDER, J. & JENNI, R. 1997. Isolated noncompaction of the myocardium in adults. *Mayo Clin Proc,* 72, 26-31.

RODIGHIERO, S., BAZZINI, C., RITTER, M., FURST, J., BOTTA, G., MEYER, G. & PAULMICHL, M. 2008. Fixation, mounting and sealing with nail polish of cell specimens lead to incorrect FRET measurements using acceptor photobleaching. *Cell Physiol Biochem,* 21, 489-98.

RONES, M. S., MCLAUGHLIN, K. A., RAFFIN, M. & MERCOLA, M. 2000. Serrate and Notch specify cell fates in the heart field by suppressing cardiomyogenesis. *Development,* 127, 3865-76.

ROY, A., KUCUKURAL, A. & ZHANG, Y. 2010. I-TASSER: a unified platform for automated protein structure and function prediction. *Nat Protoc,* 5, 725-38.

ROY, A., XU, D., POISSON, J. & ZHANG, Y. 2011. A protocol for computer-based protein structure and function prediction. *J Vis Exp*, e3259.

RUAN, Y., TECOTT, L., JIANG, M. M., JAN, L. Y. & JAN, Y. N. 2001. Ethanol hypersensitivity and olfactory discrimination defect in mice lacking a homolog of Drosophila neuralized. *Proc Natl Acad Sci U S A,* 98, 9907-12.

RUTENBERG, J. B., FISCHER, A., JIA, H., GESSLER, M., ZHONG, T. P. & MERCOLA, M. 2006. Developmental patterning of the cardiac atrioventricular canal by Notch and Hairy-related transcription factors. *Development,* 133, 4381-90.

S

SAHLGREN, C., GUSTAFSSON, M. V., JIN, S., POELLINGER, L. & LENDAHL, U. 2008. Notch signaling mediates hypoxia-induced tumor cell migration and invasion. *Proc Natl Acad Sci U S A,* 105, 6392-7.

SARMA, R. J., CHANA, A. & ELKAYAM, U. 2010. Left ventricular noncompaction. *Prog Cardiovasc Dis,* 52, 264-73.

SEDGWICK, S. G. & SMERDON, S. J. 1999. The ankyrin repeat: a diversity of interactions on a common structural framework. *Trends Biochem Sci,* 24, 311-6.

SEDMERA, D., PEXIEDER, T., HU, N. & CLARK, E. B. 1997. Developmental changes in the myocardial architecture of the chick. *Anat Rec,* 248, 421-32.

SEDMERA, D., PEXIEDER, T., VUILLEMIN, M., THOMPSON, R. P. & ANDERSON, R. H. 2000. Developmental patterning of the myocardium. *Anat Rec,* 258, 319-37.

SHAH, D. K., MOHTASHAMI, M. & ZUNIGA-PFLUCKER, J. C. 2012. Role of recycling, Mindbomb1 association, and exclusion from lipid rafts of delta-like 4 for effective Notch signaling to drive T cell development. *J Immunol,* 189, 5797-808.

SHAWBER, C., BOULTER, J., LINDSELL, C. E. & WEINMASTER, G. 1996. Jagged2: a serrate-like gene expressed during rat embryogenesis. *Dev Biol,* 180, 370-6.

SHOU, W., AGHDASI, B., ARMSTRONG, D. L., GUO, Q., BAO, S., CHARNG, M. J., MATHEWS, L. M., SCHNEIDER, M. D., HAMILTON, S. L. & MATZUK, M. M. 1998. Cardiac defects and altered ryanodine receptor function in mice lacking FKBP12. *Nature,* 391, 489-92.

SHUTTER, J. R., SCULLY, S., FAN, W., RICHARDS, W. G., KITAJEWSKI, J., DEBLANDRE, G. A., KINTNER, C. R. & STARK, K. L. 2000. Dll4, a novel Notch ligand expressed in arterial endothelium. *Genes Dev,* 14, 1313-8.

SINGH, M. K., CHRISTOFFELS, V. M., DIAS, J. M., TROWE, M. O., PETRY, M., SCHUSTER-GOSSLER, K., BURGER, A., ERICSON, J. & KISPERT, A. 2005. Tbx20 is essential for cardiac chamber differentiation and repression of Tbx2. *Development,* 132, 2697-707.

SNARR, B. S., KERN, C. B. & WESSELS, A. 2008. Origin and fate of cardiac mesenchyme. *Dev Dyn,* 237, 2804-19.

SRIVASTAVA, D. 2006. Making or breaking the heart: from lineage determination to morphogenesis. *Cell,* 126, 1037-48.

STANLEY, E. G., BIBEN, C., ELEFANTY, A., BARNETT, L., KOENTGEN, F., ROBB, L. & HARVEY, R. P. 2002. Efficient Cre-mediated deletion in cardiac progenitor cells conferred by a 3'UTR-ires-Cre allele of the homeobox gene Nkx2-5. *Int J Dev Biol,* 46, 431-9.

STOLLBERGER, C. & FINSTERER, J. 2004. Left ventricular hypertrabeculation/ noncompaction-don't forget the myologist!Concerning the article "Isolated myocardial noncompaction als seltene Ursache einer Synkope im Kindesalter" by Binz G. et al. Z Kardiol 92:1039-1044 (2003). *Z Kardiol,* 93, 242-3; author reply 243-4.

STOLLBERGER, C., FINSTERER, J. & BLAZEK, G. 2002. Left ventricular hypertrabeculation/ noncompaction and association with additional cardiac abnormalities and neuromuscular disorders. *Am J Cardiol,* 90, 899-902.

T

TAMURA, K., TANIGUCHI, Y., MINOGUCHI, S., SAKAI, T., TUN, T., FURUKAWA, T. & HONJO, T. 1995. Physical interaction between a novel domain of the receptor Notch and the transcription factor RBP-J kappa/Su(H). *Curr Biol,* 5, 1416-23.

TANIGAKI, K. & HONJO, T. 2007. Regulation of lymphocyte development by Notch signaling. *Nat Immunol,* 8, 451-6.

TAO, J., DOUGHMAN, Y., YANG, K., RAMIREZ-BERGERON, D. & WATANABE, M. 2013. Epicardial HIF signaling regulates vascular precursor cell invasion into the myocardium. *Dev Biol,* 376, 136-49.

TIMMERMAN, L. A., GREGO-BESSA, J., RAYA, A., BERTRAN, E., PEREZ-POMARES, J. M., DIEZ, J., ARANDA, S., PALOMO, S., MCCORMICK, F., IZPISUA-BELMONTE, J. C. & DE LA POMPA, J. L. 2004. Notch promotes epithelial-mesenchymal transition during cardiac development and oncogenic transformation. *Genes Dev,* 18, 99-115.

TOWBIN, J. A. 2010. Left ventricular noncompaction: a new form of heart failure. *Heart Fail Clin,* 6, 453-69, viii.

TSAI, M. F., LIN, Y. J., CHENG, Y. C., LEE, K. H., HUANG, C. C., CHEN, Y. T. & YAO, A. 2007. PrimerZ: streamlined primer design for promoters, exons and human SNPs. *Nucleic Acids Res,* 35, W63-5.

U

UYTTENDAELE, H., MARAZZI, G., WU, G., YAN, Q., SASSOON, D. & KITAJEWSKI, J. 1996. Notch4/int-3, a mammary proto-oncogene, is an endothelial cell-specific mammalian Notch gene. *Development,* 122, 2251-9.

V

VAN DE WALLE, I., DE SMET, G., DE SMEDT, M., VANDEKERCKHOVE, B., LECLERCQ, G., PLUM, J. & TAGHON, T. 2009. An early decrease in Notch activation is required for human TCR-alphabeta lineage differentiation at the expense of TCR-gammadelta T cells. *Blood,* 113, 2988-98.

VAN DIJK, R. A., ENGELS, C. C., SCHAAPHERDER, A. F., MULDER-STAPEL, A., TEN DIJKE, P., HAMMING, J. F. & LINDEMAN, J. H. 2012. Visualizing TGF-beta and BMP signaling in human atherosclerosis: a histological evaluation based on Smad activation. *Histol Histopathol,* 27, 387-96.

VAN KEMPEN, M. J., VERMEULEN, J. L., MOORMAN, A. F., GROS, D., PAUL, D. L. & LAMERS, W. H. 1996. Developmental changes of connexin40 and connexin43 mRNA distribution patterns in the rat heart. *Cardiovasc Res,* 32, 886-900.

VELTMAAT, J. M., ORELIO, C. C., WARD-VAN OOSTWAARD, D., VAN ROOIJEN, M. A., MUMMERY, C. L. & DEFIZE, L. H. 2000. Snail is an immediate early target gene of parathyroid hormone related peptide signaling in parietal endoderm formation. *Int J Dev Biol,* 44, 297-307.

VOLLRATH, B., PUDNEY, J., ASA, S., LEDER, P. & FITZGERALD, K. 2001. Isolation of a murine homologue of the Drosophila neuralized gene, a gene required for axonemal integrity in spermatozoa and terminal maturation of the mammary gland. *Mol Cell Biol,* 21, 7481-94.

W

WANG, W., CAMPOS, A. H., PRINCE, C. Z., MOU, Y. & POLLMAN, M. J. 2002. Coordinate Notch3-hairy-related transcription factor pathway regulation in response to arterial injury. Mediator role of platelet-derived growth factor and ERK. *J Biol Chem,* 277, 23165-71.

WATANABE, Y., KOKUBO, H., MIYAGAWA-TOMITA, S., ENDO, M., IGARASHI, K., AISAKI, K. I., KANNO, J. & SAGA, Y. 2006. Activation of Notch1 signaling in cardiogenic mesoderm induces abnormal heart morphogenesis in mouse. *Development,* 133, 1625-34.

WEINMASTER, G., ROBERTS, V. J. & LEMKE, G. 1992. Notch2: a second mammalian Notch gene. *Development,* 116, 931-41.

WENG, A. P., MILLHOLLAND, J. M., YASHIRO-OHTANI, Y., ARCANGELI, M. L., LAU, A., WAI, C., DEL BIANCO, C., RODRIGUEZ, C. G., SAI, H., TOBIAS, J., LI, Y., WOLFE, M. S.,

SHACHAF, C., FELSHER, D., BLACKLOW, S. C., PEAR, W. S. & ASTER, J. C. 2006. c-Myc is an important direct target of Notch1 in T-cell acute lymphoblastic leukemia/ lymphoma. *Genes Dev,* 20, 2096-109.

WESSELS, A. & SEDMERA, D. 2003. Developmental anatomy of the heart: a tale of mice and man. *Physiol Genomics,* 15, 165-76.

WESSELS, A., VAN DEN HOFF, M. J., ADAMO, R. F., PHELPS, A. L., LOCKHART, M. M., SAULS, K., BRIGGS, L. E., NORRIS, R. A., VAN WIJK, B., PEREZ-POMARES, J. M., DETTMAN, R. W. & BURCH, J. B. 2012. Epicardially derived fibroblasts preferentially contribute to the parietal leaflets of the atrioventricular valves in the murine heart. *Dev Biol,* 366, 111-24.

WHARTON, K. A., JOHANSEN, K. M., XU, T. & ARTAVANIS-TSAKONAS, S. 1985. Nucleotide sequence from the neurogenic locus notch implies a gene product that shares homology with proteins containing EGF-like repeats. *Cell,* 43, 567-81.

WU, L., ASTER, J. C., BLACKLOW, S. C., LAKE, R., ARTAVANIS-TSAKONAS, S. & GRIFFIN, J. D. 2000. MAML1, a human homologue of Drosophila mastermind, is a transcriptional co-activator for NOTCH receptors. *Nat Genet,* 26, 484-9.

Z

ZAFFRAN, S., KELLY, R. G., MEILHAC, S. M., BUCKINGHAM, M. E. & BROWN, N. A. 2004. Right ventricular myocardium derives from the anterior heart field. *Circ Res,* 95, 261-8.

ZELLER, R., BLOCH, K. D., WILLIAMS, B. S., ARCECI, R. J. & SEIDMAN, C. E. 1987. Localized expression of the atrial natriuretic factor gene during cardiac embryogenesis. *Genes Dev,* 1, 693-8.

ZHANG, C., LI, Q. & JIANG, Y. J. 2007a. Zebrafish Mib and Mib2 are mutual E3 ubiquitin ligases with common and specific delta substrates. *J Mol Biol,* 366, 1115-28.

ZHANG, C., LI, Q., LIM, C. H., QIU, X. & JIANG, Y. J. 2007b. The characterization of zebrafish antimorphZHANG, Y. 2008. I-TASSER server for protein 3D structure prediction. *BMC Bioinformatics,* 9, 40.

Acknowledgments

I would like to thank José Luis de la Pompa for letting me develop my doctoral thesis in his group, for all the years of patience, guidance and mentoring that I needed to finish this work (writing is not speaking) and for encouraging me to follow the long path that starts now even though eventually I'd like to teach. I also would like to thank my tutor, Antonio Rodriguez for his totally necessary support for this thesis to be finished.

I would like to thank all my lab mates that made that coming to the lab it is not just going to work. Belén Prados, my non-academical tutor, treated me as the older sister I never had. Quim Grego-Bessa, Luis Luna, Álvaro Gonzalez-Rajal, Gonzalo del Monte taught me everything I know and took me into the group as one of them. Beatríz Martínez-Poveda and Jesús F. Casanova helped me a lot answering the evil reviewers so that the paper could be published. Mauro Sbroggió shared not only lab protocols. Patricia Martinez, Abelón Galicia, Vanessa Bou, Ana Cabrero and Eva García made the impossible to make this work possible. Meritxell Nus, Juli Münch, Gaetano D'Amato, Lao Travisano, Dimitrios Grivas, Marcos Siguero and Paula Gomez-Apiñaniz make shorter the long evenings and Donal Macgrogan taught me part of what he knows because everything would be impossible in a lifetime.

I would also like to thank all the collaborators that make this work possible, Juan Ramón Gimeno and María Sabater from the Hospital de la Arrixaca in Murcia, Lorenzo Montserrat from Genes in Code in La Coruña, Pablo García Pavía from the Hospital Puerta de Hierro in Madrid, Gonzalo Pizarro from the Clínica Quirón in Madrid, Constancio Medrano from the Hospital Gregorio Marañón in Madrid, Borja Ibañez from the Hospital Clínico San Carlos in Madrid, Leticia Fernández from the Department of Epidemiology, Atherothrombosis and Image of the CNIC in Madrid and Jesús Borreguero from the Hospital de la Princesa in Madrid; he unveiled the secrets of cardiac imaging to us.

The CNIC is a great place to develop science not only because its great technical units. Without histopathology, where Roisin Doohan can do magic with a paraffin block, microscopy, genomics and the people in the animal house everything would have been much more difficult. But especially for the great atmosphere that have been built in the Developmental Biology Department. Working in an open space laboratory where everybody helps, everybody shares their expertise and everybody supports you has been really enriching. So I'd like to thank all the "Torres", "Flores", "Nadias", "Beneditos" and "Juanjos". Also everything would have been impossible without the help of Teresa Casaseca, Sandra Cillero and Beatríz Ferreiro. Not just in the department, but the CNIC is full of friendly faces as the "Manzanitos", Teresa it was a great pleasure to re-find you here, Edu, please never stop being so Edu, or the Mondays football troupe. But I cannot finish this list of important scientists that helped me finishing my thesis without mentioning the people that were somehow at the beginning, Holly Shiels took me in her lab as Erasmus student 45 minutes after receiving my email and Gina Galli showed me how to do my first solution.

Everything written in this book wouldn't be here if it wasn't for the support of my family. My mother and her continuous questions about when was it going to be finished, my father's lectures and encouragement, the croquetas of my abuela, my brother's example about never giving up. MariNieves, Javier, Luismi, Begoña and the whole "cocretas" bunch, Rebe, Clara, Blanca, Luis, Alba and Lua. I would also like to tank all the LuXanes that have encouraged me to do a PhD.

I had also a lot support coming from Aschaffenburg, Mülheim and Grosseto. Ulrike, Johannes, Tom, Astrid, Svenja, Josefine, Ferdi, Paulina, Juri, Lilly and Carla had a place reserved for me when I needed to escape.

My other family has been present through all the processes of this thesis and I want to thank them for all the support and love they have given to me. Carlos, Elisa, Eva, Alessia, Manolo, Mayte, Luis, Javier, Maria, Bruno and Tania the crazy aunt.

And finally I want to thank Meike for taking care of me during these last years and especially in the last two when she had to share me. For supporting me when I said I would be chained to Madrid for a "couple" of years and for dragging her almost to the Wall where they don´t know how is a brezel. For accepting me as the geek I've become and running with me to infinity and beyond.

COVER PAGE. 3D episcopic reconstruction of E16.5 *Mib1^{flox};cTnT-Cre* heart.

BACK COVER. MIB1 dimer model